FROM THE: MAX PLANCK INSTITUTE OF PSYCHIATRY

The ageing of the human brain - Transcriptomic changes throughout ageing revealed at cell-type resolution & their implications for neurodegenerative and psychiatric disorders

Dissertation zum Erwerb des
Doctor rerum naturalium (Dr. rer. nat.)
an der Fakultät für Biologie der
Ludwig-Maximilians Universität München

vorgelegt von

Anna Sophie Fröhlich

Tag der Abgabe:

25.08.2023

Mit Genehmigung der Fakultät für Biologie

Ludwig-Maximilians-Universität München

Supervisor: *Prof. Dr. Dr. med. univ. Elisabeth B. Binder*
Department of Genes and Environment
Max Planck Institute of Psychiatry

Erster Gutachter: *PD Dr. Mathias Schmidt*

Zweiter Gutachter: *Prof. Dr. Wolfgang Enard*

Dritte Gutachterin: *Prof. Dr. Laura Busse*

Vierte Gutachterin: *PD Dr. Serena Schwenkert*

Tag der Abgabe: 25.08.2023

Tag der mündlichen Prüfung: 08.02.2024

Eidesstattliche Erklärung

Ich versichere hiermit an Eides statt, dass die vorgelegte Dissertation von mir selbständig und ohne unerlaubte Hilfe angefertigt ist.

München, den .... 25.08.2023 ..... Anna Fröhlich .....

(Unterschrift)

Erklärung

Hiermit erkläre ich, *

☒ dass die Dissertation nicht ganz oder in wesentlichen Teilen einer anderen Prüfungskommission vorgelegt worden ist.

☒ dass ich mich anderweitig einer Doktorprüfung ohne Erfolg **nicht** unterzogen habe.

☐ ~~dass ich mich mit Erfolg der Doktorprüfung im Hauptfach~~ .....

~~und in den Nebenfächern~~ .....

~~bei der Fakultät für ..... der~~ .....

(Hochschule/Universität)

~~unterzogen habe.~~

☐ ~~dass ich ohne Erfolg versucht habe, eine Dissertation einzureichen oder mich der Doktorprüfung zu unterziehen.~~

München, den..... 25.08.2023 ..... Anna Fröhlich .....

(Unterschrift)

*) Nichtzutreffendes streichen

Publication Statement

The work presented in this doctoral thesis is currently part of a manuscript in review in a peer-reviewed journal with the following title “Cell-type-specific aging effects in the human OFC and implications for psychiatric disease” (Fröhlich, AS et al. in revision).

Most of the content and figures in the Results, and Material and Methods sections have been adapted from this manuscript.

Abstract

We are part of an ageing society, which is due to changes in demographics amongst others driven by a drastic increase in life expectancy over the last century. The longer life expectancy comes at a cost: a rise in the prevalence of age-related neurodegenerative disorders, debilitating diseases with currently no cure available. Another group of diseases with substantial disease burden and societal impact are psychiatric disorders. In fact, comorbidity between these two groups of disorders and genetics have demonstrated that neurodegenerative and psychiatric disorders are interconnected. Age represents the strongest risk factor for neurodegenerative disorders and a body of evidence suggests that biological ageing is accelerated in psychiatric disorders. In-depth characterization of the cellular and molecular ageing process could therefore provide insights into disease aetiology.

The ageing process affects the level of molecules, cells, and organs resulting in changes in function and physiology impacting the whole organism. The brain, with the prefrontal cortex - an area essential for higher cognitive functions - most affected, suffers structural decline during ageing. The brain consists of several different cell types each with specific features, functions and connections which together accomplish the brain's complex computations. Using different (animal) model systems, several age-related changes in cellular morphology and function and affected biological pathways have already been identified. Yet, the human cortex has expanded massively during evolution and certain features of neurodegenerative disorders only seem to be present in humans necessitating the molecular investigation of the ageing process in a human-specific model. Moreover, detailed insights on the effects of ageing on the diverse cell types in the brain are still missing resulting in our incomplete understanding of both the normal and pathological ageing process.

Therefore, this doctoral thesis aimed at characterizing how normal ageing affects gene expression in the different cell types of the prefrontal cortex. Using single nucleus RNA sequencing, the transcriptomes of ~ 800,000 nuclei, isolated from a large cohort (N=87) of human post-mortem brain samples of the orbitofrontal cortex, were examined. Since the brain samples were derived from individuals with and without a diagnosis of a psychiatric disorder, the effect of suffering from a psychiatric disorder on the ageing process could additionally be investigated. Integration of single nucleus RNA sequencing datasets derived from individuals with and without Alzheimer's disease further enabled the exploration of the relation of age-related changes in neurodegenerative disorders.

We were able to identify twenty different brain cell types and showed that ageing affects the transcriptome of nearly all cell types. The transcriptomic changes were largely cell-type specific with only a partial overlap of age-regulated genes between the different cell types. However, despite different genes being age-regulated, pathway analysis revealed a convergence of gene expression alterations across cell types onto dysregulated synaptic signalling. Moreover, an inhibitory neuron subtype, shown to be enriched in the cortex of primates (compared to mice), was identified as most strongly affected by the ageing process. Importantly, we were able to replicate our findings using previously published datasets both in bulk brain tissue and specific cell types. We could further demonstrate that age-related gene expression changes overlap with expression changes in Alzheimer's disease in specific

cell types. Lastly, we provide evidence for accelerated transcriptomic ageing in individuals with psychiatric disorders and uncover age-related gene expression trajectories across individual cell types shifted in individuals with psychiatric disorders.

In summary, the work presented in this doctoral thesis provides a comprehensive dataset of age-related gene expression changes in the individual cell types of the brain. Additionally, it offers insights into the biological processes affected by these alterations thereby expanding our knowledge of the molecular ageing process. In addition, the overlap of age-regulated genes with genes playing a role in Alzheimer's disease provides a potential molecular explanation for why age represents the strongest risk factor for their development. Moreover, in several cell types, we identified genes whose expression was influenced by both ageing and psychiatric disease which may contribute to the accelerated brain ageing observed in individuals with psychiatric disorders.

Zusammenfassung

Wir leben in einer alternden Gesellschaft, was auf demographische Veränderungen zurückzuführen ist, die unter anderem durch einen drastischen Anstieg der Lebenserwartung im letzten Jahrhundert bedingt sind. Die höhere Lebenserwartung hat jedoch ihren Preis: ein Anstieg in der Prävalenz altersbedingter neurodegenerativer Erkrankungen; belastende Krankheiten, für die es derzeit keine Heilung gibt. Eine weitere Gruppe von Krankheiten mit erheblichen gesundheitlichen Belastungen für Betroffene sowie gesellschaftlichen Auswirkungen sind psychiatrische Erkrankungen. Die Komorbidität zwischen diesen beiden Gruppen von Erkrankungen und die Genetik haben gezeigt, dass neurodegenerative und psychiatrische Erkrankungen miteinander verbunden sind. Das Alter ist der stärkste Risikofaktor für neurodegenerative Erkrankungen, und es gibt zahlreiche Hinweise darauf, dass der biologische Alterungsprozess bei psychiatrischen Erkrankungen beschleunigt ist. Eine eingehende Charakterisierung des zellulären und molekularen Alterungsprozesses könnte daher Einblicke in die Ursachen der Krankheiten liefern.

Der Alterungsprozess wirkt sich auf der Ebene von Molekülen, Zellen und Organen aus und führt zu Veränderungen in Funktion und Physiologie, die den gesamten Organismus beeinflussen. Das Gehirn, insbesondere der präfrontale Kortex - ein Bereich, der für höhere kognitive Funktionen unerlässlich ist - erleidet während des Alterns einen strukturellen Verfall. Das Gehirn besteht aus mehreren verschiedenen Zelltypen mit jeweils spezifischen Eigenschaften, Funktionen und Verknüpfungen, die zusammen die komplexen Berechnungen des Gehirns durchführen. Anhand verschiedener (Tier-)Modellsysteme wurden bereits mehrere altersbedingte Veränderungen der zellulären Morphologie und Funktion sowie betroffene biologische Signalwege identifiziert. Der menschliche Kortex hat sich jedoch im Laufe der Evolution massiv vergrößert, und bestimmte Merkmale neurodegenerativer Erkrankungen scheinen nur beim Menschen aufzutreten, was die molekulare Untersuchung des Alterungsprozesses in einem human-spezifischen Modell erforderlich macht. Darüber hinaus fehlen noch immer detaillierte Erkenntnisse über die Auswirkungen des Alterns auf die verschiedenen Zelltypen im Gehirn, was zu unserem unvollständigen Verständnis sowohl des normalen als auch des pathologischen Alterungsprozesses beiträgt.

Das Ziel dieser Doktorarbeit war, zu charakterisieren, wie normales Altern die Genexpression in den verschiedenen Zelltypen im präfrontalen Kortex beeinflusst. Mit Hilfe der single nucleus RNA Sequenzierung wurden die Transkriptome von etwa 800 000 Zellkernen untersucht, die von einer großen Kohorte (N=87) menschlicher postmortaler Gehirnproben des orbitofrontalen Kortex isoliert worden waren. Da die Gehirnproben von Personen mit und ohne Diagnose einer psychiatrischen Erkrankung stammten, konnte zusätzlich der Einfluss einer psychiatrischen Erkrankung auf den Alterungsprozess untersucht werden. Der Vergleich mit anderen single nucleus RNA Sequenzierungs-Datensätzen, von Personen mit und ohne Alzheimer, ermöglichte die Erforschung des Zusammenhangs von altersbedingten Veränderungen und neurodegenerativen Erkrankungen.

Wir waren in der Lage, zwanzig verschiedene Zelltypen zu identifizieren und konnten zeigen, dass das Altern das Transkriptom fast aller Zelltypen beeinflusst. Die transkriptomischen

Veränderungen waren weitgehend zelltypspezifisch, da sich die altersregulierten Gene zwischen den verschiedenen Zelltypen nur teilweise überschnitten. Obwohl verschiedene Gene altersreguliert wurden, ergab die Analyse der Signalwege eine Konvergenz der Genexpressionsveränderungen über alle Zelltypen hinweg auf eine dysregulierte synaptische Signalübertragung. Darüber hinaus wurde ein Subtyp von inhibitorischen Neuronen, der im Kortex von Primaten (im Vergleich zu Mäusen) vermehrt vorhanden ist, als am stärksten vom Alterungsprozess betroffen identifiziert. Zu unterstreichen ist, dass wir unsere Ergebnisse mit Hilfe von bereits veröffentlichten Datensätzen replizieren konnten, und zwar sowohl im Gesamt-Gehirngewebe als auch in spezifischen Zelltypen. Wir konnten außerdem zeigen, dass sich altersbedingte Veränderungen der Genexpression in bestimmten Zelltypen mit den Expressionsveränderungen bei Alzheimer überschneiden. Schließlich liefern wir Beweise für ein beschleunigtes transkriptomisches Altern bei Menschen mit psychiatrischen Erkrankungen und decken altersbedingte Genexpressionsverläufe in einzelnen Zelltypen auf, die bei Menschen mit psychiatrischen Erkrankungen verschoben sind.

Die in dieser Doktorarbeit vorgestellten Arbeiten umfassen einen großen Datensatz altersbedingter Veränderungen der Genexpression in den einzelnen Zelltypen des Gehirns. Außerdem bieten sie Einblicke in die biologischen Prozesse, die von diesen Veränderungen betroffen sind, und erweitern damit unser Wissen über den molekularen Alterungsprozess. Darüber hinaus liefert die Überschneidung von altersregulierten Genen mit Genen, die bei Alzheimer eine Rolle spielen, eine mögliche molekulare Erklärung dafür, warum das Alter den stärksten Risikofaktor für deren Entstehung darstellt. Des Weiteren haben wir in mehreren Zelltypen Gene identifiziert, deren Expression sowohl durch das Altern als auch durch psychiatrische Erkrankungen beeinflusst wird, welche zu der beschleunigten Alterung des Gehirns bei Menschen mit psychiatrischen Erkrankungen beitragen könnten.

Contents

List of Abbreviations

AD	Alzheimer's disease
AMPA	α-amino-3-hydroxy-5-methyl-4-isoxazolepropionic acid
ATP	adenosine triphosphate
Aβ	amyloid β
BBB	blood brain barrier
BPD	bipolar disorder
BrainAGE	brain age gap estimation
Ca^{2+}	calcium
CBT	cognitive-behavioural therapy
CpG	cytosine guanine dinucleotide
DALY	disability-adjusted life year
DE	differentially expressed
DGE	differential gene expression
DNAm	DNA methylation
ECT	electroconvulsive therapy
ER	endoplasmatic reticulum
FC	fold change
FDR	false discovery rate
GABA	γ-aminobutyric acid
GEMs	gel bead in emulsions
GO	gene ontology
GWAS	genome-wide association studies
iNeurons	induced neurons
iPSC	induced pluripotent stem cell
lib_batch	library preparation batch
MDD	major depressive disorder
MGLUR2	glutamate metabotropic receptor 2
MRI	magnetic resonance imaging
NDMA	N-methyl-D-aspartate
NEB	nuclei extraction buffer
NFTs	neurofibrillary tangles
NGS	next-generation sequencing
OFC	orbitofrontal cortex
OI	overlap index
OR	odds ratio
ORA	over-representation analysis
PC	principal component
PCA	principal component analysis
PD	Parkinson's disease
PFC	prefrontal cortex

PMI	post-mortem interval
PRS	polygenic risk scores
RIN	RNA-integrity number
ROS	reactive oxygen specie
sc-RNA-seq	single cell RNA sequencing
sc-seq	single cell sequencing
SCZ	schizophrenia
SZA	schizoaffective disorder
sn-RNA-seq	single nucleus RNA sequencing
SNP	single nucleotide polymorphism
TNF	tumour necrosis factor
UMAP	uniform manifold approximation and projection
UN	United Nations
UPS	ubiquitin–proteasome system
ρ	spearman correlation coefficient

1 | Introduction

1.1 Global population trends - our ageing society

Over the last 100 years, the world population has drastically increased from roughly 2.5 billion people in 1950 to 8 billion in November 2022. This increase is due to a rise in births combined with a decrease in child mortality and overall improvements in global health care driven by the discovery of antibiotics, the development and global rollout of vaccinations and advances in prevention, diagnosis, and treatment of a myriad of communicable and non-communicable diseases. Current estimates by the United Nations (UN) predict a continued growth of the world population until the 2080s totalling 10.35 billion people by the end of the century. However, the demographic structure is changing: While in the 1950s the number of births was high, child mortality and the overall risk of death throughout life was also high, which resulted in a demographic structure resembling a pyramid with a broad base, the new-borns, and a steep narrowing at the top, the elderly (**Figure 1.1a**). Looking at today's global population, the global median age has increased from 22.2 in 1950 to 29.7 in 2020 with the overall population structure still somewhat resembling a pyramid (**Figure 1.1b**), though with a much broader base and a less steep narrowing towards the older age groups indicating a population increase in/along all age groups. The UN's projections for 2090 foresee a decline in birth rates resulting in only a minimal increase at the base with a parallel rise in middle and older age groups due to longer life expectancy transforming the former pyramid into a bell-shaped structure (**Figure 1.1c**). This change in population structure depicts an overall healthier world population with a minimal risk of death until old age. However, the increasing share of elderly people poses new challenges not only for the economic but also for the healthcare sector [1, 2].

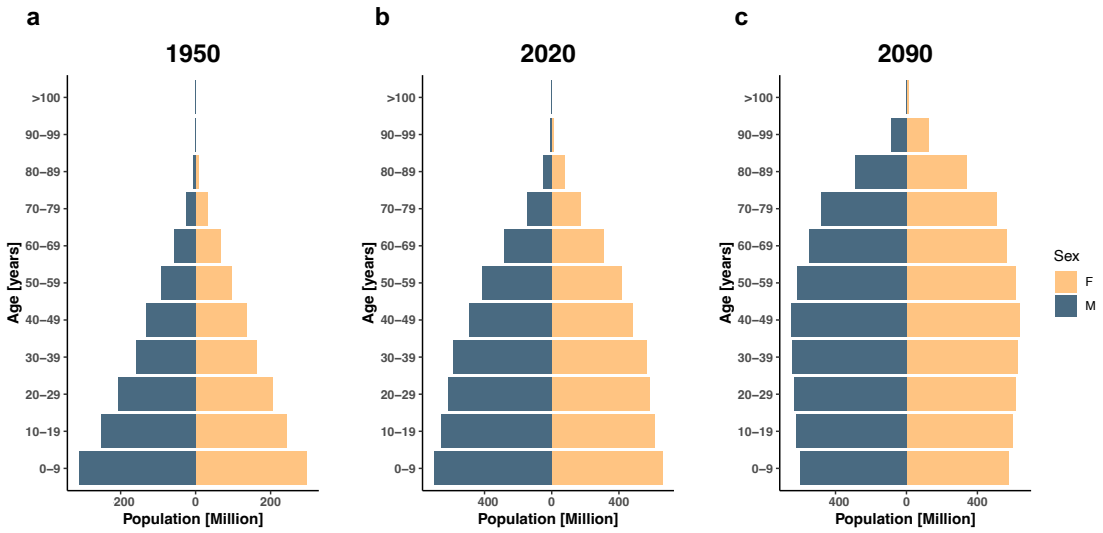

Figure 1.1: Population demographics throughout the years. **a-c**, Population demographics in 1950 (**a**), in 2020 (**b**) and projected population demographic in 2090 (**c**); F=female, M= male; Data obtained from [3].

1.2 Neurodegenerative disorders - the burden of rising life expectancy

The increase in life expectancy has been accompanied by a rise in individuals affected by age-related neurodegenerative diseases. Neurodegenerative diseases refer to a group of debilitating diseases with currently no cure available and for most only insufficient treatments. They include diseases such as Parkinson's disease (PD), Alzheimer's disease (AD), and other forms of dementia. Common to their pathology is the progressive accumulation of certain proteins, which leads to neuronal loss. This impairs normal brain function, ultimately resulting in the impairment of memory and cognition [4]. Dementia is an umbrella term for several conditions leading to deterioration in cognitive function with AD accounting for up to 60 - 70% of all cases [5].

In fact, AD is the most common neurodegenerative disease with 32 million affected people globally [6]. Neuropathologically, AD is characterized by the accumulation of amyloid β (Aβ) aggregates and neurofibrillary tangles (NFTs) made up by tau proteins. Symptoms vary from person to person but commonly include memory loss, poorer judgement, difficulties with routine tasks, changes in mood and personality, increased anxiety, and social isolation [4]. Even though the exact pathomechanisms are not fully understood, it is thought that the progressive accumulation of Aβ and NFTs results from a disruption in protein homeostasis. This leads to compromised cellular function including mitochondrial dysfunction, dysfunction in the clearance system and calcium (Ca^{2+}) signalling, which results in impaired neuronal activity and ultimately neuronal death. These alterations likely start in the entorhinal cortex and then further spread to connected regions including the hippocampus and cortex thereby affecting circuits involved in cognition and memory. [7, 8] Current treatments for AD include cholinesterase inhibitors, which reduce the enzymatic breakdown of acetylcholine, a neurotransmitter involved in memory and thinking. N-methyl-D-aspartate receptor antagonists are also used, which are thought to exhibit their effect via the regulation of glutamate levels. Other treatment options include immunotherapies, which target Aβ to reduce its aggregates. However, due to the complexity of AD pathogenesis, combination therapy rather than monotherapy may be necessary for more effective treatment. [9]

PD represents the second most frequent neurodegenerative disorder, with worldwide more than 10 million people affected [10], and involves the abnormal aggregation and insufficient clearance of the so-called Lewy bodies, which are mainly composed of α-synuclein and ubiquitin. Clinical manifestation includes movement impairments such as tremors, muscle stiffness and slowed movement, but also mild cognitive impairment, depression, and anxiety. [11] The pathomechanisms implicated in PD include a gradual loss of dopaminergic neurons in the substantia nigra resulting in the observed motor deficits. Moreover, non-motor symptoms are attributed to neuronal dysfunction caused by an accumulation of α-synuclein across the central and peripheral nervous system. [12] Pharmacological treatments include dopaminergic and anti-cholinergic medication to alleviate motor symptoms, whereas selective serotonin reuptake inhibitors may be used for psychiatric symptoms. Additionally, some patients may benefit from deep brain stimulation. [13]

Besides certain genetic and environmental risk factors [4], older age is the strongest risk factor for both AD and PD, with the prevalence rate of dementias in Europe in the age group of 65 - 69 being 1.3% compared to 12.1% in people aged 80 - 84 years [14]. Hand in hand with the changes in population demographics due to an increasing share of older people, there has been a global increase in the number of cases of neurodegenerative diseases placing dementia at the seventh leading cause of death worldwide and even fourth when focusing on individuals above 69 [15]. To quantify the burden of disease, metrics such as disability-adjusted life years (DALYs) - a measure for the years of life lost due to a reduced quality of life caused by an illness and premature death - are used. The global DALYs caused by dementia were estimated to be 28 million [16] and the global costs constituting medical care, social care and costs for unpaid care (e.g. by relatives) amounted to 818 billion USD in 2015 [17]. Moreover, it is estimated that by 2050 the number of individuals affected by dementia globally could triple (from 57 in 2019 to 152 million) [18] and nearly double in Europe (from 9.9 million in 2018 to 18.8 million) [14]. Thus, there is an urgent need for a better understanding of disease pathogenesis of neurodegenerative disease for earlier diagnosis, development of disease-modifying treatments and policy-making due to the significant impact on both the healthcare and economic sector.

1.3 Psychiatric disorders - complex disorders with substantial disease burden

Psychiatric disorders are a complex, diverse group of illnesses, which significantly affect thinking, behaviour, perception, and emotions resulting in distress and a worsened ability to execute daily tasks. The most common psychiatric disorders are depression and anxiety disorders, with a global prevalence of 280 million and 301 million in 2019 respectively. Other important psychiatric disorders include schizophrenia (SCZ) and bipolar disorder (BPD), each affecting roughly 23.6 and 39.5 million people, respectively. Psychiatric disorders severely affect the quality of life and thus represent a substantial proportion of global disease burden, with almost 100 million DALYs attributable to the aforementioned four diseases in 2019. [19]

Twin studies have demonstrated that psychiatric disorders are highly heritable, estimating the heritability at 37% for major depressive disorders (MDD), 81% for SCZ and at 85% for BPD. [20] However, with large genome-wide association studies (GWAS) it has become evident that their genetic architecture is polygenic - with up to many thousands of different genetic loci, each with small effect size, contributing to the risk. Moreover, the pleiotropy for some of these genetic loci indicates that certain genetic factors are shared between specific psychiatric disorders. [21] Mapping of identified SCZ risk loci to genes followed by enrichment analysis revealed that implicated genes are expressed in the brain, in both excitatory and inhibitory neurons, and likely result in disrupted synaptic transmission [22]. Similarly, loci implicated in MDD [23] and BPD [24] are located in/near genes expressed in neurons and involved in neurotransmission. Besides the strong evidence of genetic risk factors for psychiatric disorders, different environmental exposures, such as childhood trauma [25], severe stress [26, 27], birth complications [28] and substance abuse [29] have also been implicated in their aetiology possibly mediated via epigenetic mechanisms.

Patients suffering from MDD present a heterogenous symptom profile such as depressed mood, anhedonia, loss of energy, poor concentration, sleep disturbances, feelings of guilt and/or worthlessness, suicidal ideation, and changes in appetite and/or weight. The pathophysiological mechanisms implicated in MDD include reduced levels within the monoamine system, e.g. noradrenaline, dopamine and serotonin, dysfunction in glutamatergic and GABAergic neurotransmitter systems, and dysfunction in neuroendocrine systems including the hypothalamic-pituitary-adrenal (HPA) axis, however remain overall still poorly understood. [30, 31] Antidepressants are one possible treatment option for MDD and range from selective serotonin reuptake inhibitors, and serotonin-noradrenaline reuptake inhibitors to other compounds such as bupropion and ketamine, whose exact mechanisms of action are not known. Other treatments, with proven efficacy, include cognitive-behavioural therapy (CBT) and electroconvulsive therapy (ECT) [30].

The clinical presentation of SCZ includes hallucinations and delusions (positive symptoms), social isolation, diminished motivation, emotional blunting (negative symptoms), abnormal mood and cognitive impairments. The pathophysiology of SCZ is (partly) characterized by several abnormalities in neurotransmission such as dopaminergic, glutamatergic, and γ-aminobutyric acid (GABA)-ergic signalling, ultimately resulting in imbalances between

excitatory and inhibitory neurons. Classical antipsychotic medications block the dopamine D2 receptor, which efficiently reduces positive symptoms such as hallucinations, however, barely impact other symptom domains strongly suggesting that these are caused by different pathophysiological mechanisms. [32, 33] Other treatment options, e.g. CBT, have been shown to improve both positive and negative symptoms [34-36].

BPD is defined by unusual changes in a person's mood. It consists of two phases: the manic and depressive phase. The manic phase is characterized by feeling elated, agitated, full of energy, being delusional and having illogical thoughts whereas the depressive phase is characterized by feelings of sadness, hopelessness, guilt, self-doubt, anhedonia, lack of energy and sleep disturbances. The pathomechanisms hypothesized to be involved in BPD include a destabilization of neurotransmitter signalling (mainly dopamine and serotonin) related to inflammatory processes in the white matter which ultimately result in periodic reshaping of brain network activities causing manic and depressive episodes [37]. Treatment options include medication, such as mood stabilizers, antipsychotics, antidepressants, or combinations thereof depending on the phase [38]. Additionally, psychotherapy [38] including CBT, and ECT [39, 40] have shown to be effective treatments.

Individuals suffering from severe mental disorders (BPD, MDD, SCZ) are at an increased risk for cardiovascular disease [41], neurodegenerative disorders [42] and premature mortality [43], which means dying on average 10 - 20 years earlier compared to the general population [44]. Moreover, several studies suggest that psychiatric disease is associated with faster (accelerated) biological ageing. These studies used different proxies to assess biological age including sensory, motor and cognitive function [45], DNA methylation in blood [46-48] as well as gene expression [49] and MRI in brain [50].

Although a variety of different treatments and therapies are available, our understanding of the disease pathologies is incomplete, evidenced by relapse and even treatment resistance. Given the increase in the prevalence of psychiatric disorders [51] - mainly due to demographic changes -, with a specific increase especially in depression and anxiety disorder during the COVID-19 pandemic [52], and the chronic nature of these disorders, it is critical to further our insights in the involved pathophysiological mechanisms in search for novel, more effective, and more targeted treatments including preventative measures. In this regard, it is also highly relevant to deepen our insights into the ageing process both under healthy and pathological conditions.

1.4 Interconnection between neurodegenerative and psychiatric disorders

Epidemiological comorbidity has been reported for neurodegenerative and psychiatric disorders, and recent studies have indicated genetic correlation between them. However, our understanding of the underlying, shared pathophysiology is still limited. One of the largest longitudinal studies, conducted in New Zealand with more than 1.7 million participants over a period of 30 years, found that having a mental disorder increases the risk (relative risk of >4) of subsequently developing dementia [42]. Moreover, on average the onset of dementia was 5.6 years earlier compared to individuals without a history of mental disorder [42].

Psychiatric symptoms such as depression and psychosis are commonly observed in neurodegenerative disorders, including AD and PD [53-55]. In fact, there is a significantly increased risk for depression in individuals suffering from AD compared to individuals without dementia with prevalence estimates of up to 16% in dementia [56]. This increased risk is at least partly explained by genetic heritability due to an increased familial liability for depression [57, 58]. Familial studies as well as GWAS have also demonstrated a clear genetic component of psychosis seen in AD [54]. Both depression and psychosis have been associated with accelerated worsening of cognitive impairment in AD [59].

The prevalence of depression in PD is estimated to be up to 35% and represents one of the most frequent non-motor symptoms [60] besides psychosis, present in up to 40% of individuals suffering from PD [61]. While pharmacological treatment including anti-cholinergic and dopaminergic medication has been linked to an increased psychosis risk, other intrinsic patient characteristics, amongst others severity of disease, depression, and poorer eyesight, have also been associated with risk for psychosis. [62] Depression and psychosis in PD patients are associated with an increased disease burden as indicated by an overall worsening of quality of life, and an elevated risk of hospitalization and mortality [63].

Recently, a shared genetic aetiology between SCZ and PD was shown [64]. Moreover, a study by Wingo and colleagues [65] examined genetic correlations between neurodegenerative and psychiatric disorders and found positive genetic correlations between AD and multiple psychiatric disorders, including MDD and BPD, providing evidence for shared underlying genetic architecture. Further, the integration of GWAS results with transcriptomic and proteomic data from human brain led to the identification of several shared proteins between neurodegenerative and psychiatric disorders with causal roles for disease. Sadeghi et al. [66] performed a meta-analysis of RNA-sequencing datasets of post-mortem brain samples from several neurodegenerative and psychiatric disorders and found several common dysregulated genes. Co-expression network analysis implicated neuronal dysfunction, impaired mitochondrial function as well as astrocyte and oligodendrocyte activation as shared alterations across the disorders, consistent with mechanisms identified by Wingo et al. [65].

Despite these efforts, exact mechanistic insights are limited. Given the rising incidence of neurodegenerative and psychiatric disorders, identification of shared pathophysiological mechanisms is crucial and could open new avenues for the development of therapeutics suitable across disorders.

1.5 The diverse cell types in the neocortex and their functions

The neocortex, which together with the allocortex forms the cerebral cortex, is involved in higher cognitive functions including consciousness, perception, attention, as well as working memory and motor control [67]. It is one of the majorly affected regions in psychiatric disorders but also neurodegenerative disorders. Its complex functions are accomplished by the interplay of its diverse neuronal and glial cell types. **Figure 1.2** summarizes the most important roles of the different cell types.

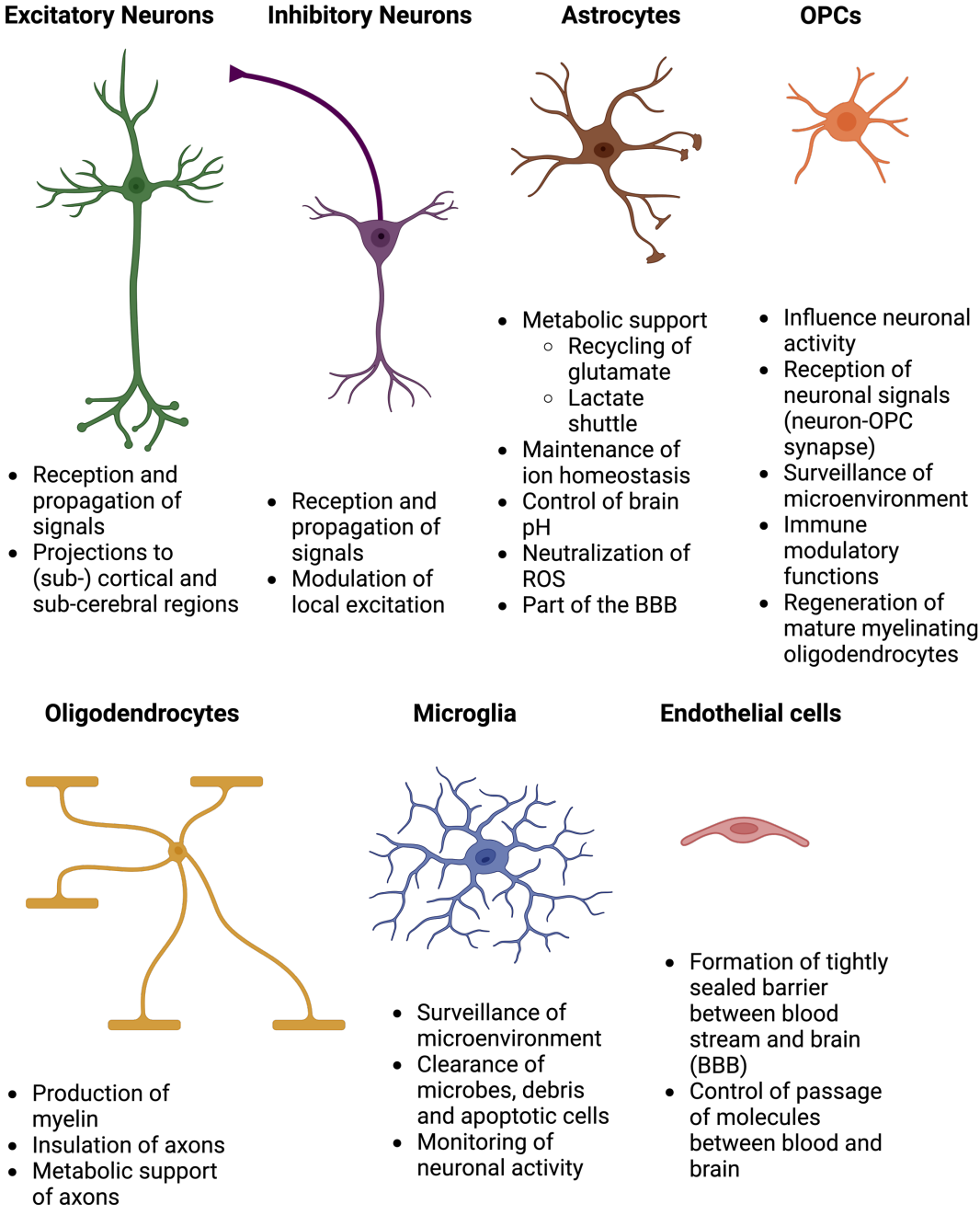

Figure 1.2: The diverse cell types in the brain and their functions. The broad cell type classes (astrocytes, endothelial cells, excitatory neurons, inhibitory neurons, microglia, oligodendrocytes, and oligodendrocyte precursors) and their main functions are displayed. Figure was created with BioRender.com.

The cytoarchitecture of the neocortex is characterized by a six-layer structure. There a two main types of cortical neurons: glutamatergic projections neurons (also referred to as excitatory neurons) and GABA-ergic interneurons (also referred to as inhibitory neurons), which are named after the neurotransmitter they release; glutamate and GABA respectively. The vast majority of cortical neurons are excitatory neurons [68], which are characterized by their long axons projecting to (sub-) cortical and even sub-cerebral regions, whereas inhibitory neurons make local connections [69]. Neurons communicate by means of electrochemical signals. Dendrites receive chemical signals, in the form of neurotransmitters, from neighbouring neurons and deliver the signal to the soma. The axon propagates the signal in the form of action potentials to the presynaptic terminals thereby enabling communication between neurons.

Different classes of excitatory neurons vary in morphology, connectivity, electrophysiology, and gene expression. On the one hand, they can be classified based on their laminar location (layer (L) 2 (L2) to layer 6 (L6)) and on the other hand, by their projection targets for both of which specific gene expression patterns have been identified [69-72]. Excitatory neurons with commissural projections are predominantly located in L2/3, L5 and L6, have ipsilateral projections to the cortex as well as the striatum and connect the two brain hemispheres by contralateral projections. Corticothalamic neurons and sub-cerebral projection neurons are classified as corticofugal. Corticothalamic neurons, primarily found in L6 and partially in L5, send projections to the thalamus, whereas sub-cerebral projection neurons, mainly localized to the deep L5, project to the brainstem and spinal cord. [69] However, studies profiling the single cell transcriptomes indicate that the diversity of excitatory neuron subtypes goes beyond these broad subclasses with more than 50 different excitatory neuron subtypes identified in the mouse neocortex [73, 74].

Inhibitory neurons also comprise a diverse group of cells with differences in developmental origin, morphology, connectivity, electrophysiology, and gene expression patterns enabling a dynamic modulation of local excitation of neighbouring neurons [75-77]. Studies focusing on electrophysiological and/or morphological characteristics identified 15 different inhibitory neuron subtypes in mouse visual cortex [78] and 10 in rat somatosensory cortex [79]. However, subclassification based on differences in single cell transcriptomes resulted in a strikingly higher number of subtypes ranging from more than 20 [73] in the visual cortex to more than 60 different interneuron subtypes within the whole mouse neocortex [74]. Though, given the fact that there is no standardized choice for the resolution parameters used in clustering algorithms of single cell expression data, it remains to be shown that these identified clusters represent true biological subtypes or simply mathematically defined groups [76]. One of the currently proposed models aims to provide an explanation for the great interneuron diversity: Once interneuron progenitors have become postmitotic four cardinal interneuron cell classes exist [77, 80]. These are characterized by the expression of LAMP5 (lysosomal-associated membrane protein family member 5), PVALB (parvalbumin), SST (somatostatin), and VIP (vasoactive intestinal peptide) and by the (excitatory) neuron compartment they target. PVALB interneurons target the soma and adjacent dendrites, whereas SST interneurons target (apical) dendrites, and VIP interneurons synapse on other interneurons, predominantly SST interneurons [77]. Further subtype specification of the four cardinal classes via extrinsic cues occurs during their migration and once an interneuron has

reached its final position. What is more, dynamic changes in gene expression upon local brain activity allow further adaptation to state-specific demands. [77]

Glial cells, including astrocytes, oligodendrocyte precursor cells (OPCs), oligodendrocytes and microglia, were originally proposed to simply represent the 'glue' of the brain passively supporting neuronal functions. This view has drastically changed since specific vital functions for each of the glial cells have been identified. Among the glial cell types, astrocytes are the most abundant and comprise two main subtypes: fibrous and protoplasmic [81]. Fibrous astrocytes are mainly located along white matter tracts and are structurally characterized by straight, less branched processes. Instead, protoplasmic astrocytes are predominantly found in the grey matter and are highly branched with many fine processes. They are spatially organized in non-overlapping domains resulting in areas of up to two million synapses that are under the control of one single astrocyte [82]. Astrocytes have various functional roles, some of which are better understood and characterized than others. One of their best-characterized properties is the uptake and recycling of the neurotransmitter glutamate to glutamine via enzymatic conversion, which is then released and taken up by neurons to be converted back to glutamate. The lactate shuttle hypothesis proposes another metabolic cycle between astrocytes and neurons: Glucose enters the brain from the bloodstream via glucose transporters in the end-feet of perivascular astrocytes and is converted to lactate, which is released and taken up by neurons and used as energy source. However, since neurons themselves express glucose transporters, it is likely that several different pathways contribute to meet the high metabolic demands of neurons. [83] Astrocytes are also responsible for the maintenance of the extracellular ion homeostasis, especially after neuronal firing increases the extracellular potassium concentrations. Moreover, they are also involved in the control of brain pH, water transport as well as neutralization of reactive oxygen species (ROS). Since astrocytic processes are not only in contact with synapses but also surround blood vessels, as mentioned before, they also play an important role in the regulation of cerebral blood flood. [83, 84]

Oligodendrocyte precursor cells (OPCs), also referred to as NG2+ glia, have a round cell body with highly branched processes and are uniformly distributed within both white and grey matter. Analogous to astrocytes, OPCs in the superficial layers of the cortex are organized in non-overlapping spatial domains [85]. Throughout the last decades, it has become evident that these highly proliferative cells do not only simply regenerate mature myelinating oligodendrocytes but also have other crucial roles in brain function. For example, OPCs have been shown to produce factors such as fibroblast growth factor 2, neuronal pentraxin 2, and prostaglandin D2 known to influence neuronal activity. In addition, OPCs express both AMPA (α-amino-3-hydroxy-5-methyl-4-isoxazolepropionic acid) and GABA receptors enabling them to receive neuronal signals and thus forming the so-called neuron-OPC synapse, whose exact functional role remains to be elucidated. Using their filopodia, OPCs constantly survey their microenvironment responding to neuronal activity, injury, and inflammatory cues. Interestingly, OPCs could themselves have immune-modulatory functions given that they express cytokine receptors, respond to chemokines, and can produce inflammatory modulators. [86] In-vitro, OPCs also have been shown to be able to present antigens after exposure to interferon-γ [87].

Oligodendrocytes are the myelin-producing cells of the brain that insulate axons with several layers of cell membrane to allow for rapid saltatory conduction of action potentials. Along an axon, stretches of myelin are interspaced with unmyelinated areas, so-called nodes of Ranvier, areas with a high density of sodium (Na^+) channels where ion exchange and thus action potentials occur and are propagated [88]. Oligodendrocytes are predominantly found in white matter where their thin processes are in contact with the myelin sheaths, but are also found in grey matter, located peri-neuronally in close association with the soma of neurons. A single oligodendrocyte myelinates numerous axons. The multi-layered myelin sheaths are tightly sealed in order to prevent leakage of ions; however, this also isolates the axons from the extracellular space and its vital metabolites. Astrocytes can provide metabolic support via contacts with neurons at the neuronal soma, synapses, or nodes, however, the long stretches of myelin-covered axons need to receive trophic support via different means. This is achieved by the metabolic coupling of the axon with the soma of the oligodendrocyte via cytoplasmic channels within the myelin sheaths. Similarly to astrocytes, oligodendrocytes may support increased metabolic demands of axons by the export of lactate via their monocarboxylate transporters in response to axonal glutamate release sensed by their N-methyl-D-aspartate (NMDA) receptors. Alternatively, gap junctions between oligodendrocytes which allow the passage of small, polar molecules, such as amino acids and sugars, could provide another route for metabolic support. [89]

Microglia, the innate immune cells of the brain, form part of the glial cell population, although they are derived from myeloid progenitors in the yolk sac [90] in contrast to all other glial cells that originate from the ectodermal lineage [91]. Microglia have a highly dynamic morphology: In their ‘surveillance’ state, they present themselves as highly ramified cells with numerous processes, which are constantly extended and retracted to sense the extracellular space. Microglia express several pattern recognition receptors enabling them to detect secreted molecules of pathogens or damaged neurons or other glial cells. Once activated, they retract processes and transform to an amoeboid shape. Clearance of microbes, debris and apoptotic cells is enabled by the large number of receptors necessary for phagocytosis and endocytosis. Moreover, migration (to injury sites) and localization of microglia are controlled by their chemokine receptors and integrins, which additionally support the phagocytic process by strengthening the binding to target cells. The magnitude and length of immune activation are regulated by their immune receptors. Microglia cooperate with astrocytes for some of their functions: After an injury, the release of adenosine triphosphate (ATP) by astrocytes helps to direct microglial processes to the injury site and the release of GABA can reduce microglial activation. Astrocytes also secrete milk fat globule protein epidermal growth factor 8, which binds apoptotic cells and thereby tags them for microglial phagocytosis. Microglia also have receptors for neurotransmitters, including AMPA, NDMA, glutamate metabotropic receptor 2 (MGLUR2) and GABA receptors, which they use to monitor neuronal activity to detect damaged neurons. At the same time, these receptors influence the release of inflammatory cytokines, e.g. AMPA inhibits whereas MGLUR2 promotes the release of tumour necrosis factor (TNF)-α. Additionally, microglia eliminate dendritic spines that do not form synaptic contacts via phagocytosis thereby impacting synapse strength and synaptic plasticity. Moreover, prevention of excitotoxicity, caused by the excess release of

neurotransmitters, is accomplished by wrapping of microglia around swollen axons, which results in membrane repolarization. [92]

Brain endothelial cells (ECs), i.e. cells of mesenchymal origin, are flat cells forming a monolayer that lines blood vessels within the brain. Within this monolayer, ECs are connected via tight, adherens and gap junctions resulting in a tightly sealed barrier that limits passive diffusion from the bloodstream into the brain. The expression of specific efflux and influx transporters strictly controls the passage of molecules while at the same time allowing passive diffusion of oxygen from the bloodstream into the brain and of carbon dioxide diffusion out of the brain. Additionally, some small lipophilic molecules can pass whereas the uptake of glucose and amino acids is carrier-mediated and the passage of larger molecules such as leptin and insulin is enabled by receptor-meditated endocytosis. Several enzymes that metabolize drugs represent an additional, metabolic barrier. Therefore, brain ECs represent a central component of the blood brain barrier (BBB), the interface between the brain and the blood circulatory system, which helps maintain brain homeostasis by controlling metabolic support and protecting against toxins both from endogenous and xenobiotic origin. [93, 94] Other cells, which form part of the BBB include pericytes and astrocytes. Pericytes enwrap ECs, are surrounded by extracellular matrix and in contact with astrocytic end-feet. Pericytes control the proliferation of ECs and together with astrocytes and OPCs help establish the junctions between ECs necessary for BBB formation, maintenance, and integrity. [86, 95, 96]

The accurate function and interplay between all different cell types is crucial for the brain's capability to achieve the complex computations involved in cognitive as well as motor functions, and ultimately behaviour. It is essential to understand how these diverse cell types and their interactions are affected during ageing and by different brain diseases including neurodegenerative and psychiatric disorder.

1.6 Effects of ageing on the brain

Ageing is accompanied by a reduction in cognitive performance, and we are only beginning to understand the underlying mechanisms. Interestingly, not all domains of cognitive function are equally affected by the ageing process: Functions including the encoding of new memories, processing speed, and working memory have been reported to linearly decline throughout adult life, whereas short-term memory and semantic knowledge seem to only decrease late in life (after the age of 70). Moreover, autobiographical knowledge, implicit memory and emotional processing remain stable across life. [97]

The strongest macroscopic changes during ageing occur in the prefrontal cortex (PFC), which shows volumetric declines both in grey and white matter. The striatum, a region with strong functional connections to the PFC, also declines with age, whereas the hippocampus exhibits only minor structural changes. Interestingly, regions like the hippocampus and the entorhinal cortex are the areas to be first affected in neurodegenerative disorders such as AD. This led to the proposal of a two-component model of ageing with on the one hand, gradual age-related volumetric loss in the fronto-striatal systems even in the absence of disease and on the other hand, volumetric loss in the hippocampus and entorhinal cortex primarily associated with pathologies like AD. On the functional level, several studies have demonstrated an overall reduced PFC activity with age when performing executive tasks and occasionally (depending on the task) an activation of specific PFC subregions that are not activated in younger individuals, which has been suggested to represent a compensatory mechanism. [97] Furthermore, a study by Andrews-Hanna and colleagues found that the coordinated activation of the default mode network - which includes regions in the prefrontal and temporal cortex - is reduced with age, which is associated with poorer cognitive performance [98]. Even though the hippocampus only shows minor structural changes, activity in the left hippocampus related to memory decreases with age. Similarly, the amygdala gets less activated in response to negative stimuli with age with only minimal structural changes. Changes in the activity of these brain regions could additionally affect connected regions such as the PFC contributing to an overall less integrated activation at the circuit level. [97]

On the microscopic level, it has been shown that there is only modest neuronal loss during ageing, however a striking change in morphological features: These include a reduction in dendritic arborizations as well as spine number and density. [97, 99, 100] A progressive loss of synapses from 16 to 98 years of age in non-demented individuals in the frontal cortex was shown by Masliah et al. [101]. Nevertheless, studies that followed only found a non-significant decrease in synapse number [102] or no reduction at all [103, 104], suggesting that synaptic loss may not be part of healthy human ageing at least not in the frontal cortex. Volumetric changes observed in white matter are further linked to the loss of myelin during ageing. On the one hand, some axons show reduced myelin sheath thickness because of incomplete re-myelination while others are completely lost. To counteract, there is a constitutive myelination activation, which however also leads to the increase in myelin sheath thickness of some axons. Reduced myelin negatively affects the conduction velocity, which together with the changes in synaptic connectivity could explain the alterations seen at the circuit level. [97, 99] Accumulation of Aβ and NFTs, besides being a hallmark of AD, is also observed in brains

of older cognitively healthy individuals. However, in normal ageing Aβ accumulation is primarily diffuse compared to dense deposits in AD. [99] Lipofuscin, aggregates made up of lipids and peroxidased proteins, also increases with age [100]. Overall, these accumulations are indicative of disruption in cellular proteostasis and clearance mechanisms.

At the molecular level, several neurotransmitters, and hormones as well as their receptors reduce during ageing thereby affecting synaptic signalling. Mitochondria are essential for the production and storage of cellular energy through oxidative phosphorylation using the electron transport chain. Intact mitochondrial function is therefore crucial to meet the high metabolic demands of neuronal cells necessary for the regulation of ion gradients as well as transport along axons and ultimately signalling. However, with age mutations in the mitochondrial DNA accumulate, which results in an increased production of ROS. ROS, whether derived endogenously or exogenously (from e.g. UV radiation, toxins, chemicals), cause oxidative damage to lipids, proteins and nucleic acids. This can result in cross-links between biomolecules (DNA, RNA, proteins, lipids) and accumulation of aggregates or structural and functional changes of proteins. Autophagy is one of the cell's mechanisms for degrading unneeded cellular components thereby recycling and producing nutrients. Autophagy declines throughout ageing, which is partly due to the accumulation of lipofuscin which impairs autophagocytic function. [99, 100] Studies in mice [105] and worms [106] have shown that increasing autophagy increases life span, whereas reduction leads to a decreased life span and neurodegeneration [107-109]. Misfolded or damaged proteins are tagged by ubiquitin thereby labelled for proteasomal degradation. The ubiquitin-proteasome system (UPS) also plays an essential role in synaptic transmission by controlling the vesicle pool and release at the presynaptic membrane and protein abundance (such as receptors) at the post-synapse [100]. During ageing, UPS activity declines, which leads to the accumulation of ubiquitinylated proteins. Interestingly, ubiquitinylated protein aggregates are found during normal brain ageing, surpassing a pathological threshold in neurodegenerative disorders including AD and tauopathies [110]. The reduction of both autophagy and the UPS contributes to the disruption of cellular homeostasis due to the accumulation of insoluble aggregates, insufficient clearance of damaged organelles including mitochondria, and excessive ROS production. [99, 100] Calcium (Ca^{2+}) acts as a second messenger, is an indicator of cellular energy demand via the mitochondrial ATP production and is involved in the regulation of synaptic signalling and plasticity, cell survival and death. The extracellular concentration of Ca^{2+} is ~ 1 mM compared to the much lower intracellular levels of ~ 100 nM in neurons [111]. Thus, calcium homeostasis is crucial and is maintained by the regulation of voltage- and ligand-gated Ca^{2+} channels, mitochondria, the endoplasmatic reticulum (ER), and Ca^{2+} binding proteins. Yet, during ageing expression changes and modulation of the activity of Ca^{2+} channels in combination with a decrease in the Ca^{2+} buffering mechanisms in the ER and mitochondria and alterations in the levels of Ca^{2+} binding proteins lead to reduced Ca^{2+} efflux and a prolonged Ca^{2+} concentration increase in the cytoplasm. This can lead to the breakdown of membranes and organelles, increased production of ROS and the activation of cell death pathways. [112]

These altered processes are also reflected by changes in the transcriptome. Examination of the brain transcriptome across different species including worms, flies, mice, rats, and (non-) human primates revealed conserved gene expression changes with age. Reduced

mitochondrial function is amongst the conserved pathways. It has been causally linked to ageing with studies in worms and mice showing that a reduced function shortens whereas an increased function prolongs life span. [110] Another common affected pathway is the stress response, which increases with age. Yet, a study by Loerch et al. [113] comparing age-related gene expression changes in the cortex of mice, rhesus macaque and humans showed that only a fraction of age-regulated genes were shared across species. Moreover, they found an evolutionary shift in age-related gene expression regulation between mice, which upregulated the majority of the genes, and primates (macaques and humans), which downregulated most of the age-regulated genes. Recent studies in mice [114] and rhesus macaque [115] have begun to look at the effect of ageing on the different cell types in the brain revealing an additional layer of complexity. These studies indicate that gene expression changes are not uniform across cell types, but rather distinct gene expression changes occur in the diverse cell types. In addition, studies in commonly used model organisms such as mice and rats have shown that these species do not naturally develop Aβ deposits, whereas studies in non-human primates have shown accumulation of Aβ but rarely NFTs with age [116, 117]. Since current research suggests a progression from Aβ to tau accumulation subsequently affecting cognition and causing neurodegeneration [118, 119], it is not clear if these Aβ deposits (alone) represent AD(-like) pathology that is accompanied by neuronal loss seen in AD and PD in humans. These findings highlight the importance of studying normal ageing and age-associated pathologies in the human brain specifically besides the use of a variety of animal models.

1.7 Transcriptomic profiling of the brain

1.7.1 Bulk vs single cell transcriptomic profiling

Since more than two decades, next-generation sequencing (NGS) approaches have been used to examine the transcriptomes across different organs, in diverse species and under different experimental and pathological conditions, including neurodegenerative and psychiatric disorders. These helped advance mechanistic insights across scientific fields. However, most of these studies performed so-called bulk RNA-sequencing, profiling tissue homogenates, thereby obtaining gene expression values averaged across multiple cell types comprising the tissue. Besides not being able to assign observed gene expression changes to specific cell types, transcriptomic changes can also be diluted out when they are subtle and only present in a specific cell type and gene expression levels get averaged across all cell types. Single cell sequencing (sc-seq) refers to techniques that can measure the DNA or RNA content of individual cells of a sample enabling the examination of cell-type-specific changes and cellular heterogeneity. [120] **Figure 1.3** provides a schematic comparison between bulk and sc-RNA-seq.

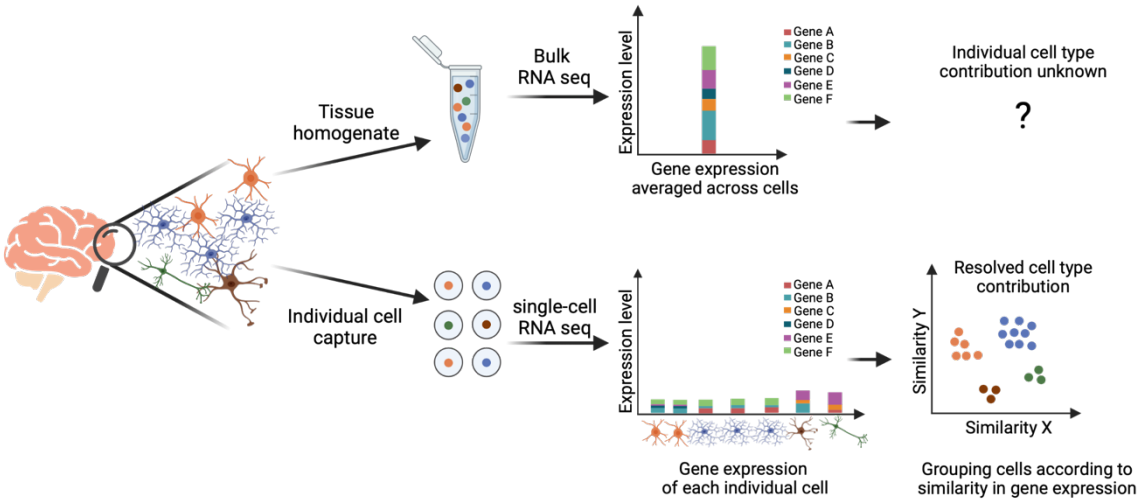

Figure 1.3: Comparison of bulk RNA seq with single cell RNA seq. The brain consists of a variety of different cell types. When performing bulk RNA seq the tissue is homogenised, and RNA is extracted and sequenced representing a mixture of transcripts from these different cell types. However, using single cell RNA seq methodologies, the individual cells can be captured and transcripts attributable to each cell can be quantified. Clustering of cells based on similarity in gene expression allows for assignment of cell-type labels and cell-type specific analysis. Figure was created with BioRender.com and modified from [121].

The first sc-RNA-seq study coupled to NGS was performed in 2009 by Tang et al. examining the whole transcriptome of a mouse blastomere [122]. Since then, different approaches for single cell isolation have been applied, amongst others fluorescence-activated cell sorting, plate-based and microdroplet-based microfluidics, resulting in different numbers of cells to be profiled ranging from low (several hundreds of cells) to high (several thousands of cells) throughput. Moreover, certain sc-RNA-seq methodologies are biased towards either the 3’

or 5' end of the transcripts whereas others examine the full-length transcript, which additionally allows for splicing analysis. [120, 123] One highly used commercial platform is the Chromium system (10x Genomics) which uses a microdroplet-based microfluidic approach to partition cells into microdroplets, so-called gel bead in emulsions (GEMs), forming a separate reaction compartment for each individual cell. Next, the cells are lysed, and RNA fragments are captured using barcoded complementary oligos. This is followed by a reverse transcription reaction, ligation of adaptors and amplification. After sequencing, the transcripts can be traced back to the cells they originated from owing to the barcode within the GEMs. Using clustering algorithms cells with similar transcriptomes are grouped together, and cell types can be assigned to these clusters based on the expression of known cell-type specific genes. [120]

1.7.2 Single cell sequencing of the human brain

One initial drawback of sc-seq methods was the requirement of intact single cells, which hindered the profiling of solid tissues and especially frozen archived tissue, such as post-mortem brain. However, the possibility to isolate intact nuclei from frozen tissue and their applicability for single nucleus RNA-seq (sn-RNA-seq) was soon demonstrated [124-126]. This permitted the examination of cell-type-specific alterations in brain disorders such as psychiatric and neurodegenerative diseases using post-mortem brain samples, as exemplified by the following studies: In autism-spectrum disorder, excitatory neurons from L2/3 and L4 as well as microglia were identified as the most severely affected [127]. A study performing sn-RNA-seq in the dorsolateral prefrontal cortex of neurotypical individuals and individuals having suffered from major depression found the strongest transcriptomic changes in deep-layer excitatory neurons and OPCs [128]. Two sn-RNA-seq studies implicated neuronal cell types in the pathophysiology of SCZ, with significant contributions from PVALB interneurons and deep-layer neurons [129, 130]. Additionally, it was shown that dysregulated genes were enriched for genes mapped to SCZ risk loci from GWAS [129, 130]. Furthermore, Smajic et al. identified a specific dysfunctional dopaminergic neuron cluster in midbrain of PD patients as well as a decrease in oligodendrocyte number, an increase in the microglia population and their activation [131]. Moreover, several studies have profiled samples of the prefrontal cortex of subjects with and without AD, implicating oligodendrocytes, and disruption of myelination as core features of AD pathology [132, 133]. Additionally, shifts in the proportions of cell subtypes, including astrocytes, were identified [132, 133].

Although these studies have advanced our understanding of brain pathologies, we have limited knowledge of the normal ageing process at the cell-type level. Since age represents the strongest risk factor for neurodegenerative disorders and accelerated ageing has been described in individuals suffering from psychiatric disorders, it is essential to deepen our insights on gradual changes that occur during normal ageing. First studies focusing on normal ageing at cell-type resolution have been performed in model organisms such as mice [114] and rhesus macaque [115] but are however still lacking in humans.

2 | Rationale and Objectives

Ageing is a continuous process that affects the level of cells, organs, and the whole organism. The brain accomplishes complex functions which are brought about by the interplay of its highly specialized neuronal and glial cells. However, some of its functions decline throughout ageing. In addition to various age-related changes in the brain being conserved across species, as outlined in the introduction, certain aspects of ageing are primate or even human-specific [110]. Our current knowledge of ageing is limited since most studies (in humans) have studied ageing with a focus on neurodegeneration (by comparing individuals with and without neurodegenerative disease) but have hardly looked at ageing as a continuous process [99]. We therefore have little insight into the individual cell type contribution to ageing in the brain and whether all cells are equally vulnerable to the ageing process. Moreover, it is not clear whether genes changing their expression throughout ageing play a role in neurodegenerative disorders and could thus potentially help us explain why age is such a strong risk factor for their development. Furthermore, several studies have indicated that psychiatric disorders are associated with accelerated biological ageing, but whether this is seen across all cell types in the brain, which genes could be driving this process and how much of it is attributable to heritable genetic factors remains to be elucidated.

The aim of this thesis was to better characterize the transcriptomic changes associated with the ageing process across individual cell types in the human brain and to understand how these are related to neurodegenerative and psychiatric disorders. In order to do so, post-mortem brain samples from a cohort of neurotypical individuals and individuals having suffered from psychiatric disease spanning an age range from 26 to 84 years of age were used. Samples from the orbitofrontal cortex were chosen due to its involvement in cognitive function [134], structural and functional decline during ageing [135], and its implication in the pathophysiology of several psychiatric disorders [136, 137]. Using single nucleus RNA seq, the transcriptomes of several thousand nuclei per individual were profiled to understand the individual cell-type specific changes across ageing. Additionally, individuals were genotyped, and bulk DNA methylation was profiled to address the following questions:

<u>sn-RNA-seq:</u>

1) Which genes linearly change their expression along ageing and in which cell types?
2) Which molecular pathways and cellular functions are affected by these gene expression changes in the affected cell types?
3) Have these genes been implicated in the disease pathogenesis of neurodegenerative disorders, focusing on Alzheimer's disease?

<u>sn-RNA-seq, DNA methylation measurement, genotyping:</u>

4) Do we find evidence of biological age acceleration at the epigenetic and transcriptomic level in individuals suffering from psychiatric disease?
5) Are linear age-related gene expression changes shifted when suffering from a psychiatric disease and if so in which cell types and how much is driven by genetic factors?

3 | Material and Methods

3.1 Description of post-mortem brain cohort

Ethical approval for this study was obtained by the Ludwig Maximilians-Universität Munich (22-0523) and the Human Research Ethics Committees at the University of Wollongong (HE2018/351). Brain samples (from the orbitofrontal cortex) were obtained from 87 individuals from the NSW Brain Tissue Resource Centre in Sydney, Australia. Donors or their next of kin provided written informed consent for brain autopsy. For this study, donors were classified as either controls based on the absence of any psychiatric diagnosis, or as cases, who had been diagnosed with one of the following psychiatric disorders (schizophrenia (SCZ), schizoaffective disorder (SZA), bipolar disorder (BPD) or major depressive disorder (MDD)). All included brains were neuropathologically examined to determine Braak stage. Out of all donors, only one individual (case) showed macro- and microscopic changes (Braak NFT stage III), but not in cortical areas. None of the brain donors had been diagnosed with a neurodegenerative disorder. **Table 3.1** summarises cohort characteristics (mean ± SEM) including age, biological sex, diagnosis, post-mortem interval (PMI), brain pH, and RNA-integrity number (RIN). Cases and controls did not differ in any of these parameters.

Table 3.1: Cohort Description

	Controls (n=33)	Cases (n=54)
Age [years]	57.15 ± 2.18	53.44 ± 1.86
Sex	13 F | 20 M	19 F | 35 M
Psychiatric diagnosis	0	BPD (5), MDD (6), SZA (7), SCZ (36)
PMI [h]	30.91 ± 1.91	34.54 ± 2.26
pH	6.68 ± 0.04	6.58 ± 0.03
RIN	7.20 ± 0.24	7.36 ± 0.15

Figure 3.1 displays an overview of the cohort showing the distribution of individuals along age coloured for cases and controls (**Figure 3.1a**) and for females and males (**Figure 3.1b**).

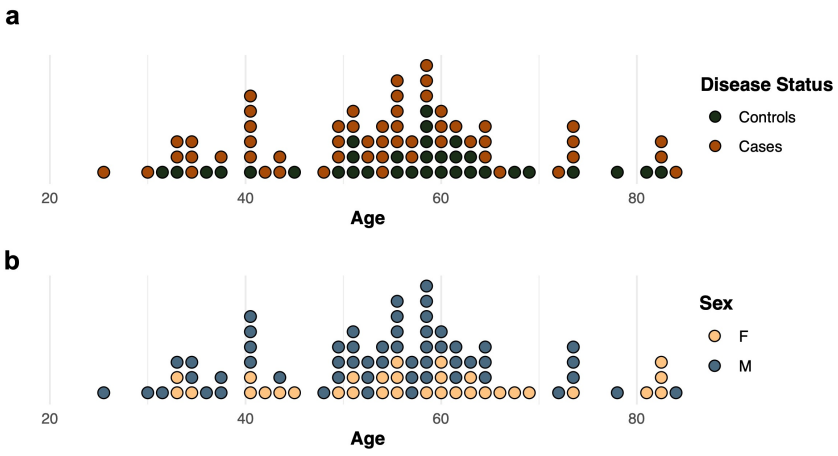

Figure 3.1: Age distribution of post-mortem brain cohort. **a-b**, Age distribution of controls (green) and cases (orange) (**a**) and females (F; yellow) and males (M; blue) (**b**) used in this study. Each dot represents one individual.

Tissue dissection from fresh-frozen post-mortem tissues of the orbitofrontal cortex (BA11) was performed by the NSW Brain Tissue Resource Centre in Sydney, Australia. Tissue was used for single nucleus RNA sequencing (sn-RNA-seq), and DNA extraction for genotyping as well as DNA methylation measurement.

3.2 Nuclei Extraction & single nucleus RNA library preparation

Figure 3.2 shows a schematic overview of the nuclei extraction and sn-RNA-seq procedure.

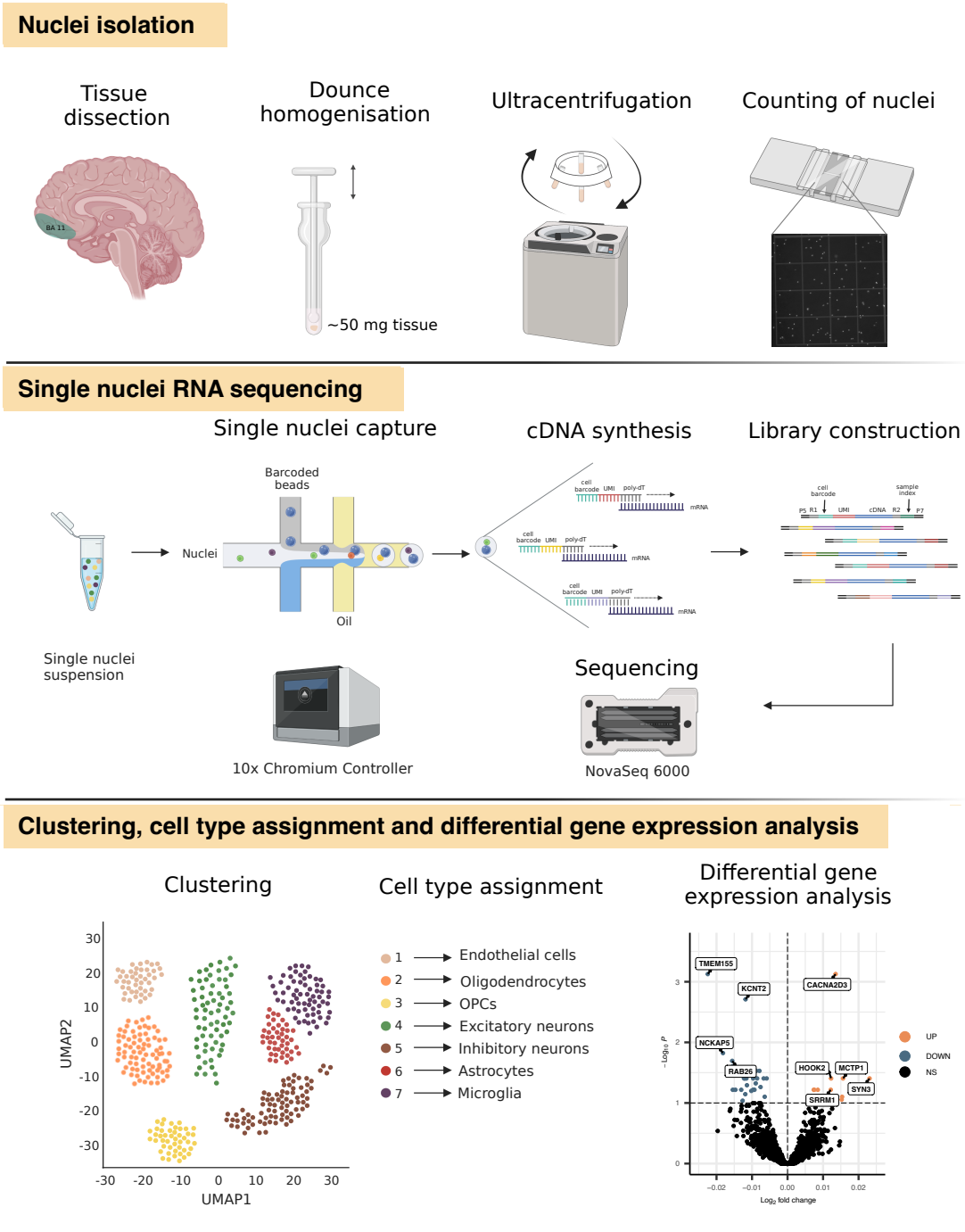

Figure 3.2: Schematic overview of single nucleus RNA-sequencing procedure. Dissected brain tissue was dounce-homogenized and ultracentrifuged to obtain nuclei. Individual nuclei were captured into GEMs using the 10x Genomics microfluidics device. Each of the beads is covered with an oligonucleotide sequence consisting of a cell barcode (unique for each GEM), unique UMIs for transcript quantification and a poly-T stretch to hybridize with the mRNA's poly-A-tail necessary for cDNA synthesis. cDNA synthesis is followed by library construction adding the required P5 and P7 oligonucleotide sequences enabling hybridization and bridge amplification on the Illumina flow cell. Read 1 (R1) and Read 2 (R2) sequences are required for the annealing of sequencing primers to read the cell barcode and UMI as well as the sample index and cDNA while sequencing. After sequencing on the Illumina NovaSeq 6000 and alignment, cells are clustered based on similarity in their gene expression. These separate groups of cells can then be assigned a cell type label based on the expression of cell-type specific (known) marker genes. Finally, differential gene expression analysis for each cluster/cell type can be performed. Figure was created using Biorender.com and modified from [138, 139].

3.2.1 Randomisation

For a balanced experimental design not confounded by the variables of interest, samples were divided into 16 batches using OSAT [140] randomised for age, sex, and disease status for nuclei extraction and subsequent sn-RNA-seq library preparation.

3.2.2 Nuclei Extraction

From the frozen tissue pieces, 50 - 60 mg were cut using a sterile scalpel on dry ice, transferred to a 1.5 ml Eppendorf tube and stored at -80°C until nuclei extraction. All buffers were prepared the day before the start of each batch. Nuclei extraction buffer (NEB) and sucrose cushion were prepared with autoclaved milliQ water whereas resuspension buffer was prepared with DPBS (**Table 3.2** shows the details of needed equipment as well as buffer composition). Buffers were stored at 4°C. Extraction protocol was modified from [141]: All steps were performed on ice. On the day of the experiment, IGEPAL-CA630 and RiboLock RNase-Inhibitor were added to the NEB to a final concentration of 0.1% and 40 U/ml respectively. Tissue pieces were transferred into the dounce homogenizer and 600 µl of ice-cold NEB buffer were added to each sample, followed by a 5 min incubation. Next, dounce homogenisation with the loose pestle was performed for 30 strokes followed by 15 strokes with the tight pestle. Walls of dounce-homogenizer were rinsed with 400 µl of NEB buffer. Nuclei suspension was transferred to an ultracentrifuge tube. Then, 1.8 ml sucrose cushion were added to the bottom of the ultracentrifuge tube (leaving the nuclei suspension layered on top of the sucrose cushion). For balancing of the ultracentrifuge, tubes were weighed and if necessary, weight adjustments were performed by adding a corresponding volume of NEB buffer on top. Samples were ultra-centrifuged at 28,100 rpm, 4°C for 2 h 30 min. RiboLock RNase-Inhibitor (to a final concentration 40 U/ml) and DAPI (1:1000) were added to the resuspension buffer. Immediately after ultracentrifugation, tubes were placed on ice and supernatant was removed using vacuum suction leaving only the nuclei pellet behind. To each nuclei pellet 80 µl of resuspension buffer were added, followed by a 30 min incubation and subsequent gently resuspension of nuclei pellet. Pre-separation filters were washed with 200 µl of resuspension buffer. Next, nuclei suspension was filtered through. Filters were then

washed with 50 µl of resuspension buffer. Nuclei concentration was determined via manual counting using a C-Chip Neubauer chamber.

Table 3.2: Overview of equipment, chemicals, and buffer composition for nuclei extraction

Equipment	Manufacturer	Catalog Number
Dounce homogenizer (7ml)	neoLab	WD-1292
C-Chip Counting Chamber	NanoEnTek	NE63508-01
Pre-separation filter (20 µm)	Milteny Biotec	130-101-812
Ultracentrifuge tubes, PA Thin-Walled Tube	Thermo Scientific	3955
Ultracentrifuge	Thermo Scientific	75000100

Chemical	Manufacturer	Catalog Number
Bovine Serum Albumin Fraction V (BSA)	Carl Roth	8076.2
$CaCl_2$	Carl Roth	T8885.2
DAPI	Sigma-Aldrich	D9542-1MG
EDTA	Carl Roth	8043.2
$Mg(Ac)_2$	Sigma-Aldrich	M5661-50G
IGEPAL® CA-630	Sigma-Aldrich	I8896-50ml
PBS	Gibco	14190094
RiboLock RNase Inhibitor (40 U/µl)	Thermo Scientific	EO0381
D(+)-Saccharose (Sucrose)	Carl Roth	9097.1
TRIS (Tris-(hydroxymethyl)-amino methane)	Carl Roth	4855.1

Nuclei extraction buffer (NEB)	Sucrose Cushion	Resuspension buffer
0.32 M Sucrose	1.8 M Sucrose	1X DPBS
5 mM $CaCl_2$	3 mM $Mg(Ac)_2$	5 mM $CaCl_2$
3 mM $Mg(Ac)_2$	10 mM Tris-HCl pH 8	3 mM $Mg(Ac)_2$
0.1 mM EDTA		1 % BSA
10 mM Tris-HCl pH 8		filter with 0.22 µm filter

3.2.3 Single nucleus RNA library preparation

Using the Chromium Single Cell 3' Reagents kit v3.1 (10x Genomics) sn-RNA-seq libraries were prepared according to the manufacturer's instructions (10x Genomics user guide). **Table 3.3** provides an overview of necessary chemicals and equipment. As target recovery per sample 10,000 nuclei were chosen. **Figure 3.3** shows representative traces of the Bioanalyzer Chip after cDNA synthesis and of a completed library. Libraries were stored at -20°C until completion of all libraries (two batches per week were processed). Libraries were pooled equimolarly, followed by treatment with the Illumina Free Adapter Blocking Reagent. Library pools were sent for sequencing to the Core Facility Genomics at Helmholtz Munich and sequenced in two batches on the NovaSeq 6000 System (Illumina, San Diego, California, USA).

Table 3.3: Overview of equipment, chemicals for single nucleus RNA seq

Chemical/Equipment/Kit	Manufacturer	Catalog Number
Chromium Controller	10x Genomics	PN-120270
Chromium Next GEM Single Cell 3' GEM, Library & Gel Bead Kit v3.1	10x Genomics	PN-1000121
Chromium Next GEM Chip G Single Cell Kit	10x Genomics	PN-1000120
Single Index Kit T Set A, 96 rxns	10x Genomics	PN-1000213
Low TE buffer (100 ml)	G-Biosciences	786-150
Illumina Free Adapter Blocking Reagent	Illumina	20024145
10% Tween-20	Sigma Aldrich	11332465001
Agilent High Sensitivity DNA Kit	Agilent	5067-4626
AMPure beads XP	Beckman Coulter	A63881
Qiagen EB buffer	Qiagen	19086

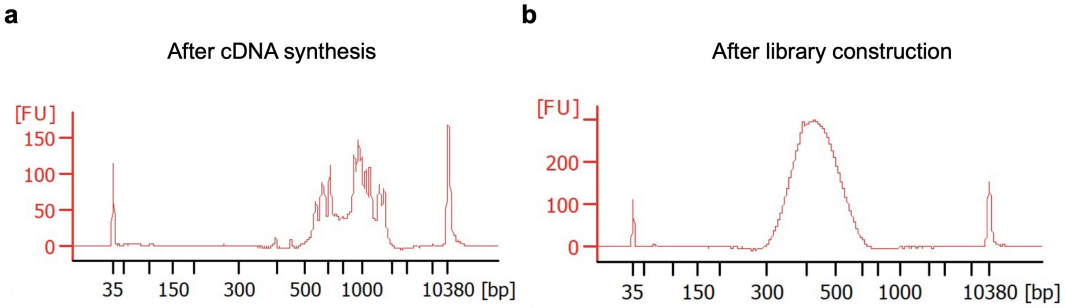

Figure 3.3: Library construction quality control. a-b: Representative Bioanalyzer traces during sn-RNA-seq library preparation; after cDNA synthesis (**a**) and after completion of library construction (**b**).

3.3 Pre-processing - sequence alignment, filtering, and normalization

Pre-processing and alignment were performed using the Cell Ranger software v6.0.1 (10x Genomics). First, sequencing reads of each sample were demultiplexing using their sample index. Since nuclei (and not cells) were sequenced, sequencing reads were aligned to a pre-mRNA reference. Next, individual nuclei were demultiplexed using the nuclei barcodes and subsequently unique molecular identifiers (UMI) were counted. The mean reads per nuclei were 13,536.69 (ranging between 7,305 and 33,1105; **Figure 3.4**). Mean sequencing saturation per sample was 24.8% (ranging between 14.5% and 57.3%).

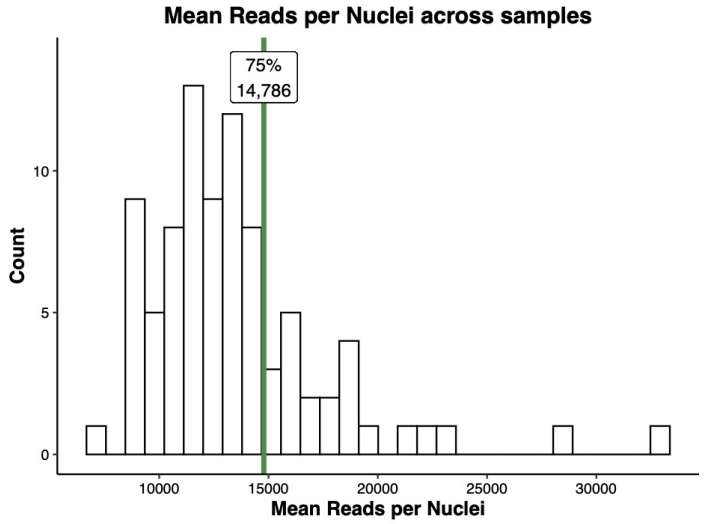

Figure 3.4: Distribution of mean reads per nuclei **a**, Histogram depicting the mean reads per nuclei across samples. The green line marks 75% quartile of reads per nuclei.

In order to avoid bias from samples with very high number of reads per nuclei, a downsampling per nuclei to the 75% quartile of reads per nuclei (14,786 reads) was performed. For further quality control and clustering using scanpy v1.7.1 [142], count matrices of all individuals were combined. Several thresholds were used to filter nuclei: Nuclei with <500 counts, <300 genes and a mitochondrial percentage ≥ 15 were discarded. Moreover, genes not expressed in ≥ 500 nuclei were filtered out. Next, doublets were called using DoubletDetection v3.0 [143] and removed, which resulted in a dataset of 813,095 nuclei. Finally, data was normalized using sctransform v0.3.2 [144].

3.4 Clustering and assignment of cell types

3.4.1 Clustering

For clustering highly variable genes were selected and Leiden clustering was applied. Different resolution parameters from 0.5 to 1 were tested. One cluster was removed since 3 individuals contributed > 25% of nuclei of that cluster, resulting in a final dataset containing 787,685 nuclei.

3.4.2 Cell type assignment

For initial cell-type assignment, a label transfer algorithm (scarches v0.4.0 [145]) was applied, with cell-type labels from the Allen Brain Atlas (Human Multiple Cortical Areas SMART-seq, available at: https://portal.brain-map.org/atlases-and-data/rnaseq/human-multiple-cortical-areas-smart-seq) serving as reference for our clusters. After initial assignment, cluster labels were refined by a manual curation based on marker gene expression [125, 127, 128]. **Table 3.4** summarizes marker genes used.

Table 3.4: Marker genes used for cell type assignment.

Cell Type/Subtype	Marker genes
Astrocytes	AQP4, *GFAP*, *GJA1*
Fibrous astrocytes (Astro_FB)	Higher *GFAP*
Protoplasmic astrocytes (Astro_PP)	Higher *ATP1A2* and *GJA1*
Endothelial cells	CLDN5, FLT1, SYNE2
Excitatory neurons	SLC17A7, *SLC17A6*, *SATB2*
Excitatory neurons layer 2-3	CUX2, *RFX3*
Excitatory neurons layer 4	IL1RAPL2, *CRIM1, RORB*
Excitatory neurons layer 5-6	RXFP1, *TOX*, *DLC1, TLE4*
Inhibitory neurons	GAD1, *GAD2*, *NXPH1*
LAMP5 inhibitory neurons	LAMP5, *ID2*
PVALB inhibitory neurons	PVALB
PVALB inhibitory neurons (Chandelier cells)	PVALB, high *RORA*, *TRPS1*, *NFIB*, *UNC5B*
RELN inhibitory neurons	RELN
SST inhibitory neurons	SST
VIP inhibitory neurons	VIP, *CALB2*
Microglia	APBB1IP, *C3*, *P2RY12*
Oligodendrocytes	MPB, *MOBP*, *PLP1*
Oligodendrocyte Precursors (OPC):	OLIG1, *PDGFRA*, *VCAN*

3.4.3 Subclustering of LAMP5 inhibitory neurons

Subclustering of cluster In_LAMP5 cluster was performed using Leiden clustering at resolution 0.1. This revealed two subtypes: In_LAMP5_1 (highly expressing *LAMP5*, *NRG1*, and *FREM1*) and In_LAMP5_2 (highly expressing, *LAMP5*, *CHST9*, and *LHX6*).

3.5 Exploration and choice of covariates

Since technical differences between the samples (such as the library preparation batch) are expected to be the same across all cell types, the influence of covariates was explored using a full pseudobulk count matrix. This full pseudobulk count matrix was generated by summing the gene-wise counts within one individual across all cell types. Next, a strict filter, retaining only genes with ≥ 10 counts in ≥ 90% of all individuals, was applied, followed by variance stabilizing transformation (vsd, DESeq2 [146]) and principal component analysis (PCA). **Figure 3.5a** shows a scree plot depicting the variance explained by each PC. PC1-PC4 explain more than 50% of the variance in the data. Significant correlation of continuous variables with PCs was observed for RIN, PMI, pH and age (**Figure 3.5b**). Canonical correlation analysis (CCA) further identified library preparation batch (lib_batch) as a covariate (**Figure 3.5c**). Additionally, biological sex and disease status were included as covariates. Next, a batch-corrected expression matrix was generated by calculation of normfactors, voom transformation and applying the removebatchEffect function [147]. Thereafter PCA was performed on the batch-corrected expression matrix and the first PC was included as an additional covariate representing hidden confounders. To obtain the variance explained by each of the individual covariates, variance partitioning [148] was performed (**Figure 3.5d**). Most of the variance was explained by the library preparation batch, followed by pH and PC1. Since information on RIN was missing for one individual, value was imputed using impute function from Hmisc package v5.0-1 [149].

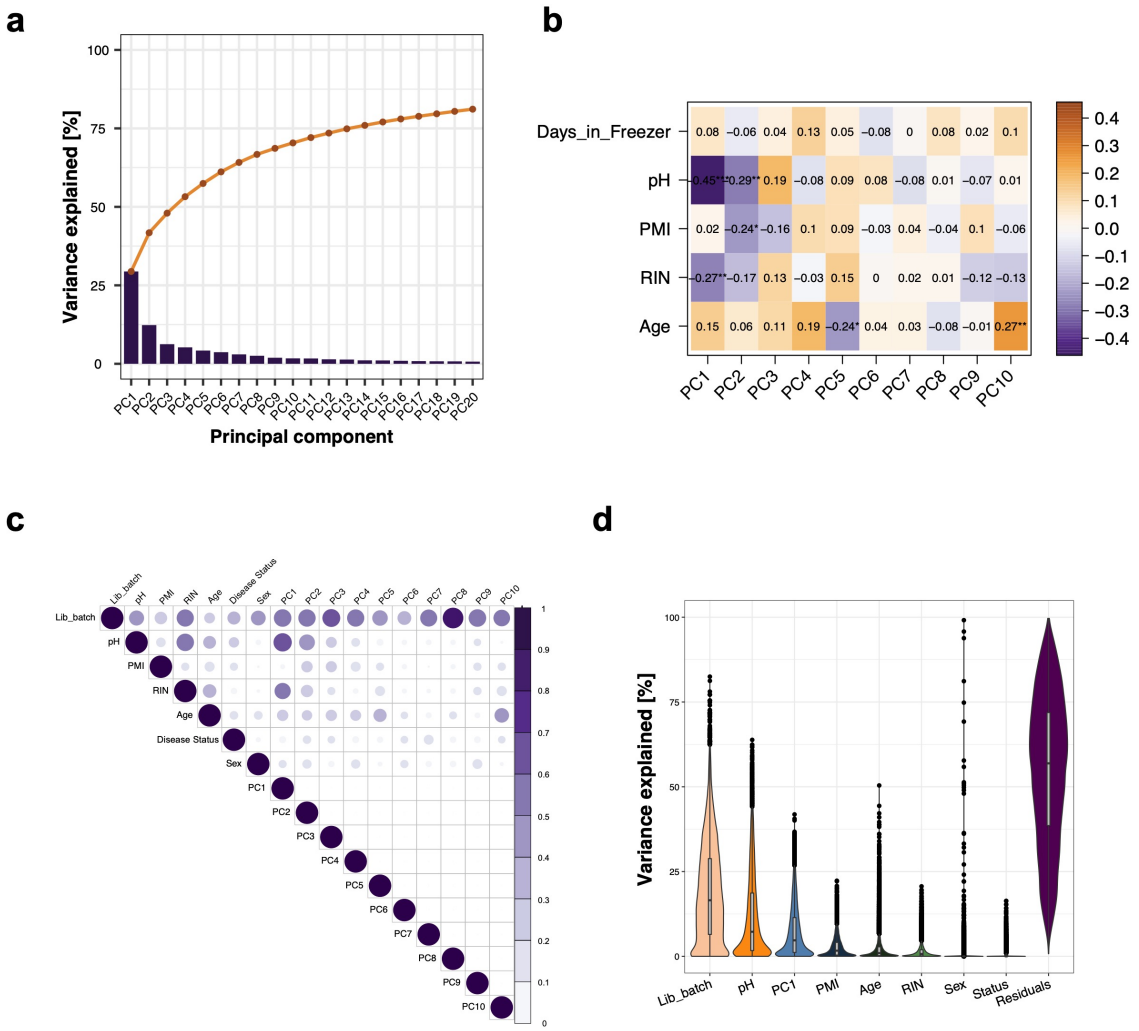

Figure 3.5: Exploration and choice of covariates. **a**, Scree plot depicts the explained variance for principal components (PCs; PC1-PC20). The orange line represents the cumulative explained variance. **b**, Heatmap displaying the Kendall correlation of continuous covariates with PCs. Asterisk (*) marks significant correlation after multiple testing correction (using the Benjamini-Hochberg (FDR) method). **c**, correlogram depicting the correlation of covariates with PCs obtained via canonical correlation analysis. **d**, violin plot of explained variance (from full pseudobulk dataset) for the different experimental variables and covariates chosen to be adjusted for in the differential expression analysis.

3.6 Differential gene expression analysis

For differential gene expression (DGE) analysis, a pseudobulk approach was chosen, since two recent studies showed that single cell specific differential expression tools, such as MAST, suffer from pseudoreplication bias leading to an increase in false positives [83, 84].

Thus, pseudobulk count matrices for each individual were computed by summing the gene-wise counts within each cell type respectively. For each of these count matrices, the same filter was applied removing genes with less than 10 counts in 75% of individuals. **Table 3.5** shows the number of expressed genes in each cell type after filtering as well as the number of individuals contributing nuclei to each cell type.

Table 3.5: Number of genes expressed per cell type and individuals contributing to each cell type.

Cell Type	# Genes expressed	# Individuals
Astro_FB	3914	87
Astro_PP	9162	87
Endothelial	2241	87
Exc_L2-3	17960	87
Exc_L3-5	8031	87
Exc_L4-6_1	12593	87
Exc_L4-6_2	11954	87
Exc_L4-6_3	8617	85
Exc_L5-6_1	4376	86
Exc_L5-6_2	1264	82
Exc_L5-6_HTR2C	3598	85
In_LAMP5	9127	87
In_PVALB_Ba	11667	87
In_PVALB_Ch	4444	87
In_RELN	9519	87
In_SST	9532	87
In_VIP	11954	87
Microglia	4007	87
Oligodendrocyte	7629	87
OPC	9143	87

DGE analysis was performed using edgeR's glmQLFtest function [150, 151] including the selected covariates (final model: ~ Age + Disease Status + Sex + pH + RIN + PMI + lib_batch + PC1). Disease status was a binary variable (0= controls, 1 = psychiatric cases). Differentially expressed (DE) genes with FDR-adjusted p-value of < 0.1 were considered for downstream analysis. This slightly more lenient cut-off was chosen since pseudobulk approaches are considered to be more conservative than single cell specific methods [152, 153]. To test for interactive effects, the interaction term (Age*Disease Status) was additionally included in the model. To test for genes associated with polygenic risk scores (PRS), the term Disease Status was replaced by the respective PRS.

3.7 Similarity measure for differentially expressed genes between cell types

The overlap index (OI) of DE genes between two cell types (C1 and C2), to estimate the similarity in gene expression change, was calculated as follows:

$$\mathrm{OI}(\mathrm{C1},\mathrm{C2}) = (\frac{|C1 \cap C2|}{|C1|} + \frac{|C1 \cap C2|}{|C2|})/2$$

Compared to the Jaccard index, this OI considers the overlap proportion in comparison to each of the two cell types separately and not the union (as for the Jaccard index). Thus, equal weight is given to each of the two cell types, which is essential given the (sometimes) large difference in total number of DE genes between cell types.

3.8 Visualisation of differentially expressed genes

Batch-corrected count matrices were computed to be able to visualise DE genes: The filtered pseudobulk count matrices for each cell type were first normalised using edgeR's [81] function calcNormFactors. Then voom-transformation (limma) was applied, followed by removal of batch effects (disease status + sex + pH + RIN + PMI + lib_batch + PC1) using the function removeBatchEffect (limma, v3.48.3 [79]). For the visualisation of age- and disease-related changes, removeBatchEffect was applied to remove all batch effects except disease status.

3.9 Cell type abundance

To investigate if cell types change in abundance during the course of ageing, cell type proportions of each cell type for each individual were estimated by dividing the number of nuclei in a specific cell type by the total number of nuclei of the respective individual. Next, multiple linear regression was used to test for association between age and cell type composition for each cell type respectively controlling for covariates (sex, disease status, pH, RIN, PMI and lib_batch). At an FDR-adjusted p-value of < 0.05 associations were considered significant.

3.10 Validation using previously published datasets

Different datasets were used to validate observed age-related gene expression changes: Two studies (Lu et al. [154] and Kumar et al. [155]) had identified age-related transcriptional changes in the human cortex using bulk sequencing approaches. Differentially expressed Affymetrix probes (Lu et al.) were mapped to ensembl IDs and IDs not expressed in the filtered full pseudobulk dataset were removed. Using Fisher's exact test (GeneOverlap v1.28.0 [156]) overlap between the two datasets for up- and downregulated genes respectively was tested. Kumar et al. provided a discovery and replication dataset. For validation, only significant DE genes present in both discovery and replication datasets were used. After mapping gene symbols to ensembl IDs and filtering out IDs not expressed in the filtered full pseudobulk dataset, overlap was determined. The direction of effect (up- or downregulation) was not provided in Kumar et al.'s supplementary data and thus not considered for the overlap.

For validation of cell-type specific age-regulated genes, another sn-RNA-seq dataset [157] as well as two datasets one from sorted microglia [158] and another one from sorted astrocytes [159] were leveraged. To validate age-related genes in In_LAMP5, differential expression for age was performed in the same cell type "In_LAMP5_validation". Its summed pseudobulk expression matrix was filtered and voom-normalized before performing differential expression using limma [147]. The model was adjusted for all covariates (identified by the authors of the original publication): age, sex, PMI, genetic PC1, psychiatric diagnosis (controls, MDD, post-traumatic stress disorder), lifetime antipsychotic use, day of the experiment, percentage of cells in the cluster over the total of cells and batch. For the Fisher's exact test, up- and downregulated age-regulated genes respectively at an FDR-adjusted p-value of < 0.1 for In_LAMP5 from this study and age-regulated genes at nominal p-value < 0.05 for In_LAMP5_validation were used.

Next, age-regulated genes identified in purified populations of microglia [158] and astrocytes [159] (FDR-adjusted p-value < 0.05) were compared to age-regulated genes in microglia and astrocytes (broad cell type cluster; FDR-adjusted p-value < 0.1) of this study. Analogous to the comparisons above, ensembl IDs not expressed in the filtered pseudobulk expression matrix (of microglia and astrocytes respectively) were removed before testing for overlap. To investigate the comparability of effect sizes, spearman correlation of log2FC of overlapping genes was calculated for the respective comparisons in In_LAMP5, microglia and astrocytes.

3.11 Over-representation analysis of biological pathways and disease

In order to understand, which biological pathways are affected by the gene expression changes during ageing, over-representation analysis (ORA) for up- and downregulated age DE genes was performed using clusterProfiler (v4.0.5 [160]). Moreover, to investigate in which diseases the age-regulated genes are implicated, disease enrichment analysis using DOSE (v3.18.3 [161]) was conducted. All genes expressed in the respective cell type (at minimum of 10 counts in 75% of the individuals) were considered as background. Since the different cell types have different numbers of DE genes (**Table 4.2**), only GO/disease terms were considered that had ≥ 5% of the DE genes overlapping with the term genes and > 2 genes per term. At an FDR-adjusted p-value < 0.05, terms were considered significant. To reduce redundancies in the list of GO-terms and for visualization, semantic similarity analysis using GO-Figure! [162], with default parameters, was applied.

3.12 Comparison of transcriptomic changes between age and Alzheimer's disease

Two studies (Mathys et al. [132] and Lau et al. [133]) had previously uncovered cell-type-specific transcriptomic changes related to Alzheimer's disease (AD) in prefrontal cortex using sn-RNA-seq. Both AD studies had assigned broad cell type labels and had identified astrocytes, endothelial cells, excitatory and inhibitory neurons, microglia, and oligodendrocytes (and oligodendrocyte precursors only in [132]). To examine the cell-type specific overlap between age-associated and AD-associated genes, the cell-type specific AD DE genes were overlapped with the age DE genes in the corresponding broad cell type (after filtering out AD DE genes not expressed in the filtered pseudobulk expression matrix of the corresponding cell type).

3.13 Calculation of transcriptomic age

To estimate the biological age based on gene expression in brain, a transcriptomic age predictor derived from brain samples of the same region (BA11), developed by Lin and colleagues [49], was used. The transcriptomic age predictor was derived from bulk expression; therefore, the full pseudobulk count matrix was used. After removing genes with less than 10 counts in 75% of individuals, counts were normalized using the calcNormFactors function (edgeR [150]) and voom transformation (limma, v3.48.3 [147]). The transcriptomic age predictor is based on the weighted expression of 76 genes. Gene symbols were first mapped to ensembl IDs. Next, missing ensembl IDs (i.e. genes not expressed in the filtered pseudobulk count matrix) were identified: Out of the 76 genes only 3 were missing (*APLNR*, *KCNA6*, and *MIR29C*). Transcriptomic age for each individual was calculated by multiplying the gene expression value by its provided coefficient (weight) summed for all 73 genes. To

re-scale the unit of the transcriptomic age back to the unit of chronological age by year a linear regression was fit between chronological age and transcriptomic age. As a measure for deviation of biological from chronological age, transcriptomic age acceleration was computed by regressing transcriptomic age on chronological age adjusting for the library preparation batch (lib_batch; the strongest batch effect - see **Figure 3.5d**). Using multiple linear regression, the association of disease status (cases) with transcriptomic age acceleration (correcting for covariates (sex, pH, RIN, PMI and PC1)) was investigated.

3.14 DNA extraction

Isolation of genomic DNA from ~10 mg frozen OFC tissue was performed using the QIAamp DNA mini kit (Qiagen) following the manufacturer's instruction 'Protocol: DNA purification from Tissues' without performing the RNase A treatment. Next, DNA was concentrated using the DNA Clean & Concentrator-5 (Zymo Research) kit. Genomic DNA was used for DNA methylation measurement as well as genotyping (see next sections).

3.15 DNA methylation measurement and calculation of epigenetic clocks

For a balanced experimental design not confounded by our variables of interest, sample position (column and row) on a 96-well plate was randomised for age, sex, and disease status using OSAT [140].

The EZ-96 DNA Methylation kit (Zymo Research, Irvine, CA) was used for bisulfite-conversion of 400 ng DNA on a 96-well plate. The Illumina Infinium MethylationEPIC BeadChip (Illumina, San Diego, CA, USA) was used according to manufacturer's guidelines to measure epigenome-wide DNA methylation (DNAm). Each column of the 96-well plate represented one batch of the Infinium MethylationEPIC BeadChip.

To estimate biological age based on DNAm, two DNAm clocks were computed; Horvath's multi-tissue clock [163] and a recently developed cortical clock [164]. For each of the two DNAm clocks, processing of raw intensity values was performed as suggested by the original publications. Thus, for Horvath's multi-tissue clock raw intensity values were transformed into beta-values followed by quality control with the *minfi* R package [165, 166]. Next, stratified quantile normalization [167] and subsequent beta-mixture quantile normalization (BMIQ) [168][96] was applied. For the cortical clock [164], raw intensity values were processed using the *watermelon* and *bigmelon* R packages according to the preprocessing pipeline by Shireby et al. [164, 169, 170]. PCA was performed separately after transformation of beta-values to M-values for each of the two clocks to detect potential outliers (>3 SD on two first principal components). None of the samples met exclusion criteria during quality control (mean detection of p-value > 0.05, distribution artefacts in raw beta-values, sex mismatches, or outliers). Next, technical batch effects (array and row) showed the strongest associations with principal components and were thus corrected for sequentially with ComBat (*sva*

package) [171]. Batch-corrected M-values were transformed into beta-values and sample mix-ups were excluded using MixupMapper [172]. Other covariates (brain pH and freezer storage time) significantly correlated with the first 5 PCs and were thus included as covariates in all subsequent analyses.

Epigenetic age (DNAmAge) was calculated for Horvath's multi-tissue clock using the methylclock package [163, 173] and for the cortical clock using code provided by the authors [164, 174]. Epigenetic age was then used for estimating epigenetic age acceleration (AgeAccel), i.e. the residuals of the regression of epigenetic age on chronological age adjusted for the covariates pH and freezer storage time. Since different cells contribute to the bulk DNA methylation profile, proportions of neuronal cells were estimated from the epigenome-wide DNA methylation as suggested by Guintivano et al. [175]. To examine the association of disease status (cases) with epigenetic age acceleration multiple linear regression was used controlling for sex, smoking status and neuronal cell proportions. Out of the 87 individuals, one individual could not be profiled for DNA methylation due to too low DNA yield. Moreover, for seven individuals smoking status was unknown, which led to a final cohort of 79 individuals (controls n=27, cases n=52) for multiple linear regression analysis.

3.16 Genotyping

For a balanced experimental design not confounded by our variables of interest, sample position (column and row) on a 96-well plate was randomised for age, sex, and disease status using OSAT [140]. Three columns represented one batch (24 samples per genotyping array).

With the Illumina GSA-24v2-0_A1 arrays genome-wide single nucleotide polymorphism (SNP) genotyping was performed according to the manufacturer's guidelines (Illumina Inc., San Diego, CA, USA). *PLINK* [176] was used for genotypic quality control. SNPs with a call-rate <98%, MAF < 1% or a p-value for deviation from Hardy-Weinberg-Equilibrium $<1x10^{-5}$ were removed. Next, individuals were removed if their call-rate was < 98%. If two individuals presented relatedness (pihat)> 0.125, the individual with the higher call-rate was kept in the analysis. Individuals defined as genetic outliers (based on deviation of more than 4 standard deviation (SD) on the first 3 MDS-components of the IBS-matrix after LD-pruning) were also excluded. None of the 87 individuals qualified for any of the above-mentioned exclusion criteria. After quality control, genotypes were subjected to imputation using *shapeit2* [177] and *impute2* [178] using the 1000 Genomes Phase III reference sample. Next, SNPs with an info score > 0.6, a minor allele frequency > 1%, or deviating from Hardy–Weinberg equilibrium (p-value < 1×10^{-5}) were excluded from further analysis resulting in 9,652,209 SNPs.

3.17 Calculation of polygenic risk scores

GWAS studies for a cross-disorder psychiatric phenotype [179] and schizophrenia [22] were used for the calculation of polygenic risk scores (PRS). To infer posterior SNP effect sizes in the summary statistics of GWAS, the PRS-CS package (v1.0.0 [180]) in python (v3.6.8) was used. The linkage disequilibrium reference panel computed from the 1000 Genomes Project phase 3 European samples was used (linked on the PRS-CS GitHub page [181]). The parameter for global shrinkage of PRS-CS, phi, was not specified for the cross-disorder phenotype since the large sample size of the GWAS allowed for phi to be learned from the data. For SCZ, however, phi was specified to 1e-2, as suggested for highly polygenic traits. For the calculation of PRS per individual, based on the previously inferred posterior effect sizes, PLINK (v2.00a2.3LM) [182, 183] with the score parameter was used.

4 | Results

4.1 Experimental Design

To study the cell-type specific transcriptomic changes that occur during (non-pathological) ageing, post-mortem brain samples from a cohort of 87 individuals that spanned an age range from 26 to 84 years of age were used. Neuropathological examination of all brains revealed no signs of neurodegenerative processes ensuring to minimize their possible influence on the investigated ageing process. The inclusion of both neurotypical individuals (controls) and individuals having suffered from psychiatric disease (cases) enabled the additional investigation of the influence of disease status on ageing.

First, several aspects were evaluated to ensure no systematic bias was present between controls and cases. There was no difference in mean age, PMI, and RIN, number of nuclei recovered by sn-RNA-seq as well as the median number of genes and counts (**Figure 4.1a-f**).

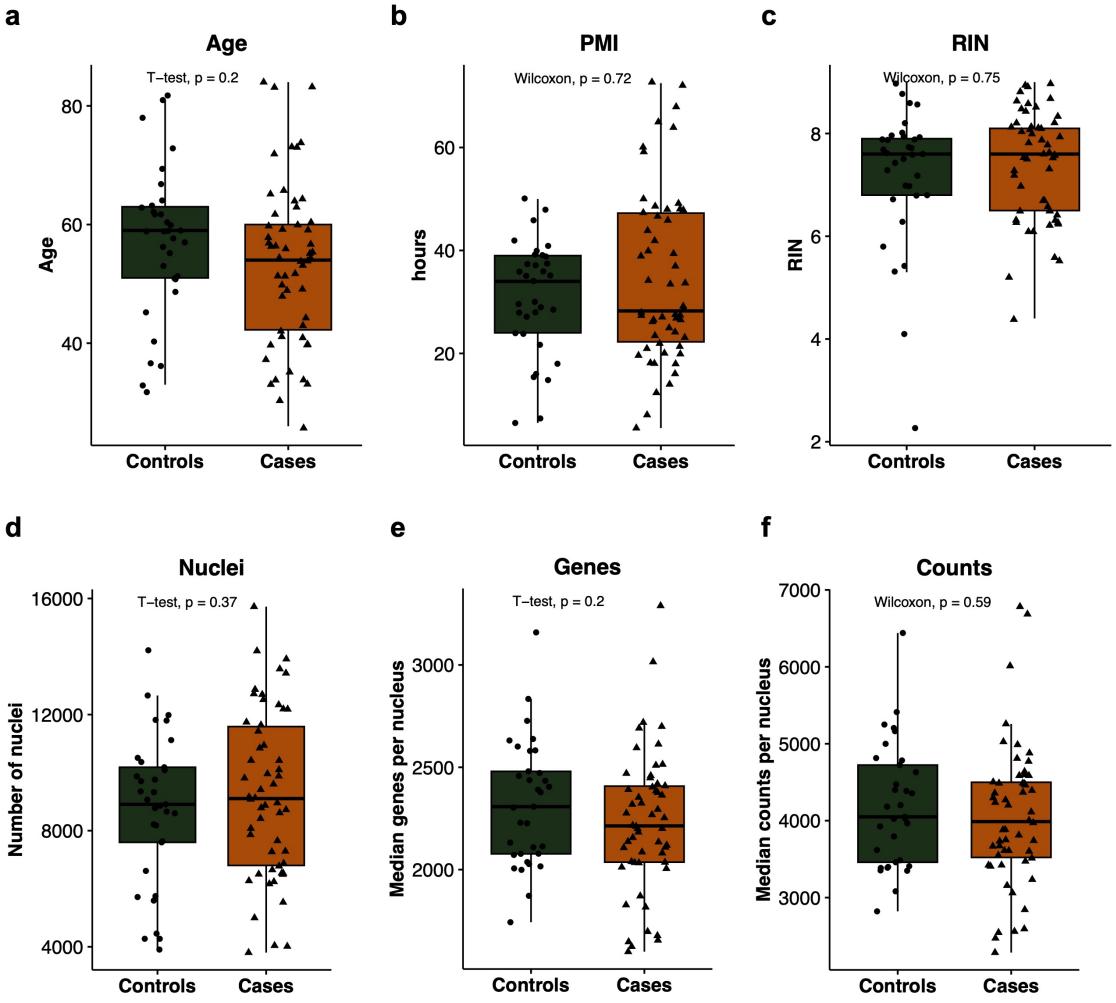

Figure 4.1: No systematic differences between healthy controls and psychiatric cases. a-f, Boxplots showing age (**a**), post-mortem interval (PMI) (**b**), RNA-integrity number (RIN) (**c**), number of nuclei (**d**), median number of genes (**e**) and median number of counts (**f**) between controls (coloured in green) and cases (coloured in orange). P-value obtained from t-test (normally distributed data) and Wilcoxon-test (non-normally distributed data) is shown.

Next, correlation of age (the variable of interest) with the covariates was tested. No correlation of age with PMI, or age with median number of genes or median number of counts were found (**Figure 4.2a-d**). However, there was a modest, negative correlation between age and RIN (**Figure 4.2e**), which has previously been reported [184].

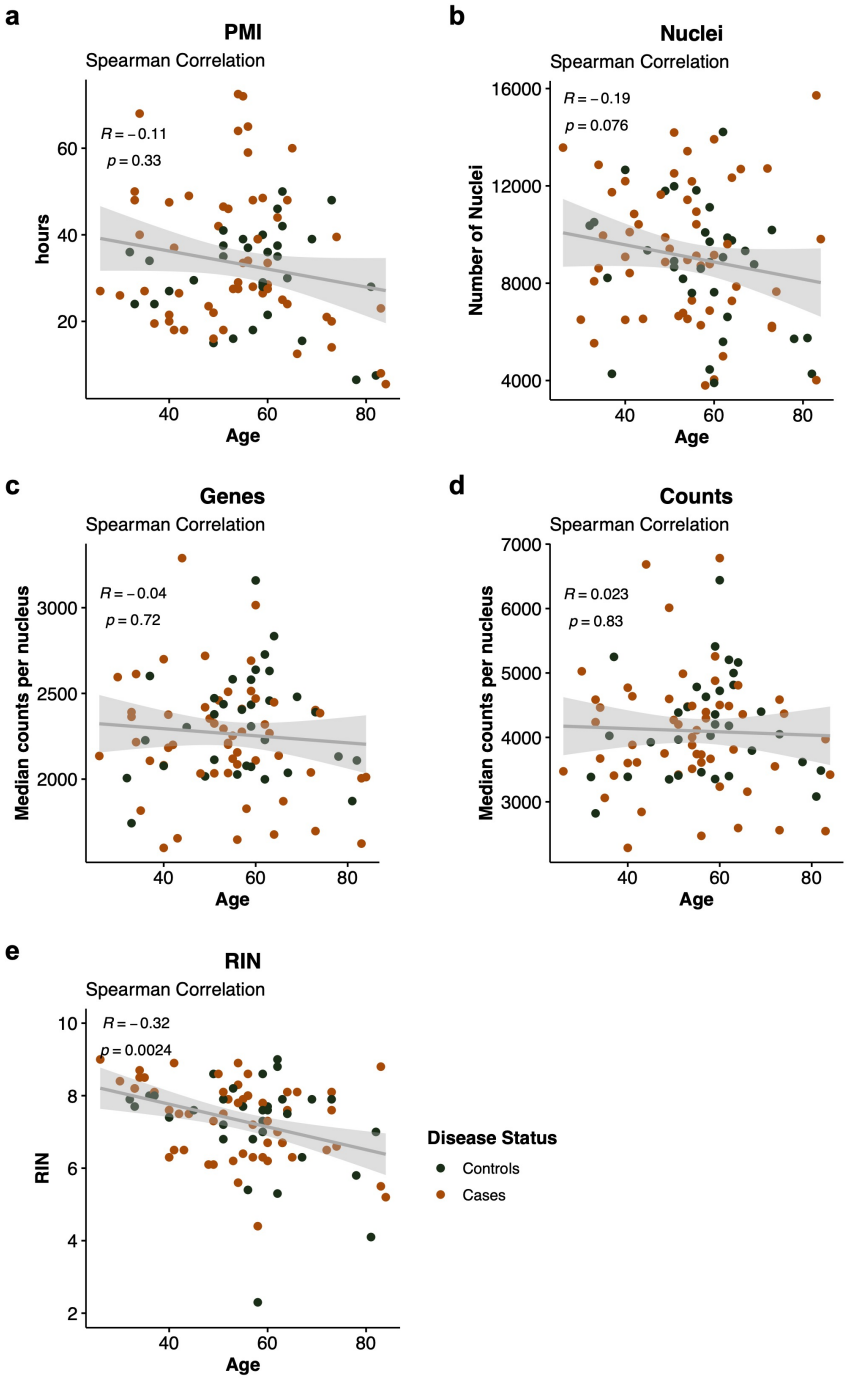

Figure 4.2: Correlation of age with covariates. **a-e**, Scatterplots depicting the correlation of age with PMI (**a**), number of nuclei (**b**), median number of genes (**c**), median number of counts (**d**) and RIN (**e**). Each dot represents one individual with controls coloured in green and cases coloured in orange. Spearman correlation coefficient and p-value are shown.

4.2 Identification of the diverse cell types in human orbitofrontal cortex

After quality control, filtering and normalization, Leiden clustering was applied using highly variable genes to group the nuclei based on similarity in gene expression profiles. The clustering of the nuclei was not driven by experimental variables (batch) or covariates (sex, disease status) or individual donors (**Figure 4.3a-h**).

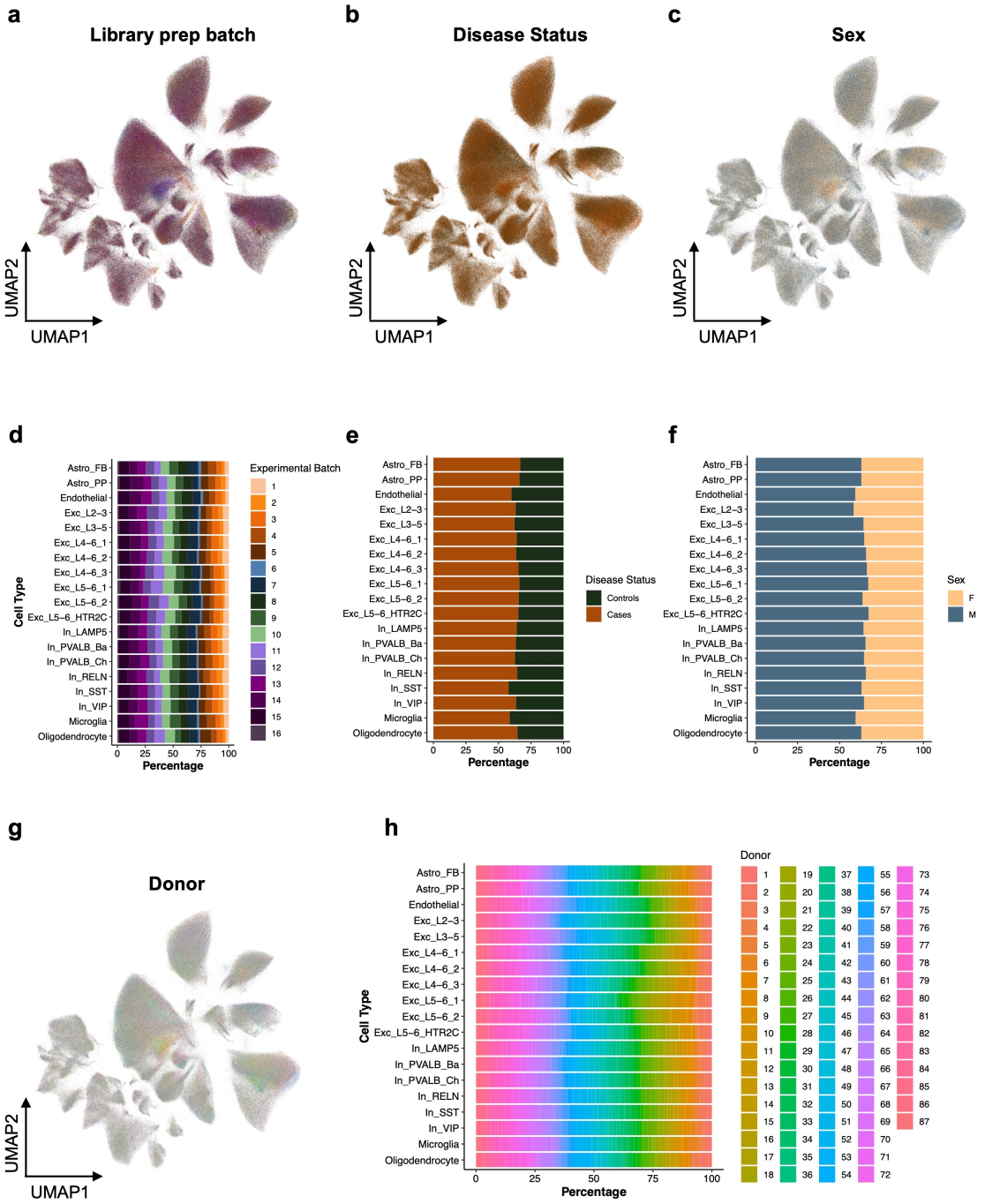

Figure 4.3: Clustering of nuclei. **a-c**, Uniform manifold approximation and projection (UMAP) showing ~800 000 nuclei from 87 donors from the orbitofrontal cortex coloured by experimental batch (**a**), disease status (**b**), and sex (**c**) indicating that clustering was not driven by these parameters. Each dot represents one nucleus. **d-f**, Stacked bar plots showing the percentage contribution to the

respective cell type cluster from experimental batch (**d**), disease status (**e**) and sex (**f**). **g**, UMAP showing ~800 000 nuclei from 87 donors from the orbitofrontal cortex coloured by donor. **h**, Stacked bar plot showing the percentage contribution to the respective cell type cluster from each donor. Each dot represents one nucleus.

Next, a label transfer algorithm was used to transfer cell type labels from the Allen Brain Atlas to identified cell type clusters. This was followed by manual curation of assigned labels using known marker genes expression. Overall, seven broad cell types (**Figure 4.4a**) and 20 cell subtypes could be identified (**Figure 4.4b**). This included endothelial cells, diverse glial cell types (two astrocyte sub-types (fibrous (Astro_FB) and protoplasmic (Astro_PP), microglia, oligodendrocytes, and oligodendrocyte precursor cells (OPC)) and several subtypes of excitatory and inhibitory neurons. Importantly, there was no difference between controls in cases in the mean number of nuclei per cell type (**Supplementary Table 1**).

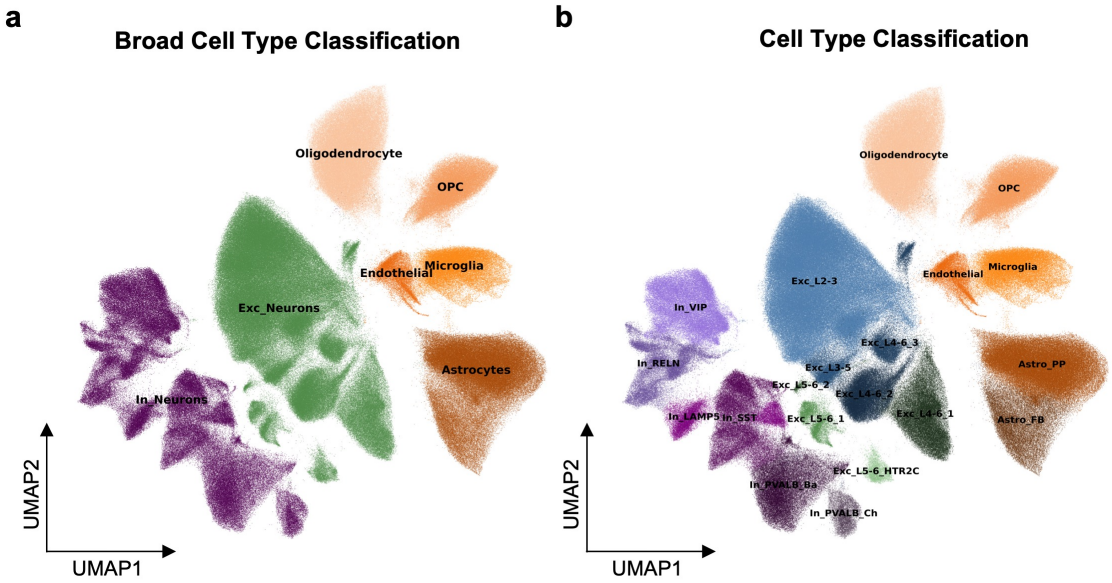

Figure 4.4: Cell type assignment. **a-b**, Uniform manifold approximation and projection (UMAP) showing ~800 000 nuclei coloured by broad cell type (**a**) and cell subtypes (**b**).

Table 4.1 shows the number of nuclei per cell type class for both broad and cell subtype classification.

Table 4.1: Number of nuclei per broad cell type cluster and per cell type cluster.

Broad Cell Type	# nuclei
Astrocytes	113334
Endothelial	13567
Exc_Neurons	329012
In_Neurons	153826
Microglia	39154
Oligodendrocyte	93357
OPC	45435

Cell Type	# nuclei
Astro_FB	25410
Astro_PP	87924
Endothelial	13567
Exc_L2-3	218679
Exc_L3-5	11815
Exc_L4-6_1	36486
Exc_L4-6_2	34813
Exc_L4-6_3	14470
Exc_L5-6_1	7541
Exc_L5-6_2	1069
Exc_L5-6_HTR2C	4139
In_LAMP5	15089
In_PVALB_Ba	31796
In_PVALB_Ch	6709
In_RELN	24191
In_SST	33791
In_VIP	42250
Microglia	39154
Oligodendrocyte	93357
OPC	45435

Figure 4.5a-d shows an overview of the expression of the marker genes used for cell type assignment.

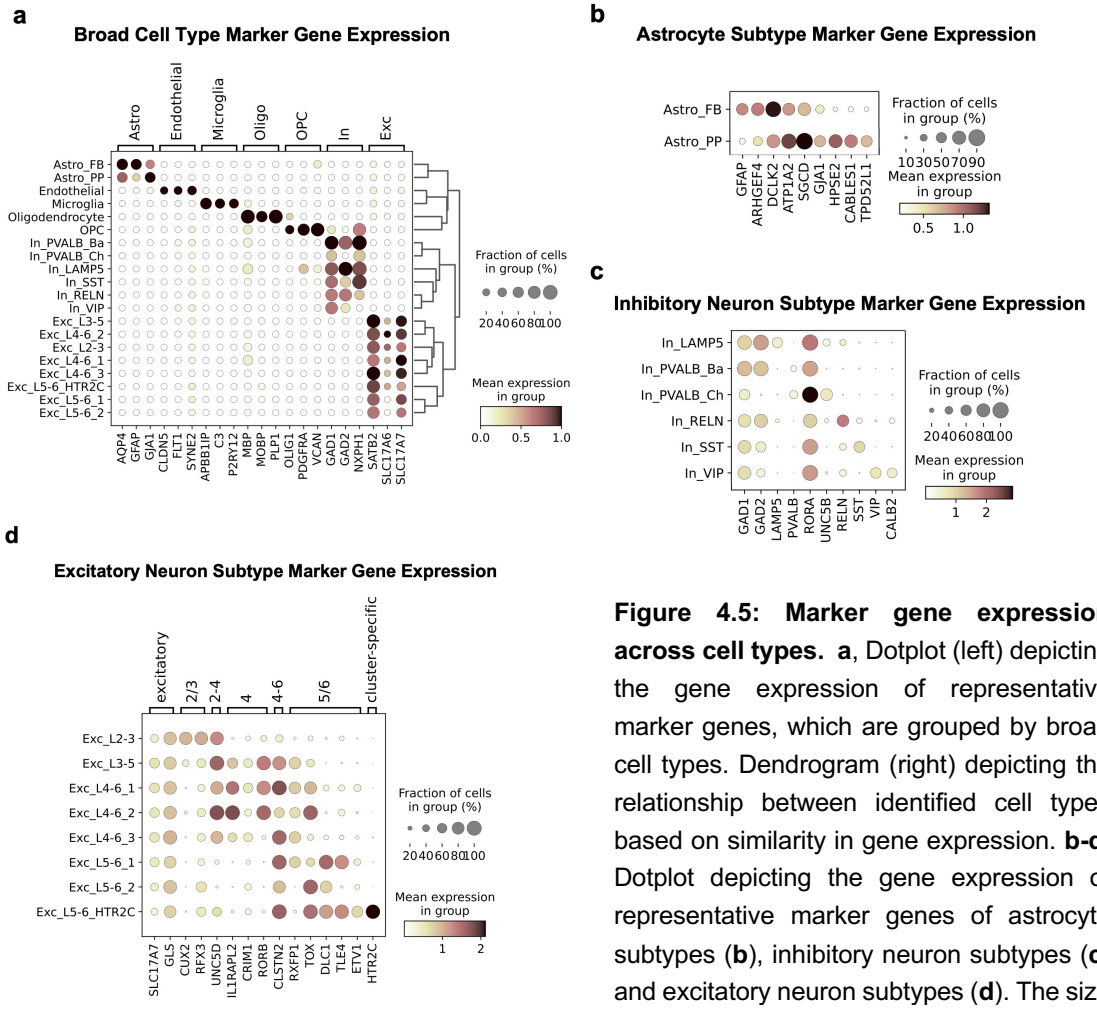

Figure 4.5: Marker gene expression across cell types. a, Dotplot (left) depicting the gene expression of representative marker genes, which are grouped by broad cell types. Dendrogram (right) depicting the relationship between identified cell types based on similarity in gene expression. **b-d**, Dotplot depicting the gene expression of representative marker genes of astrocyte subtypes (**b**), inhibitory neuron subtypes (**c**) and excitatory neuron subtypes (**d**). The size

of the dot is proportional to the fraction (%) of nuclei expressing the gene and the colour represents the mean expression level. Astro = Astrocytes, FB= fibrous, PP= protoplasmic, Exc = excitatory, In= inhibitory, L= cortical layer, OPC= oligodendrocyte precursors, Ba= Basket, Ch=Chandelier

4.3 The transcriptome of all cell types is affected by ageing

After cell-type assignment, gene counts were summed for each cell type within each individual respectively. Next, differential gene expression (DGE) analysis using edgeR [150, 151] was performed to identify genes that linearly change their expression along ageing (independent of case-control status). The following covariates were adjusted for in all analyses: disease status, sex, pH, RIN, PMI, library preparation batch, and PC1 followed by multiple testing correction using the Benjamini-Hochberg (FDR) method [185]. Out of the 20 identified cell types, all except endothelial cells had significant age-regulated genes (**Table 4.2**). Overall, 5,161 genes were differentially expressed (DE) with age (FDR adjusted p-value < 0.1) in at least one cell subtype. The majority of the DE genes encode protein-coding genes (mean across cell types: 91%).

Table 4.2: Number of differentially expressed genes with age shown for broad and cell subtypes at FDR-adjusted p-value < 0.1 and < 0.05.

Broad Cell Type	FDR < 0.1	FDR < 0.05
Astrocytes	100	37
Endothelial	0	0
Exc_Neurons	2869	1789
In_Neurons	1080	530
Microglia	144	66
Oligodendrocytes	60	27
OPC	208	89

Cell Type	FDR < 0.1	FDR < 0.05
Astro_FB	92	57
Astro_PP	87	35
Endothelial	0	0
Exc_L2-3	2598	1613
Exc_L3-5	231	115
Exc_L4-6_1	1088	660
Exc_L4-6_2	1399	936
Exc_L4-6_3	429	247
Exc_L5-6_1	129	63
Exc_L5-6_2	25	8
Exc_L5-6_HTR2C	53	22
In_LAMP5	1093	594
In_PVALB_Ba	66	10
In_PVALB_Ch	91	40
In_RELN	59	10
In_SST	399	194
In_VIP	796	427
Microglia	144	66
Oligodendrocyte	60	27
OPC	208	89

The top ten up- and downregulated DE genes within each cell type are listed in **Supplementary Table 2** and **Supplementary Table 3**. Up- and downregulated DE genes displayed high symmetry in the extent of change (fold change (FC)) as shown in **Figure 4.6**.

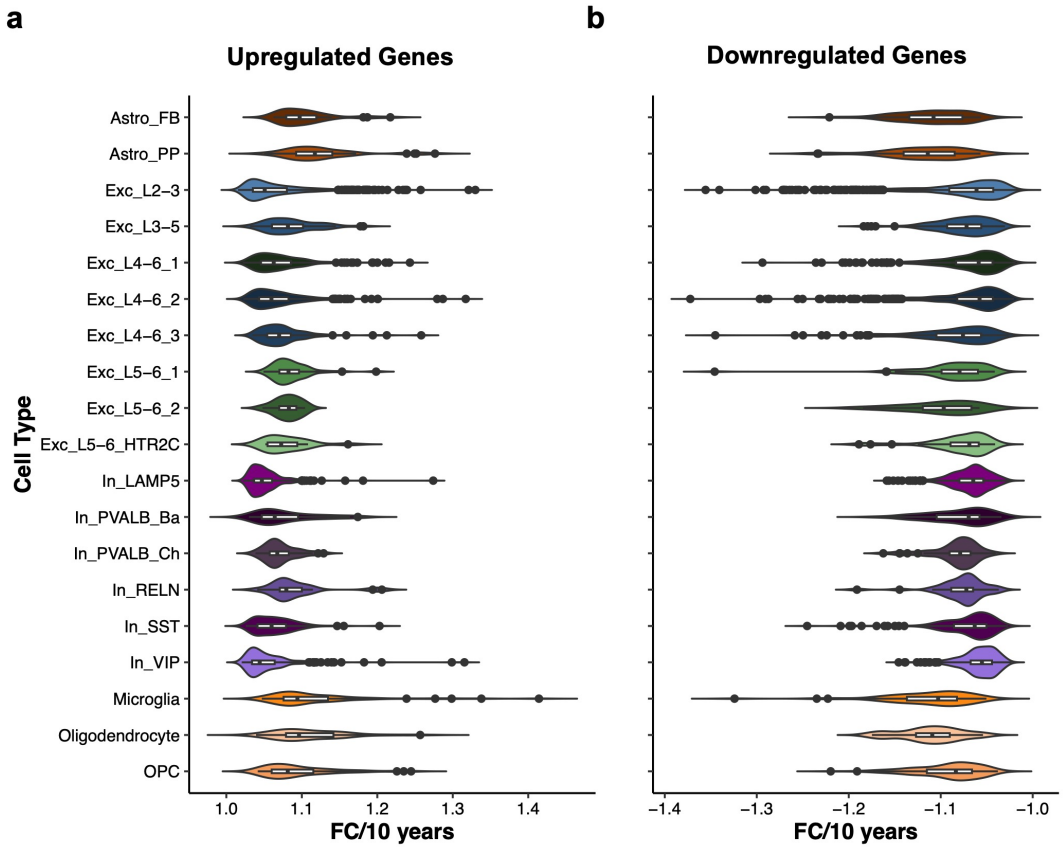

Figure 4.6: Fold change distribution of differentially expressed genes. a-b, Violin plots showing distribution of the FC per 10 years of differentially expressed genes (at FDR-adjusted p-value < 0.1) for up- (**a**) and downregulated (**b**) genes.

Except for oligodendrocytes, more than 50% of the DE genes in each cell type were downregulated with increasing age (**Figure 4.7**), which is consistent with results obtained from bulk brain tissue in both humans and rhesus macaque [110, 115].

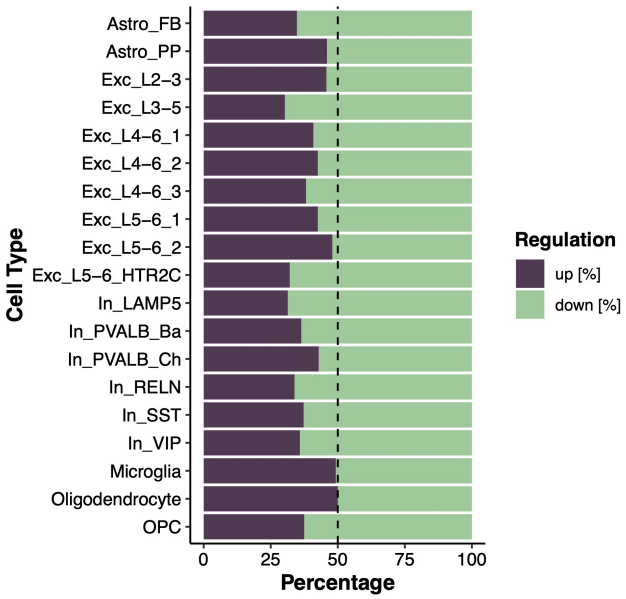

Figure 4.7: Quantification of up- and downregulated genes. Barplot depicting the percentage of up- and downregulated differentially expressed (DE) genes (at FDR-adjusted p-value <0.1) for the respective cell types.

The cell type with the highest number of DE genes were upper layer excitatory neurons (Exc_L2-3, **Table 4.2**). However, differences in the statistical power between cell types to detect DE genes exist due to factors such as the number of nuclei as well as the number of sequencing reads per cell type [186]. Thus, to estimate how strongly each cell type was affected by the ageing process irrespective of these confounding factors, we normalized the number of DE genes per cell type to the total sequencing reads of the respective cell type. Using this metric (number of DE genes per one million reads), we found that In_LAMP5, one inhibitory neuron subtype, showed the most striking changes with age (**Figure 4.8a**). Since there was a prominent gap in the relative number of DE genes between the most (In_LAMP5) and second most (Exc_L4-6_2) affected cell type, we further focused on In_LAMP5. Sub-clustering of In_LAMP5 revealed two subtypes (**Figure 4.8b**): In_LAMP5_1 highly expressed *LAMP5*, *NRG1* and *FREM1* and constituted ~65% of the nuclei, whereas In_LAMP5_2 (35% of the nuclei) showed strong co-expression of *LAMP5*, *LHX6* and *CHST9* (**Figure 4.8c**). Comparison of the relative number of DE genes revealed that In_LAMP5_2 had the highest ratio mainly contributing to the effect seen in In_LAMP5 (**Figure 4.8d**). Interestingly, LAMP5 inhibitory neurons expressing *LHX6* have been previously reported to have increased during evolution and to have become abundant in the cortex of primates [187].

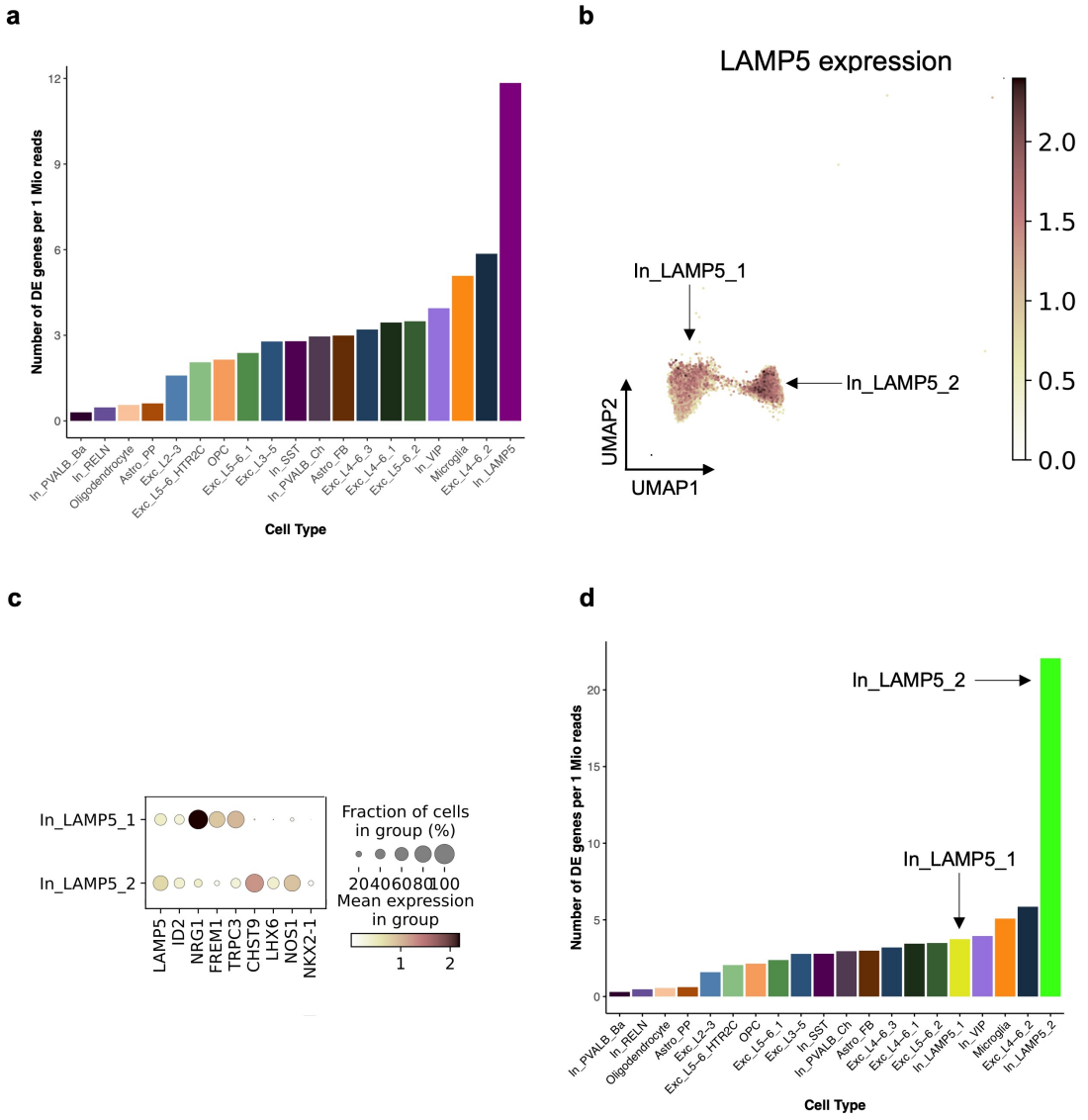

Figure 4.8: Severity of DE changes. **a**, Barplot depicting how strongly each cell type is affected by ageing estimated by the relative number of differentially expressed (DE) genes; y-axis shows the ratio of the number of DE genes (at FDR-adjusted p-value <0.1) per 1 million reads. **b**, Uniform manifold approximation and projection (UMAP) showing the expression level of LAMP5 within the identified two LAMP5 inhibitory neuron subtypes. **c**, Dotplot showing the expression of representative marker genes for the two identified LAMP5 inhibitory neuron subtypes. **d**, Barplot depicting how strongly each cell type is affected by ageing estimated by the relative number of differentially expressed (DE) genes; y-axis shows the ratio of the number of DE genes (at FDR-adjusted p-value <0.1) per 1 million reads. The two identified LAMP5 inhibitory neuron subtypes are highlighted.

4.4 Cell-type specific and universal transcriptomic changes during ageing

After having identified age DE genes in the different cell types, we wanted to understand the extent of coordinated as well as universal changes across cell types. In general, there were no age DE genes present in all of the 19 cell types that showed changes with age. Even, when comparing the broad cell type classes, only three common age DE genes - *ARPP19*, *NFKBIA* and *OLFM1* - could be identified (**Figure 4.9**). These three genes have been linked to ageing before, yet not always based on data from brain tissue.

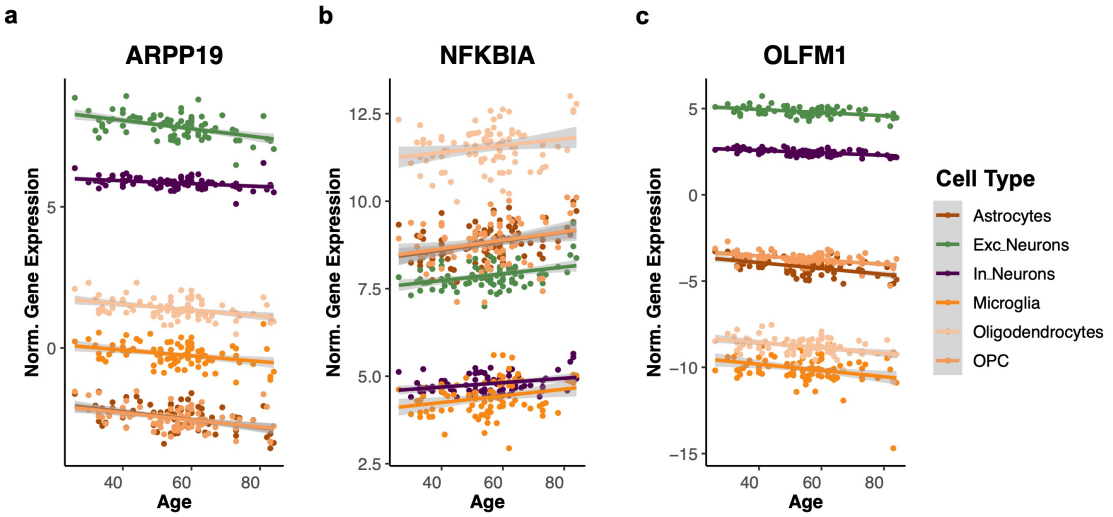

Figure 4.9: Shared differentially expressed genes across broad cell type classes. **a-c**, Scatterplots showing log normalized gene expression corrected for covariates across ageing of significantly differentially expressed genes (*ARPP19* (**a**), *NFKBIA* (**b**), *OLFM1* (**c**)) across all broad cell types. Error bands represent the 95% confidence interval. Exc=excitatory, In=inhibitory neurons.

To visualize the overlap of DE genes between the cell types for up- and downregulated DE genes, we normalized the number of shared DE genes between two cell types to the total number of DE genes of each of the two cell types and took the average. As shown in **Figure 4.10**, downregulated age DE genes showed a higher degree of overlap than upregulated age DE genes indicated by the darker colour and thicker lines connecting the different cell types. Interestingly, downregulated age DE genes did not only show an overlap between the neuronal cell types (both excitatory and inhibitory) but also with glial cells, including astrocytes, oligodendrocytes and OPCs, except microglia. Within the upregulated age DE genes, neuronal cell types showed overlap whereas all glial cells showed rather unique profiles indicated by the large size of the circles.

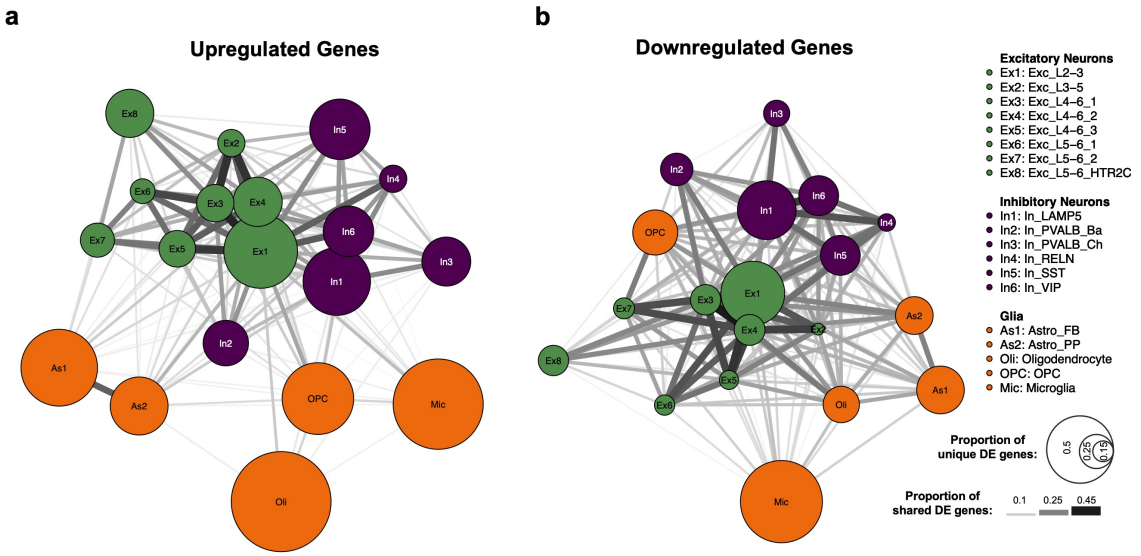

Figure 4.10: Similarity in age-regulated genes across cell types **a-b**, Visualisation of shared and cell-type specific DE genes for upregulated (**a**) and downregulated (**b**) DE genes (at FDR-adjusted p-value <0.1). The number of overlapping DE genes between two cell types was normalized to the total number of DE genes of each of the two cell types and the average was taken (overlap index (OI) - see section 3.7). The thickness of the grey line connecting two cell types is representative of this shared proportion of DE genes; with a thicker line indicating a higher overlap. The size of the circle for each cell type indicates the proportion of cell-type-specific DE genes with a bigger circle indicating a higher number of unique DE genes.

The large proportion of unique age-regulated genes is partly driven by genes uniquely expressed in these cell types. Cell types including protoplasmic astrocytes (Astro_PP), microglia, oligodendrocytes, OPCs and upper-layer excitatory neurons (Exc_L2-3) show cell-type specific expression for some of their upregulated genes (**Figure 4.11a**). Within the downregulated genes only microglia and upper-layer excitatory neurons had cell-type specific expressed genes that were differentially expressed with age (**Figure 4.11b**). The high proportion of uniquely age-regulated genes in Exc_L2-3 is likely due to the fact that this cell type had the largest number of nuclei, sequencing reads and thus detected/expressed genes. Interestingly, LAMP5 inhibitory neurons, besides being the most strongly affected cell type, had no uniquely expressed DE genes.

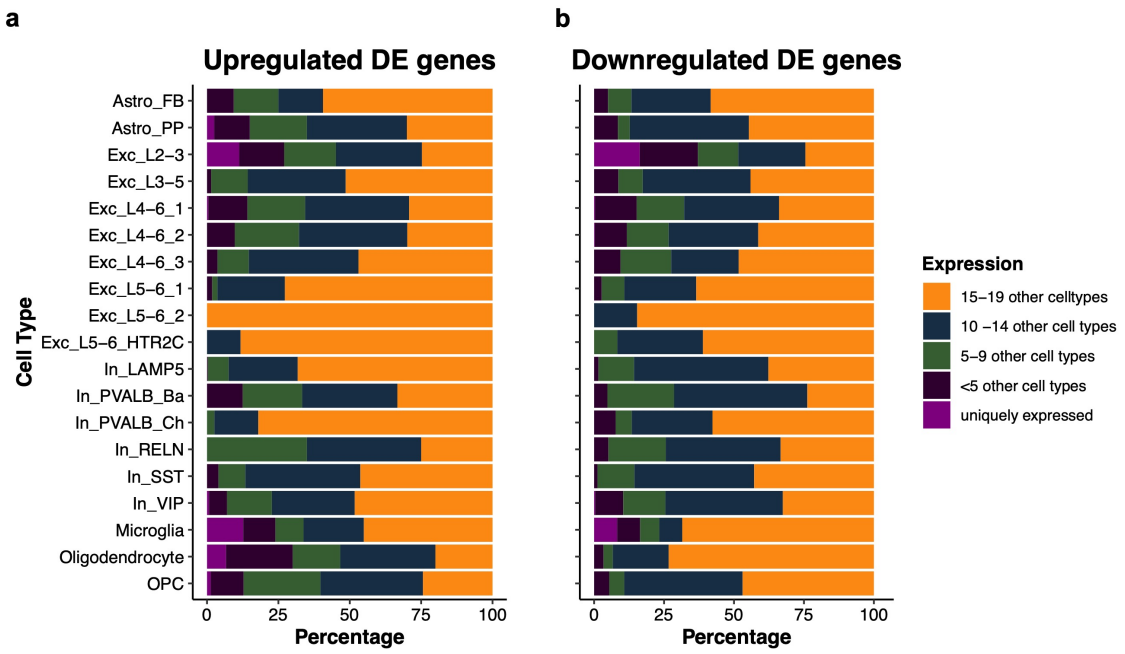

Figure 4.11: Cell-type specific expression of differentially expressed genes. a-b, Barplot quantifying the proportion of DE genes per cell type that are either uniquely expressed in the respective cell type or are expressed in <5 other cell types, between 5-9 other cell types, between 10-14 other cell types or 15 -19 other cell types shown for up- (**a**) and downregulated (**b**) DE genes.

In general, several genes previously linked to ageing, such as *CAMK4* (Calcium/Calmodulin Dependent Protein Kinase IV) and *FKBP5* (FKBP prolyl isomerase 5), were coordinately regulated across multiple cell types **(Figure 4.12a-b**). *CAMK4* has been previously identified to be downregulated with age across several species [113]. It acts as a transcriptional regulator and is involved in synaptic signalling [188]. *FKBP5* is amongst the genes with the highest magnitude of change (log2FC from 0.029 to 0.047 per year) with upper-layer excitatory neurons (Exc_L2-3) showing the highest up-regulation with age (**Figure 4.12b**), as previously reported [189]. *FKBP5* has been linked to AD by hindering tau degradation and SNPs in *FKBP5* have been shown to increase the risk for psychiatric diseases. Several genes involved in neuronal signalling are downregulated with age in multiple cell types. For example, *NREP* (neuronal regeneration related protein) significantly decreases with age in 11 cell types (both neuronal and glial) with excitatory neurons showing the strongest changes (**Figure 4.12c**). *NREP* is important for both neuronal differentiation and axon regeneration. *NPTX2* (neuronal pentraxin 2), a gene involved in excitatory synapse formation, significantly decreased with age in five excitatory neuron types and was amongst the top five downregulated DE genes in four of these cell types (**Figure 4.12d**). As mentioned above, in microglia we observed a lot of DE genes not differentially expressed in other cell types (**Figure 4.11a-b**). Additionally, several genes uniquely expressed in microglia were among the DE genes such as *MS4A6A* and *HLA-DRB1*. *MS4A6A* displays the highest magnitude of change (log2FC: 0.059 per year) of all DE genes (**Figure 4.12e)**. It has crucial roles in immune response and SNPs in this gene have been linked to AD [190, 191]. *HLA*-DRB1 shows a significant increase with age (**Figure 4.12f)** and genetic associations

with longevity [192] and AD [193] have been reported for this gene. Overall, this provides evidence that age affects the expression of a multitude of genes with certain genes being regulated only in specific cell types and others changing in a coordinated manner across several cell types.

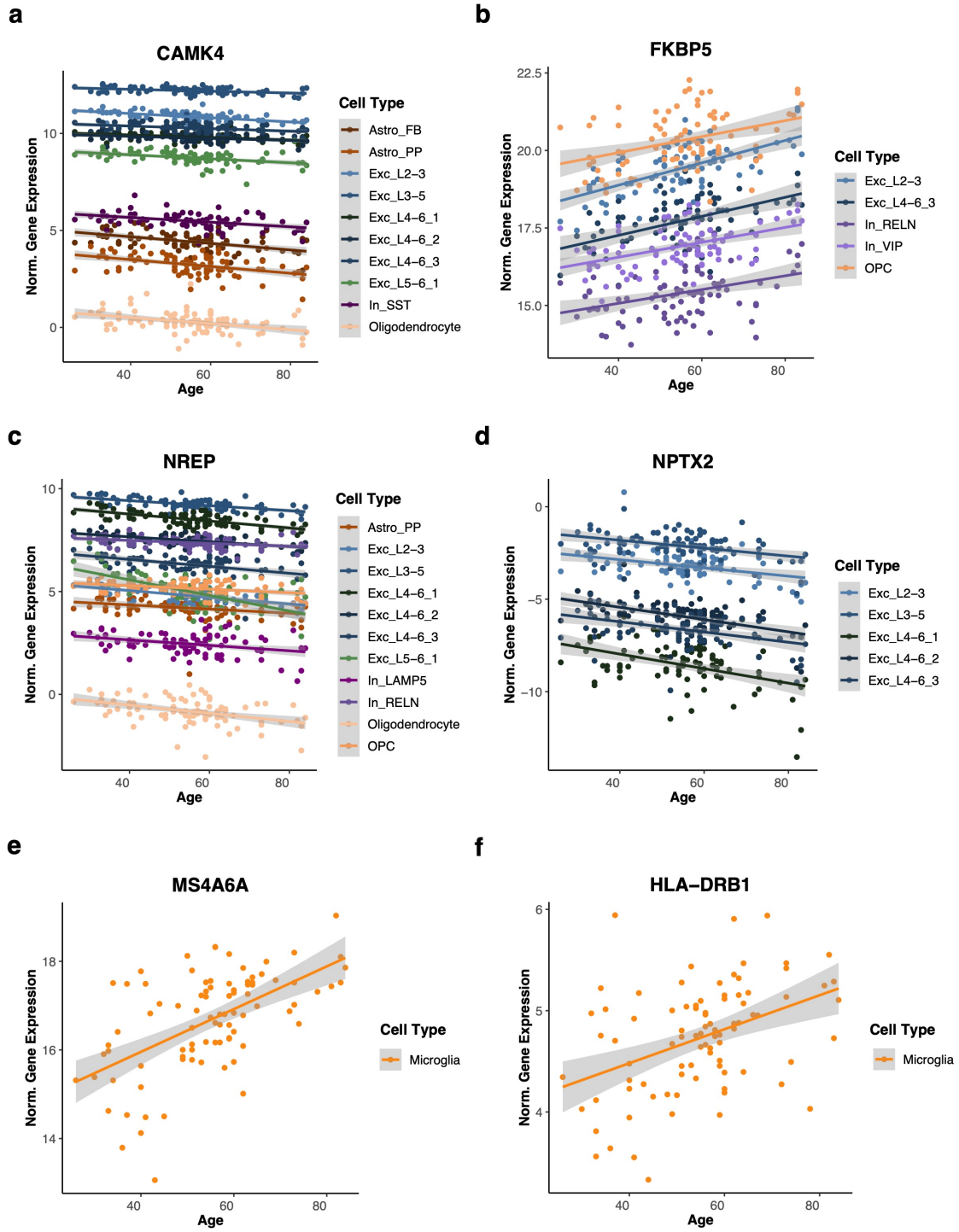

Figure 4.12: Shared and cell-type specific age-regulated genes **a-f**, Scatterplots showing log normalized gene expression corrected for covariates across ageing of significantly differentially expressed genes in respective cell types for *CAMK4* (**a**), *FKBP5* (**b**), *NREP* (**c**), *NPTX2* (**d**), *MS4A6A* (**e**) and *HLA-DRB1* (**f**). Error bands represent the 95% confidence interval.

4.5 Changes in cell-type abundance during ageing

Next, we examined if cellular composition changes during ageing. We calculated the proportion of each cell type per individual and then applied multiple linear regression to test for an association of age and cell type proportion. We found that the majority of the cell types do not change in abundance (**Table 4.3**). However, In_VIP and OPCs showed a significant reduction with age whereas oligodendrocytes increased with age.

Table 4.3: Most cell types do not change in abundance with age

Cell Type	Estimate	t statistic	p value	FDR adj. p value
Astro_FB	-0.026	-1.667	0.100	0.170
Astro_PP	-0.096	-2.224	0.030	0.099
Endothelial	-0.006	-0.667	0.507	0.534
Exc_L2-3	0.056	0.720	0.474	0.527
Exc_L3-5	0.007	1.340	0.185	0.247
Exc_L4-6_1	0.023	1.658	0.102	0.170
Exc_L4-6_2	0.026	1.849	0.069	0.165
Exc_L4-6_3	0.021	1.891	0.063	0.165
Exc_L5-6_1	0.009	1.264	0.211	0.264
Exc_L5-6_2	0.001	1.373	0.175	0.247
Exc_L5-6_HTR2C	0.003	1.397	0.167	0.247
In_LAMP5	-0.003	-0.724	0.472	0.527
In_PVALB_Ba	0.004	0.502	0.617	0.617
In_PVALB_Ch	-0.005	-2.511	0.015	0.058
In_RELN	-0.018	-1.815	0.074	0.165
In_SST	-0.030	-2.543	0.013	0.058
In_VIP	-0.033	-2.892	0.005	0.048
Microglia	-0.038	-1.719	0.090	0.170
Oligodendrocyte	0.151	2.772	0.007	0.048
OPC	-0.047	-4.163	0.000	0.002

4.6 Validation of transcriptomic changes across ageing in bulk brain datasets

After having identified cell-type-specific age-regulated genes, we wanted to evaluate how our results compared to previous studies. Most of the published studies examining gene expression changes with age in human brain, have used bulk sequencing methods. Thus, to be able to compare with these bulk studies, we generated a 'full pseudobulk' dataset by summing the gene-wise counts within each individual across all cell types before performing DGE analysis. In total, 2387 genes were identified as age-regulated (FDR-adjusted p-value <0.1). Next, we used Fisher's exact test, to test for overlap of our identified DE genes with two studies by Lu and colleagues [154] and Kumar and colleagues [155] having identified age-regulated genes in human cortex. We could show a significant overlap for both age up- and downregulated DE genes with the study by Lu et al. as well as a significant overlap with age-regulated genes identified by Kumar et al. (directionality of effect was not available) underscoring the validity of our analysis (**Table 4.4a-b**).

Table 4.4: Validation of transcriptomic changes across ageing with previously published bulk datasets.

a

Age DE genes this study	Age DE genes Lu et al.	n overlap genes	Genome size	overlap p-value	Odds Ratio	direction
961	262	18	22025	0.039	1.629	up
1426	157	36	22025	0.000	4.383	down

b

Age DE genes this study	Age DE genes Kumar et al.	n overlap genes	Genome size	overlap p-value	Odds Ratio	direction
2387	48	13	22025	0.001	3.067	not considered

4.7 Validation of transcriptomic changes across ageing in several cell types

Next, we wanted to validate our cell-type-specific age-regulated genes. Since LAMP5 inhibitory neurons were identified as the cell type most severely affected by age, we wanted to validate the extent of age-regulated genes in this cell type in an independent dataset. Chatzinakos and colleagues [157] had identified the same cell type in their sn-RNA-seq dataset derived from 32 samples from the dorsolateral prefrontal cortex (of a cohort consisting of controls and individuals having suffered from MDD and post-traumatic stress disorder). We performed DGE analysis for age in this cell type and observed a significant overlap for both up- and downregulated age DE genes (**Table 4.5a, Figure 4.13a**). Next, we used Spearman correlation to compare the effect sizes (log2FC) and found highly congruent directionality of effect and effect sizes as evidenced by a Spearman correlation coefficient (ρ) of log2FC of 0.74 (p-value < 2.2e-16). Then, we compared our identified DE genes in microglia and astrocytes (broad cell type cluster) with studies that combined cell purification with bulk RNA-sequencing. Krawczyk and colleagues [159] had isolated astrocytes whereas Galatro and colleagues [158] had purified microglia to study gene expression changes over the course of ageing in these cell types. For astrocytes, we identified a significant overlap in downregulated age DE genes and in microglia both up- and downregulated age DE genes showed a significant overlap between the two studies (**Table 4.5b-c**). The directionality of effect was highly congruent for both astrocytes and microglia, with high correlations of the effect sizes between the overlapping DE genes in astrocytes (ρ of log2FC: 0.66, p-value: 0.024; **Figure 4.13b**) and in microglia (ρ of log2FC: 0.88, p-value: 1.6e-6**; Figure 4.13c**). These analyses provide validation of age-regulated genes within specific cell types and across methodological approaches, emphasizing the consistency of findings between different sn-RNA-seq datasets as well as the comparability between data from sn-RNA-seq and sequencing in sorted cell populations.

Table 4.5: Validation of transcriptomic changes across ageing In_LAMP5 (a), astrocytes (b) and microglia (c).

a

Cell type	In_LAMP5 Age DE genes this study	In_LAMP5 Age DE genes Chatzinakos et al.	n overlap genes	Genome size	overlap p-value	Odds Ratio	direction
In_LAMP5	343	484	78	9127	1.23E-29	6.07	up
In_LAMP5	750	742	285	9127	4.41E-133	10.62	down

b

Cell type	Astro Age DE genes this study	Astro Age DE genes Krawczyk et al.	n overlap genes	Genome size	overlap p-value	Odds Ratio	direction
Astrocytes	47	34	1	10499	1.42E-01	6.86	up
Astrocytes	53	97	12	10499	3.76E-14	35.59	down

c

Cell type	Mic Age DE genes this study	Mic Age DE genes Galatro et al.	n overlap genes	Genome size	overlap p-value	Odds Ratio	direction
Microglia	71	38	8	4007	2.08E-07	16.49	up
Microglia	73	114	14	4007	9.24E-09	9.08	down

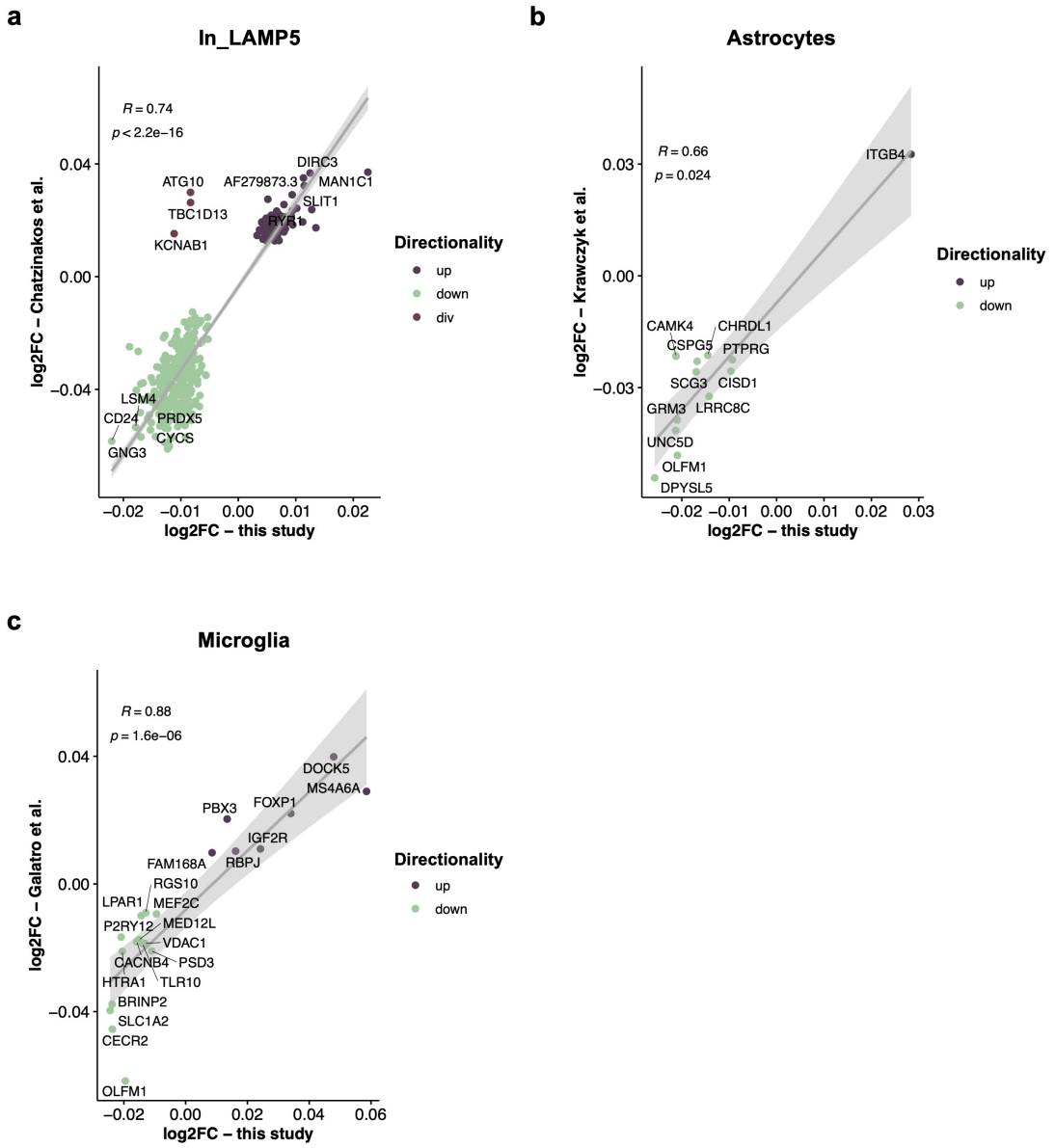

Figure 4.13: Validation of transcriptomic changes across several cell types **a**, Scatterplot depicting log2FC of overlapping DE genes and spearman correlation (**a**) in In_LAMP5 between this study (x-axis; DE genes with FDR-adjusted p-value < 0.1) and DE genes identified in In_LAMP5 by Chatzinakos et al. [157] (y-axis; DE genes with nominal p-value < 0.05); The five genes with highest positive and negative log2FC (in both studies) and genes with divergent (div) directionality are labelled **b-c**, Scatterplot depicting log2FC of overlapping DE genes and spearman correlation (**b**) in astrocytes between this study (x-axis; DE genes with FDR-adjusted p-value < 0.1) and a study by Krawczyk et al. [159] (y-axis; DE genes with FDR-adjusted p-value < 0.05); (**c**) in microglia between this study (x-axis; DE genes with FDR-adjusted p-value < 0.1) and a study by Galatro et al. [158] (y-axis; DE genes with FDR-adjusted p-value < 0.05). All overlapping genes are labelled. Error bands represent the 95% confidence interval.

4.8 Affected biological pathways in ageing

To identify in which biological pathways the age-regulated genes are involved, we split age DE genes (at FDR-adjusted p-value <0.1) in up- and downregulated and performed over-representation analysis (ORA). Since often-times several gene-ontology (GO) terms contain a similar set of genes and are therefore related, we next applied semantic similarity analysis. This groups similar terms thereby decreasing redundancies within the list of significantly enriched GO terms. Seven cell types showed significantly enriched pathways within their upregulated DE genes (**Supplementary Table 4**), whereas seventeen cell types showed significantly enriched pathways within their downregulated DE genes (**Supplementary Table 5**). A commonly upregulated process between the excitatory and inhibitory neurons was cytoskeleton organisation. However, most of the processes were specific for the respective cell type which relates back to a less coordinated transcriptional response within upregulated genes between cell types (as shown in **Figure 4.10**). Upregulated DE genes in microglia were involved in several immune processes including T-cell mediated immunity, regulation of leukocyte apoptotic process, and protein autoubiquitination (**Figure 4.14a**). This upregulation of immune pathways with age in microglia is consistent with findings from studies in both mice and humans (31,33). Interestingly, within the downregulated DE genes enrichment for GO-terms involved in synaptic signalling (e.g. chemical synaptic transmission, synapse organization, signal release), cellular ion homeostasis and G-protein-coupled receptor signalling was found across excitatory and inhibitory neurons but also all glial cells, except microglia (**Figure 4.14b-d)**. Several metabolic processes including nucleotide metabolic process, glycoprotein biosynthetic process and carbohydrate metabolic process were affected in inhibitory neurons. LAMP5 inhibitory neurons specifically showed enrichment for cellular respiration (oxidative phosphorylation) pathways (**Figure 4.14d)**. Overall, this indicates that besides different genes changing during ageing in the different cell types, these are involved in similar pathways, especially neurotransmission. Additionally, certain pathways are dysregulated specifically in inhibitory neurons.

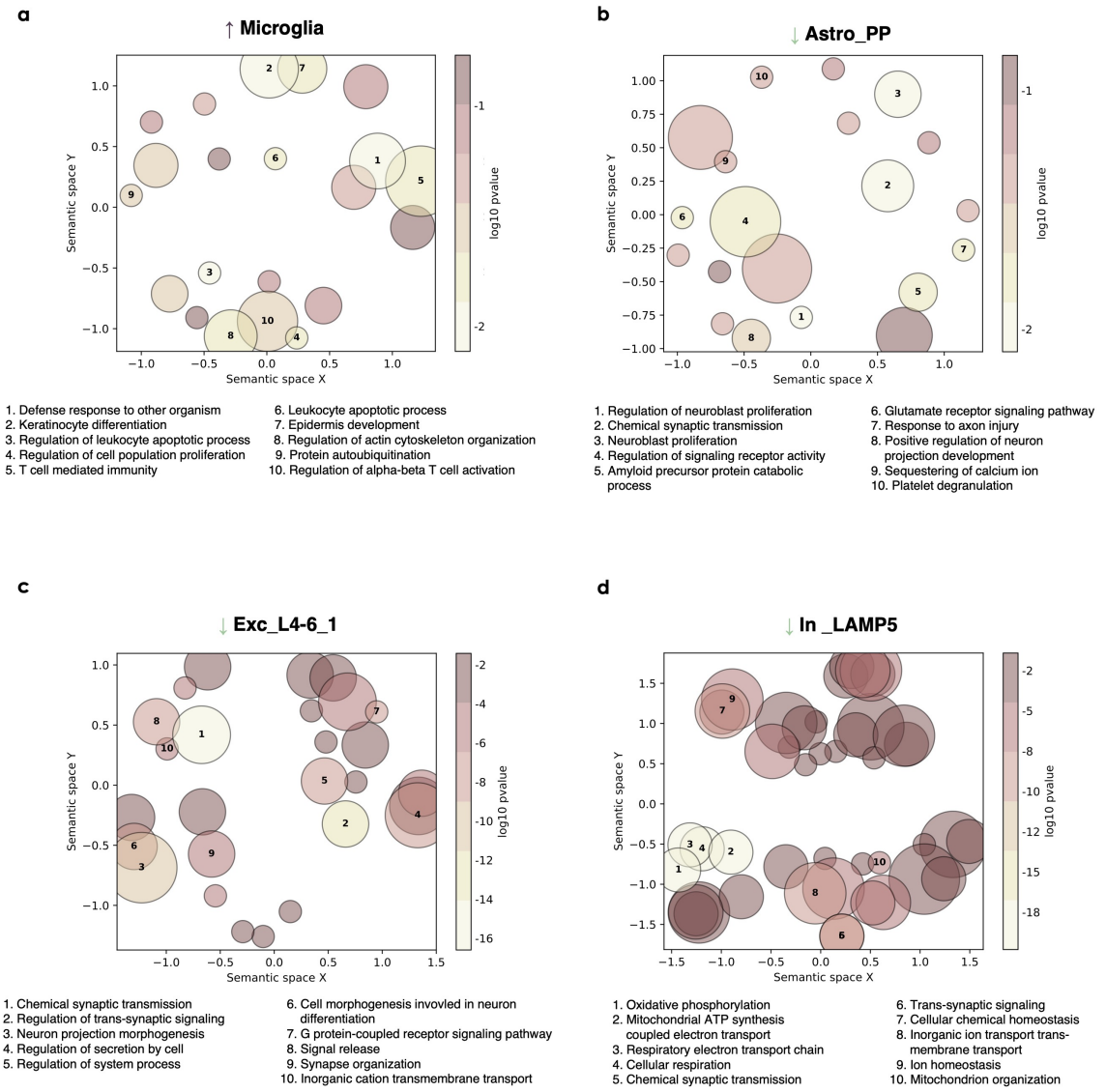

Figure 4.14: Affected biological pathways in ageing **a-d**, Representative semantic similarity scatterplots depicting significantly enriched biological processes (at FDR-adjusted p-value < 0.05) in the upregulated age DE genes in microglia (**a**) and the downregulated age DE genes in Astro_PP (**b**), Exc_L4-6_1 (**c**) and In_LAMP5 (**d**). Semantic similarity analysis places similar GO terms more closely together on a semantic space x and y. The circle is proportional to the number of GO terms representing the circle and the colour represents the log10 p-value.

4.9 Enrichment of diseases in age-regulated genes

Next, we wanted to investigate whether age-regulated genes have been associated with specific diseases. We therefore performed disease enrichment analysis and found that downregulated age DE genes across several cell types showed an enrichment for genes linked to cognitive disorder as well as psychiatric disorders including schizophrenia (**Figure 4.15a-h**). Upregulated age DE genes did not show enrichment for any brain-related disorders (**Supplementary Table 6**).

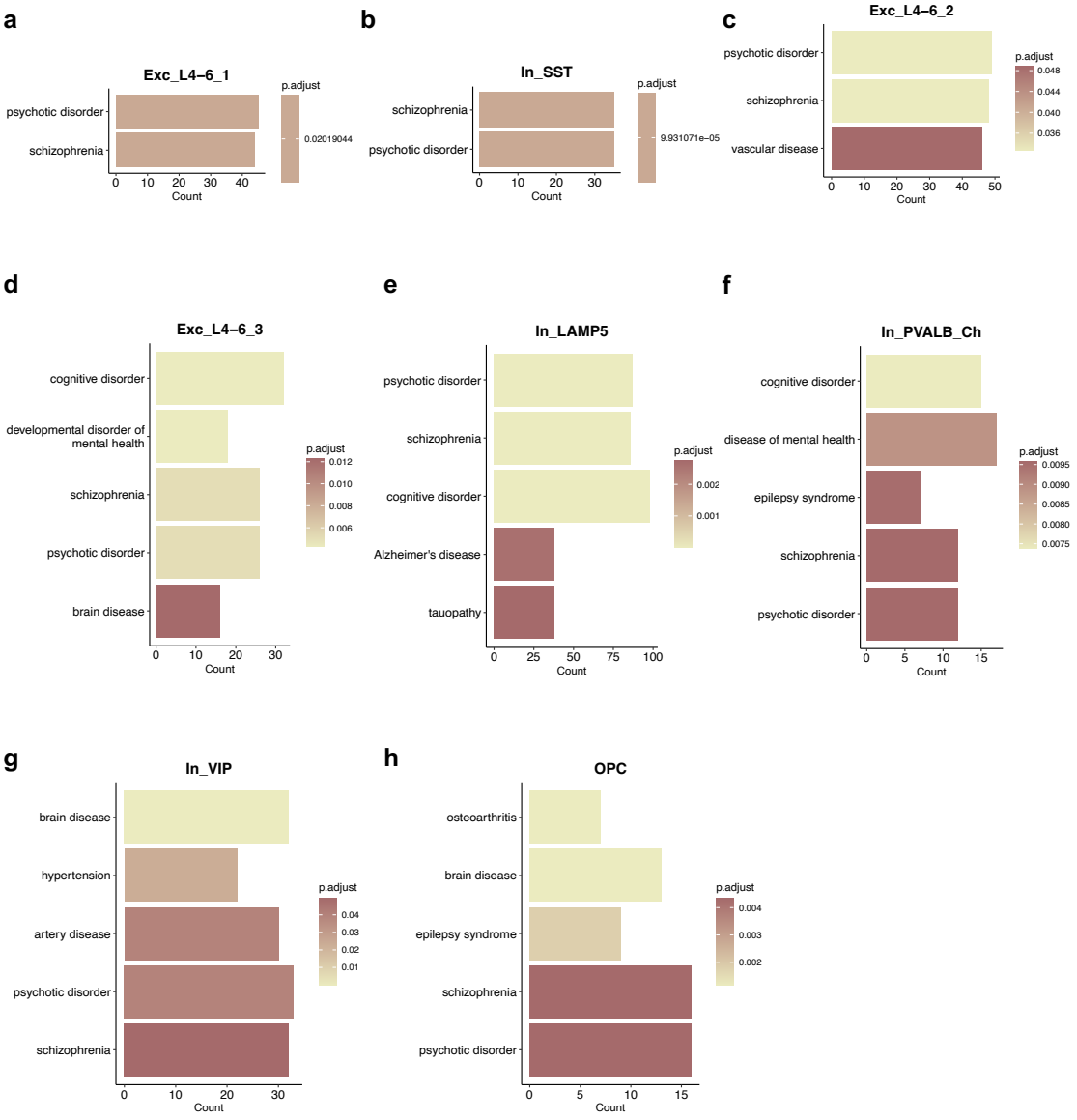

Figure 4.15: Enrichment of diseases in age-regulated genes **a-h**, Bar plots depicting the disease enrichment (at FDR-adjusted p-value < 0.05) of downregulated age DE genes across cell types. Top five disease terms (based on FDR-adjusted p-value) are shown. For cell types that had less than five significantly enriched terms, all terms are shown (**a-c**; Exc_L4-6_1, In_SST, Exc_L4-6_2). The colour of the bars represents the FDR-adjusted p-value.

4.10 Age-regulated genes overlap with genes associated with Alzheimer's disease

Since age is the biggest risk factor for neurodegenerative diseases such as AD, we next investigated whether age-regulated genes could play a role in AD. We therefore compared age DE genes with DE genes identified in AD. Two studies, one by Mathys and colleagues [132] and another one by Lau and colleagues [133], had compared gene expression in controls and individuals with AD at the single cell level in the prefrontal cortex. These two AD studies had assigned broad cell type classes only (astrocytes, endothelial cells, excitatory and inhibitory neurons, microglia, oligodendrocytes, and OPCs (only in [132])) and we therefore compared them to our DE results in broad cell type clusters. We used Fisher's exact test to evaluate the overlap of genes upregulated in AD and upregulated with age and of genes downregulated in AD and downregulated with age. Consistent with both AD studies, we show that genes upregulated in individuals with AD in astrocytes and oligodendrocytes significantly overlap with up-regulated age DE genes in the respective cell types (**Figure 4.16, Table 4.6a,c).** Moreover, genes downregulated in individuals with AD in astrocytes and excitatory neurons significantly overlap with up-regulated age DE genes in the respective cell type (**Figure 4.16, Table 4.6b,d**).

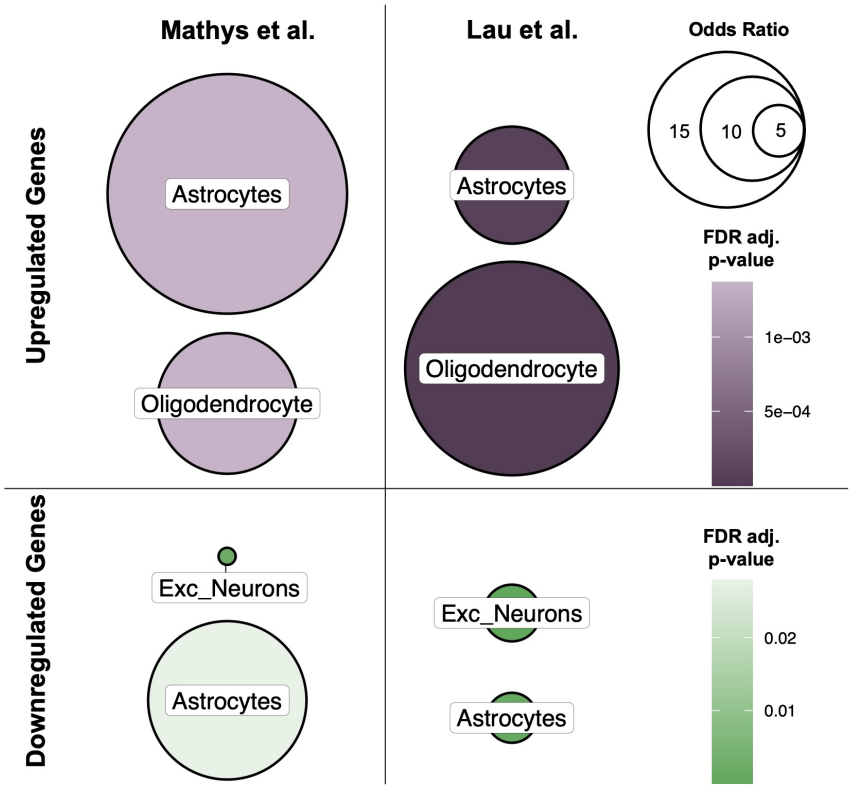

Figure 4.16: Overlap of age-regulated genes with genes dysregulated in AD Visualisation of the overlap of age DE genes with AD DE genes (from two AD sn-RNA-seq datasets; Mathys et al. [132] and Lau et al. [133]) for up- and downregulated genes respectively. Overlaps are only shown if these were significant in both AD datasets. The circle is proportional to the odds ratio and the colour represents the FDR-adjusted p-value (see also **Table 4.6**).

Table 4.6: Overlap of age-regulated genes with genes dysregulated in AD.

a – Comparison of upregulated age DE genes with upregulated AD DE genes (Mathys et al.)

Broad Cell Type	Age DE genes this study	AD DE genes Mathys et al.	n overlap genes	Genome size	overlap p-value	FDR adj. p-value	Odds Ratio
Astrocytes	47	34	3	10499	4.56E-04	1.37E-03	22.87
Exc_Neurons	1324	181	15	19752	2.33E-01	3.50E-01	1.26
In_Neurons	358	3	0	16108	1.00E+00	1.00E+00	0.00
Microglia	71	18	0	4007	1.00E+00	1.00E+00	0.00
Oligodendrocyte	30	90	4	7629	3.93E-04	1.37E-03	13.42
OPC	78	7	1	9143	5.82E-02	1.16E-01	19.57

b – Comparison of downregulated age DE genes with downregulated AD DE genes (Mathys et al.)

Broad Cell Type	Age DE genes this study	AD DE genes Mathys et al.	n overlap genes	Genome size	overlap p-value	FDR adj. p-value	Odds Ratio
Astrocytes	53	29	2	10499	9.30E-03	2.79E-02	15.12
Exc_Neurons	1545	533	64	19752	3.92E-04	2.35E-03	1.63
In_Neurons	722	46	5	16108	5.39E-02	1.08E-01	2.61
Microglia	73	10	0	4007	1.00E+00	1.00E+00	0.00
Oligodendrocyte	30	64	0	7629	1.00E+00	1.00E+00	0.00
OPC	130	16	1	9143	2.05E-01	3.07E-01	4.65

c – Comparison of upregulated age DE genes with upregulated AD DE genes (Lau et al.)

Broad Cell Type	Age DE genes this study	AD DE genes Lau et al.	n overlap genes	Genome size	overlap p-value	FDR adj. p value	Odds Ratio
Astrocytes	47	141	6	10499	3.60E-05	6.00E-05	11.17
Exc_Neurons	1324	193	7	19752	9.77E-01	9.77E-01	0.52
In_Neurons	358	26	1	16108	4.43E-01	5.53E-01	1.76
Microglia	71	91	14	4007	2.95E-10	1.47E-09	12.28
Oligodendrocyte	30	141	8	7629	4.63E-08	1.16E-07	20.38

d – Comparison of downregulated age DE genes with downregulated AD DE genes (Lau et al.)

Broad Cell Type	Age DE genes this study	AD DE genes Lau et al.	n overlap genes	Genome size	overlap p-value	FDR adj. p value	Odds Ratio
Astrocytes	53	383	8	10499	6.13E-04	1.02E-03	4.77
Exc_Neurons	1545	142	44	19752	6.24E-16	3.12E-15	5.42
In_Neurons	722	91	17	16108	5.05E-07	1.26E-06	4.99
Microglia	73	193	6	4007	1.38E-01	1.72E-01	1.79
Oligodendrocyte	30	359	2	7629	4.16E-01	4.16E-01	1.45

Examples of genes with this concordant change with age and in AD include *SLC6A15*, *GRM3* and *RPH3A* (**Figure 4.17**). *SLC6A15*, an amino acid transporter, is significantly upregulated with age and shows higher expression in AD cases in oligodendrocytes (**Figure 4.17a-b**). It is a risk gene for MDD [194] but also has been genetically linked to AD [195]. *GRM3* is downregulated with age and downregulated in AD (**Figure 4.17c-d)**. SNPs within *GRM3* have been associated with increased risk for schizophrenia as well as poorer cognitive function [196]. *RPH3A*, a gene involved in neurotransmitter release, is downregulated in excitatory neurons both with age and in AD (**Figure 4.17e-f)**. Higher RPH3A protein levels in human prefrontal cortex have been associated with cognitive resilience [197], whereas lower levels have been associated with higher Aβ burden [198]. These results suggest that the development of AD could possibly be favoured when gradual changes in gene expression during ageing, especially in astrocytes, surpass a certain threshold level.

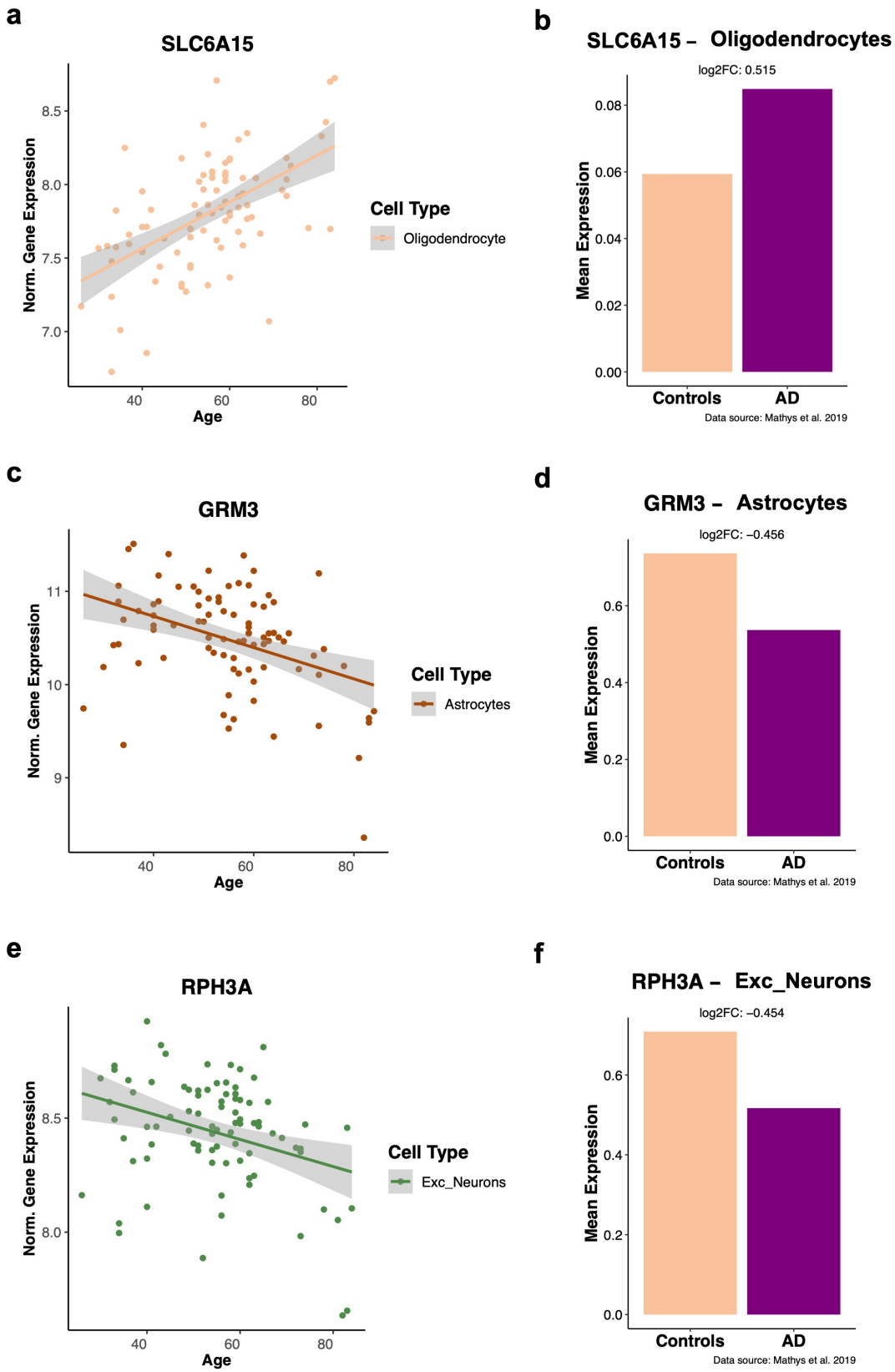

Figure 4.17: Examples of genes with concordant change with age and in AD. a,c,e, Scatterplots depicting log normalized gene expression corrected for covariates across ageing in the respective cell types for *SLC6A15* (**a**), *GRM3* (**c**), and *RPH3A* (**e**). **b,d,f**, Bar plots depicting mean expression level of *SLC6A15* (**b**), *GRM3* (**d**), and *RPH3A* (**f**) and fold change (log2FC) between controls and cases with AD. Data was taken from Mathys et al. [132].

As a next step, we investigated whether we could identify genes with an opposite regulation between ageing and AD. To this end, we compared upregulated age DE genes (at an FDR-adjusted p-value <0.1) with AD downregulated genes and vice versa for each broad cell type. We were able to identify two genes, *LINGO1* and *KCTD17*, which decrease with age (**Figure 4.18a,c**) however are increased in individuals with AD in excitatory neurons (**Figure 4.18b,d**). These genes could be of interest for drug targeting as they may serve as protective factors.

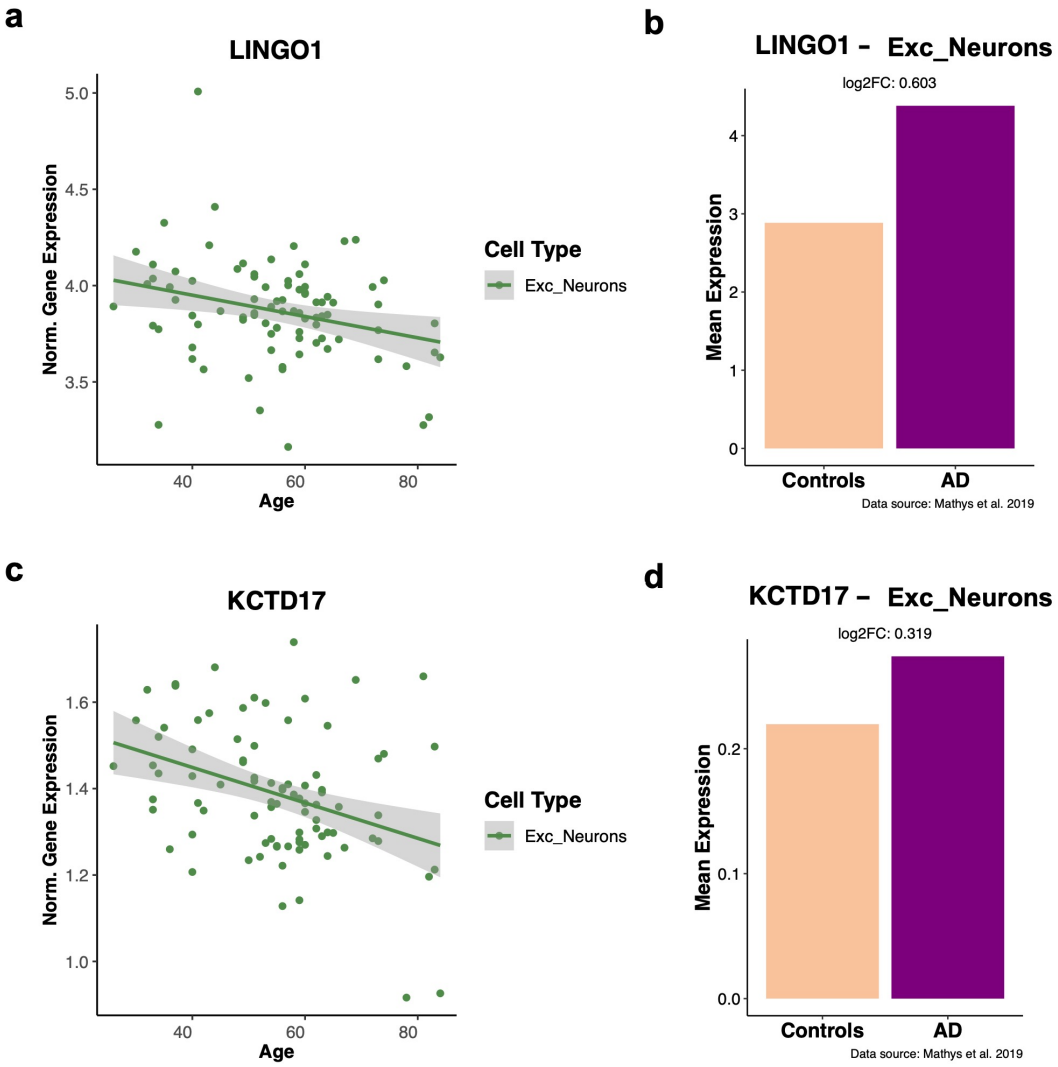

Figure 4.18: Divergent gene expression changes between ageing and AD. **a,c**, Scatterplots depicting log normalized gene expression corrected for covariates across ageing of the two DE genes whose expression decreases with age - *LINGO1* (**a**) and *KCTD17* (**c**) - but is increased in cases of AD compared to controls. Error bands represent the 95% confidence interval. **b,d**, Bar plots depicting mean expression level of *LINGO1* (**b**), and *KCTD17* (**d**) and fold change (log2FC) between controls and cases with AD. Data was taken from Mathys et al. [132].

4.11 Evidence of accelerated transcriptomic ageing in psychiatric disorders across multiple cell types

Transdiagnostically, severe mental disorders, which include BPD, MDD, and SCZ, have been associated with lower life expectancy [199] and elevated risk of developing neurodegenerative disorders [42], which are further linked to a higher mortality rate. Moreover, previous research provides evidence that biological ageing is accelerated in psychiatric disorders. These studies used diverse modalities in different tissues such as DNA methylation in blood [46-48], gene expression [49] and magnetic resonance imaging (MRI) [50] in brain for the estimation of biological age. Therefore, we calculated both epigenetic and transcriptomic age (acceleration) in our cohort to investigate differences between controls and psychiatric cases.

Using EPIC arrays, we quantified bulk DNA methylation (DNAm) levels from the same OFC tissue. Next, we computed DNAm age using two epigenetic clocks, the CorticalClock derived from human cortex as well as Horvath's multi-tissue clock. We found that the estimated DNAm age correlated highly with the chronological age (**Figure 4.19**; CorticalClock: Pearson correlation coefficient (R) of 0.96, p-value: < 2.2e-16; Horvath's multi-tissue clock: R=0.94, p-value: < 2.2e-16). We then calculated DNAm age acceleration by regressing DNAm age estimate on chronological age and used multiple linear regression to evaluate differences between controls and psychiatric cases. However, no difference in epigenetic age acceleration between the two groups was found (**Table 4.7**).

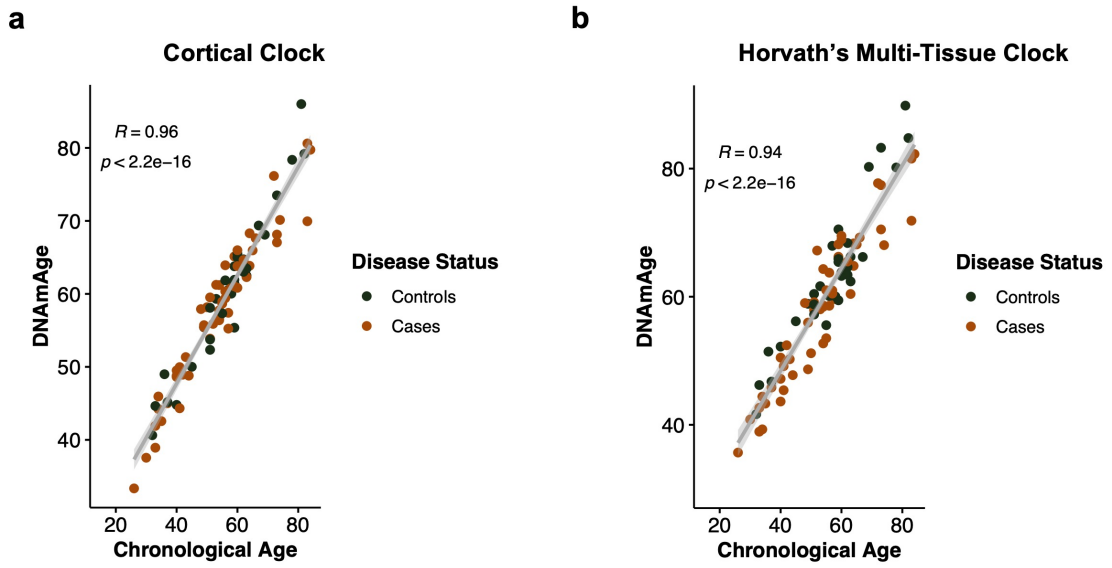

Figure 4.19: Estimation of epigenetic age. a-b, Scatterplots depicting the Pearson correlation coefficient (R) of chronological age (x-axis) with DNA methylation age (DNAmAge; y-axis) estimated using the CorticalClock (**a**) and Horvath's multi-tissue clock (**b**). Error bands represent the 95% confidence interval.

Table 4.7: Multiple linear regression of epigenetic age acceleration

a – Cortical Clock

Predictors	Estimates	CI	p-value	FDR adj. p-value
(Intercept)	-0.44	-9.60 – 8.71	0.923	1
Sex [Male]	0.47	-0.92 – 1.87	0.499	0.998
Smoking status [Ex-smoker]	0.21	-1.73 – 2.14	0.831	1
Smoking status [Current]	0.11	-1.36 – 1.57	0.885	1
propNeuron	0.17	-19.35 – 19.68	0.986	1
Disease Status [Cases]	-0.33	-1.67 – 1.02	0.628	1
Observations	79			
R^2 / R^2 adjusted	0.013 / -0.055			

b – Horvath's multi-tissue clock

Predictors	Estimates	CI	p-value	FDR adj. p-value
(Intercept)	11.85	-0.42 – 24.12	0.058	0.116
Sex [Male]	0.48	-1.39 – 2.35	0.612	1
Smoking status [Ex-smoker]	0.25	-2.35 – 2.84	0.851	1
Smoking status [Current]	0.81	-1.15 – 2.78	0.413	0.826
propNeuron	-24.80	-50.96 – 1.36	0.063	0.126
Disease Status [Cases]	-2.05	-3.85 – -0.24	0.027	0.054
Observations	79			
R^2 / R^2 adjusted	0.125 / 0.065			

We next estimated transcriptomic age using a transcriptomic brain age predictor developed by Lin et al. [49] that was derived from the exact same cortical brain region, BA11. Since the transcriptomic brain age predictor was developed using bulk gene expression, we used our 'full pseudobulk' dataset. We obtained age acceleration by regressing transcriptomic brain age estimates on chronological age. The predicted transcriptomic age correlated highly with chronological age (**Figure 4.20**, R=0.83, p-value: < 2.2e-16). Moreover, we were able to replicate within our cohort the previously reported age acceleration in cases of severe mental disorders using multiple linear regression (p-value: 0.02; **Table 4.8)**

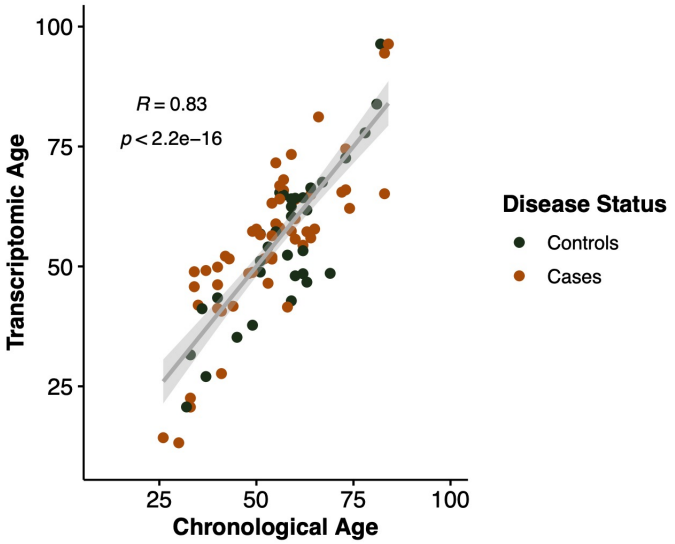

Figure 4.20: Estimation of transcriptomic age. Scatterplot depicting the Pearson correlation coefficient (R) of chronological age (x-axis) with transcriptomic age (y-axis). Error band represents the 95% confidence interval.

Table 4.8: Multiple linear regression of transcriptomic age acceleration

Predictors	Estimates	CI	p-value
(Intercept)	-22.60	-79.85 – 34.66	0.435
PC1	-0.03	-0.12 – 0.06	0.517
RIN	0.39	-1.40 – 2.17	0.667
PMI	-0.07	-0.19 – 0.04	0.200
Brain pH	2.70	-6.98 – 12.37	0.581
Sex [Male]	2.76	-0.65 – 6.16	0.111
Disease Status [Cases]	4.27	0.68 – 7.87	0.020
Observations	87		
R^2 / R^2 adjusted	0.119 / 0.053		

The fact that we found evidence for accelerated transcriptomic age in psychiatric cases as well as an enrichment of age-downregulated DE genes for genes implicated in psychiatric disorders, led us to further investigate how ageing trajectories of gene expression may be shifted in severe mental disorders. Thus, we first tested for interactive effects of age and disease status. Only two genes, namely *SLC25A37* in fibrous astrocytes (Astro_FB) and *GTPBP6* in a deep-layer neuronal cluster (Exc_L4-6_3), with an interactive effect of age and disease status, were identified (**Figure 4.21**). This small number of detected genes could be due to insufficient power for these types of statistical analysis. *SLC25A37* encodes a mitochondrial iron carrier and is a risk gene for major depression [200]. *GTPBP6*, a GTP-binding protein, is involved in the assembly and dissociation of mitochondrial ribosomes [201].

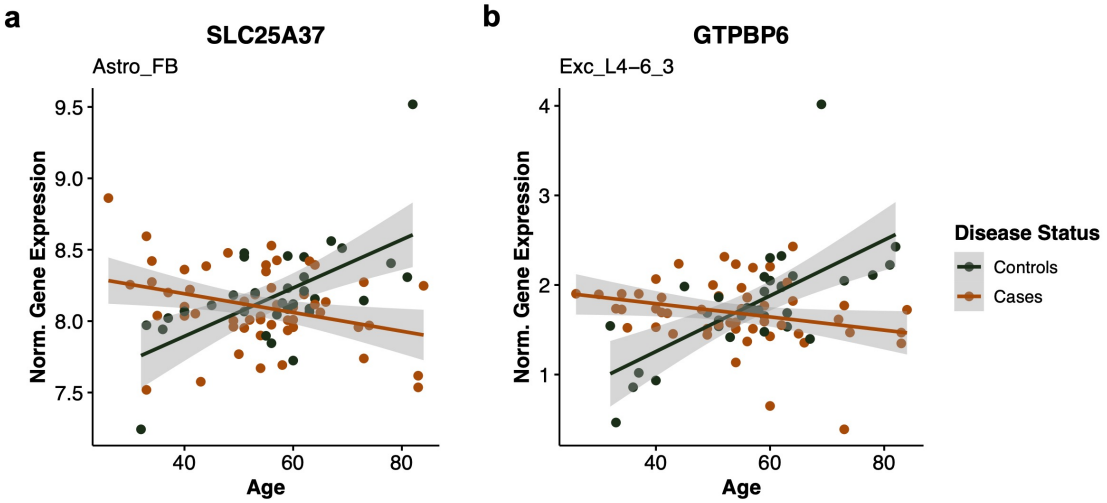

Figure 4.21: Genes with an interactive effect of age and disease status. a-b, Scatterplots depicting log normalized gene expression corrected for covariates across ageing for genes with an interactive effect between ageing and disease status; *SLC25A37* in Astro_FB (**a**) and *GTPBP6* in Exc_L4-6_3 (**b**). Error bands represent the 95% confidence interval.

Next, we wanted to understand the extent of the overlap of age-regulated genes with disease-status-associated genes. We therefore performed differential gene expression analysis for disease status and found several genes significantly associated with disease status within different cell types as shown in **Table 4.9**. The much lower number of disease-associated DE genes compared to age-regulated DE genes is consistent with the result from variance partitioning (**Figure 3.5d**) which showed that age contributed much more to the variance of gene expression than disease status. Therefore, to detect small changes, large statistical power is needed. In line with this, the highest number of disease-associated genes was detected in upper-layer excitatory neurons (Exc_L2-3); the cell type with the largest number of nuclei. We then compared the age-regulated with the disease-associated genes (at FDR-adjusted p-value <0.1) and found that, within four excitatory neuron clusters and OPCs, a substantial proportion of disease-associated genes was also age-regulated (**Figure 4.22**).

Table 4.9: Number of differentially expressed genes associated with disease status shown per cell type at FDR-adjusted p-value < 0.1 and < 0.05.

Cell type	FDR < 0.1	FDR < 0.05
Astro_FB	0	0
Astro_PP	0	0
Endothelial	0	0
Exc_L2-3	136	44
Exc_L3-5	0	0
Exc_L4-6_1	125	49
Exc_L4-6_2	70	9
Exc_L4-6_3	9	0
Exc_L5-6_1	0	0
Exc_L5-6_2	0	0
Exc_L5-6_HTR2C	0	0
In_LAMP5	0	0
In_PVALB_Ba	0	0
In_PVALB_Ch	0	0
In_RELN	0	0
In_SST	0	0
In_VIP	0	0
Microglia	0	0
Oligodendrocyte	1	1
OPC	2	2

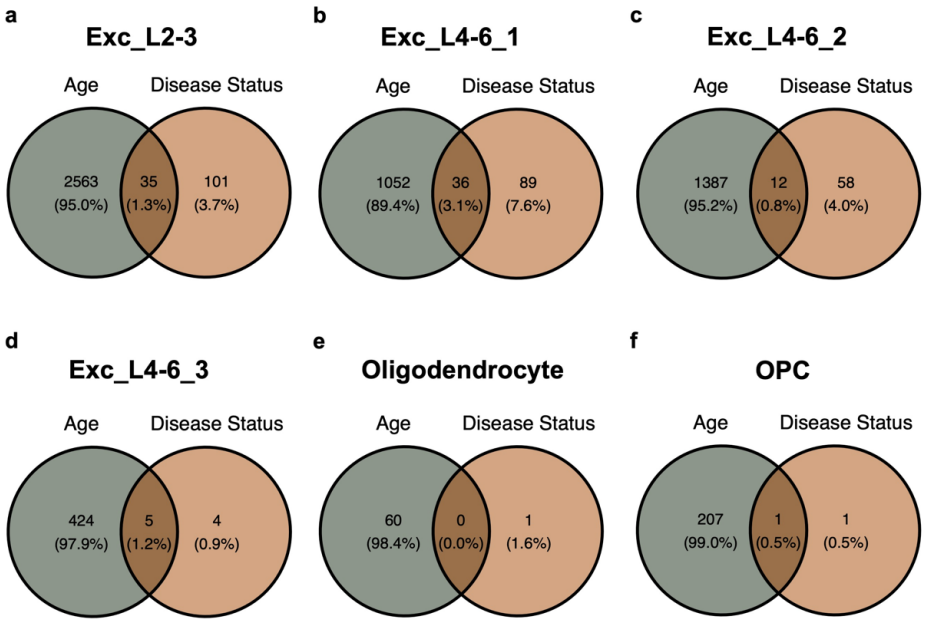

Figure 4.22: Comparison of age-regulated genes with disease-associated genes across cell types. a-f, Venn diagram showing the overlapping genes of age-regulated and disease-associated genes (at FDR-adjusted p-value < 0.1) for the respective cell type.

Fisher's exact test revealed a significant overlap for three excitatory neuron clusters (Exc_L2-3, Exc_L4-6_1, and Exc_L4-6_3; **Table 4.10**) between disease-associated and age-regulated genes.

Table 4.10: Overlap of age-regulated genes with disease-associated genes across cell types

Cell type	DE genes Disease Status	DE genes Age	n overlap genes	Genome size	overlap p-value	FDR adj. p-value	Odds Ratio
Exc_L2-3	136	2598	35	17960	0.0004	0.0008	2.06
Exc_L4-6_1	125	1088	36	12593	4.80E-11	2.88E-10	4.39
Exc_L4-6_2	70	1399	12	11954	0.1120	0.1344	1.57
Exc_L4-6_3	9	429	5	8617	3.19E-05	9.57E-05	24.10
Oligodendrocyte	1	60	0	7629	1	1	0.00
OPC	2	208	1	9143	0.0450	0.0675	43.06

Importantly, genes whose expression is influenced by both age and disease status can display a congruent or opposing directionality of effect of age and disease status. Congruent refers to genes with an upregulation with age and a higher expression in psychiatric cases or downregulation with age and a lower expression in psychiatric cases. Opposing, however, refers to genes with an upregulation with age and lower expression in psychiatric cases and vice versa. We therefore calculated the proportion of DE genes with a congruent or opposing directionality for the cell types that showed an overlap between age-regulated and disease-associated genes. This analysis revealed a concordance in expression change in all of the tested cell types (**Figure 4.23**). This concordance was especially pronounced in one of the deeper-layer neuron clusters (Exc_L4-6_3). These results indicate a convergent signature in gene expression change with ageing and in psychiatric disease providing evidence for accelerated ageing across multiple cell types.

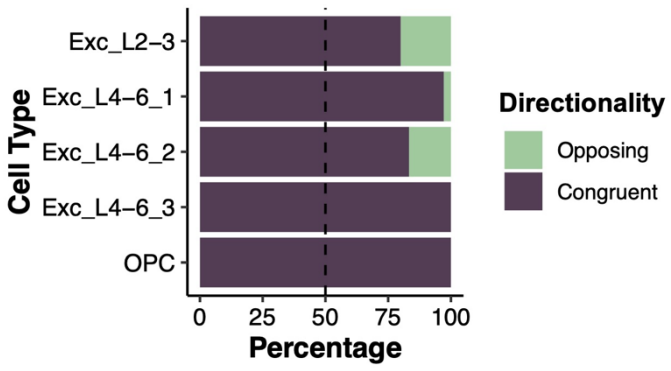

Figure 4.23: Concordance in expression change for genes associated with both age and disease status. Bar plot showing the percentage of DE genes (at FDR adj. p-value < 0.1) regulated in the same (congruent) direction or opposing directions amongst genes associated with both age and disease status for the respective cell types.

Genes displaying shifted ageing trajectories in psychiatric cases include genes previously linked to ageing. For example, *RHBDL3* is age and disease-regulated in Exc_L4-6-2 (**Figure 4.24a**) and has been previously associated with age [155]. It shows one of the most pronounced increases in expression with age. *LINC00507* is downregulated with age and in cases in Exc_L4-6_1 (**Figure 4.24b**) and has been shown to be age-regulated [202] and to show cortex-specific expression [203]. *APLF* shows one of the strongest decreases with age and a reduction in psychiatric cases in Exc_L2-3 (**Figure 4.24c**). *APLF* is involved in DNA repair, which has been linked to the ageing process [204] but up until now not to psychiatric disease. *COL19A1*, downregulated with age and disease in Exc_L4-6_3 (**Figure 4.24d**), is part of the family of nonfibrillar collagens and contributes to synapse formation [205]. UNC13C, the only gene which was age- and disease-downregulated in OPCs (**Figure 4.24e**), belongs to the Unc13 protein family, which is involved in (synaptic) vesicle fusion [206].

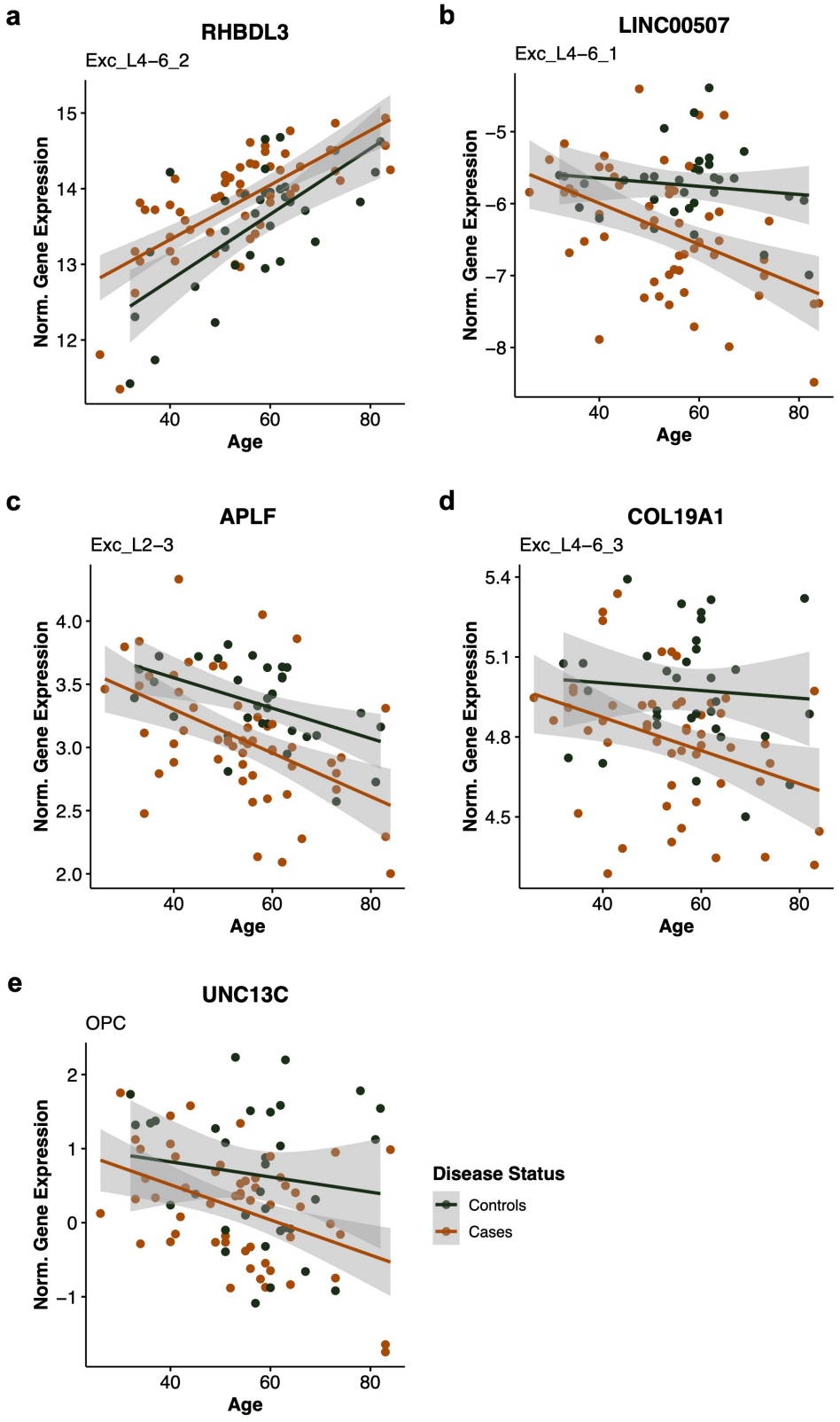

Figure 4.24: Examples of genes associated with both age and disease status. **a-e**, Scatterplots depicting log normalized gene expression corrected for covariates across ageing for genes associated with both age and disease status in the respective cell type; *RHBLD3* (**a**), *LINC00507* (**b**), *APLF* (**c**), *COL19A1* (**d**), *UNC13C* (**e**). Error bands represent the 95% confidence interval.

Since genetic factors contribute to the risk for psychiatric diseases, we wanted to examine if gene expression was influenced by polygenic risk. Using the genotype data, we calculated polygenic risk scores for each individual in our cohort for a cross-disorder psychiatric phenotype [179] and schizophrenia [22]. As expected, PRS for the cross-disorder phenotype was significantly higher (p-value: 0.0056; **Figure 4.25a**) in psychiatric cases and PRS for SCZ was trend-line increased (p-value: 0.054; **Figure 4.25b**), consistent with the mixed diagnosis within our cohort.

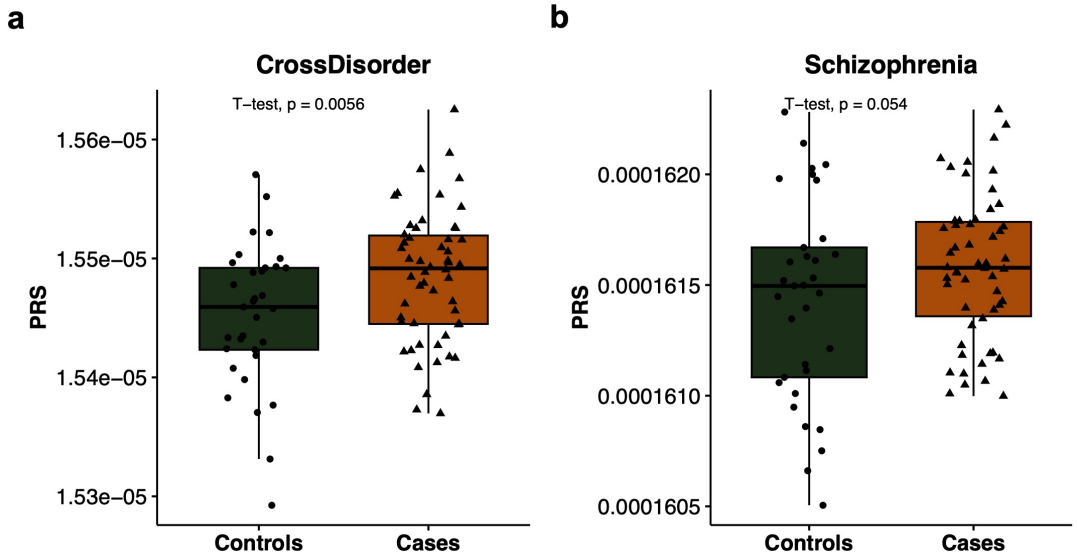

Figure 4.25: Polygenic risk scores between controls and psychiatric cases **a-b**, Boxplots depicting polygenic risk score (PRS) for the cross-disorder psychiatric phenotype (**a**) and schizophrenia (**b**) between controls and psychiatric cases. Groups were compared using one-sided t-test and p-value is shown.

Next, we stratified the cohort based on cross-disorder or SCZ PRS (instead of disease status) and performed differential gene expression analysis for PRS. However, we found that polygenic risk score was not associated with any genes in most of the cell types (**Supplementary Table 7**). This could be due to the fact that SNP-based heritability only explains a proportion of the heritability estimated by family and twin studies; SNP-based heritability in the case of schizophrenia is 24% [22]. To reduce the multiple testing burden, in an exploratory analysis, we only focused on the subset of disease-associated genes (at FDR-adj. p-value < 0.1; **Table 4.9**). We performed multiple testing correction on the nominal p-value only considering this subset. We reasoned that disease-associated genes are most likely to be associated with PRS, and that we might have enough power to detect small effects. Even amongst this subset, very few genes were associated with PRS at FDR <0.1, some of which overlapped with age-regulated genes and were regulated in a congruent manner (**Table 4.11** and **Table 4.12**). One example, *NREP*, is shown in **Figure 4.26**. It is downregulated with ageing, psychiatric cases show a lower expression and a higher cross-disorder-PRS is associated with a lower expression. This could indicate that a hypothetical

critical expression threshold of *NREP* is reached earlier in psychiatric cases and thereby could contribute to accelerated ageing. An underlying driver for this shift in the ageing trajectory between healthy controls and psychiatric cases could be genetic factors (as indicated by the association with cross-disorder-PRS). Yet, the exploratory nature of this analysis must be emphasized. Thus, genes with shifted ageing trajectories in psychiatric disease are likely the result of different factors including genetics, socio-economic and behavioural changes linked to the experience of living with the illness, environmental exposures as well as medication.

Table 4.11: Number of genes associated with cross-disorder PRS (within the subset of disease-associated genes). Genes overlapping with age-regulated genes are also shown.

Cell type	PRS_CrossD FDR <0.1	overlap with age-regulated genes	overlapping genes
Exc_L2-3	3	0	
Exc_L4-6_1	23	2	NREP; HES4
Exc_L4-6_2	2	0	
Exc_L4-6_3	7	3	AL158077.2; AC015943.1; AC034268.2
Oligodendrocyte	0	0	
OPC	2	1	UNC13C

Table 4.12: Number of genes associated with schizophrenia (SCZ) PRS (within the subset of disease-associated genes). Genes overlapping with age-regulated genes are also shown.

Cell type	PRS_SCZ FDR <0.1	overlap with age-regulated genes	overlapping genes
Exc_L2-3	0		
Exc_L4-6_1	0		
Exc_L4-6_2	0		
Exc_L4-6_3	2	1	AL158077.2
Oligodendrocyte	0		
OPC	0		

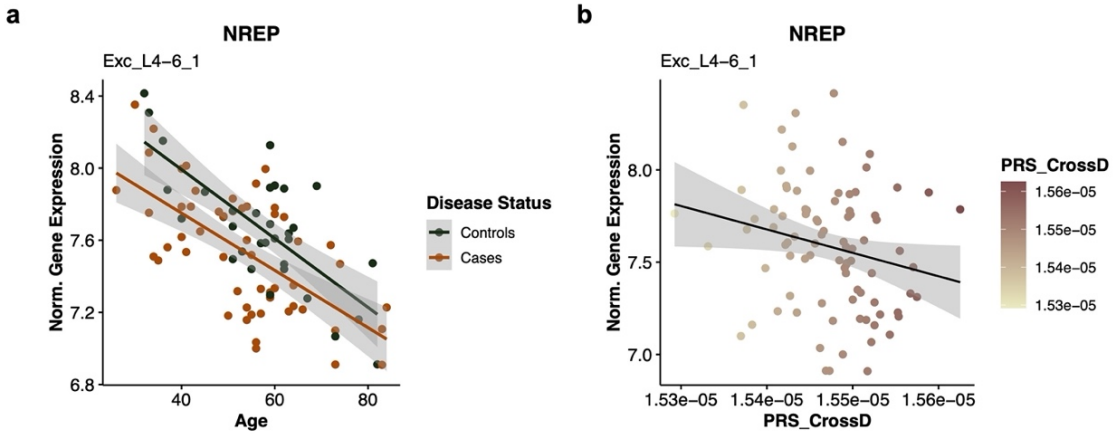

Figure 4.26: Example of a gene associated with age, disease status and cross-disorder PRS. a-b, Scatterplots depicting log normalized gene expression corrected for covariates for *NREP*. Expression shown along ageing with controls coloured in green and psychiatric cases in orange (**a**) and along cross-disorder (CrossD) PRS (**b**). Error bands represent the 95% confidence interval.

5 | Discussion

In this thesis, single nucleus RNA sequencing was used to characterize cell-type-specific gene expression changes associated with the ageing process in the human orbitofrontal cortex. Since the post-mortem brain cohort consisted of control individuals and individuals diagnosed with a psychiatric disease, the influence of disease status on ageing could further be explored. Integration of publicly available sn-RNA-seq datasets from healthy controls and individuals with AD allowed us to examine the potential role of age-related gene expression changes in AD in individual cell types. We were able to show that ageing affects the transcription of a substantial fraction of genes and that cell-type specific gene expression changes across cell types result in dysregulation of synaptic transmission on the pathway level. Moreover, we replicated age-regulated genes as well as the extent of gene expression change in several cell types using publicly available datasets. Further, an inhibitory neuron subtype, LAMP5 inhibitory neurons, was identified as severely affected by age. Next, we found a significant overlap in age-regulated genes and genes implicated in AD, most notably in astrocytes. We replicated previously shown transcriptomic age acceleration in individuals suffering from psychiatric disease. Finally, we show that gene expression of several genes is not only influenced by age but additionally by psychiatric diagnosis thereby revealing a convergent signature of ageing and psychopathology. In summary, the research presented in this thesis offers a comprehensive dataset that encompasses a substantial number of age-regulated genes and pathways. Additionally, it provides evidence for an implication of age-regulated genes in both neurodegenerative and psychiatric disease.

5.1 Model systems for the study of ageing and ageing-related pathologies - post-mortem brain as an essential resource

A lot of the insights into the ageing process at the cellular and molecular level stem from studies in animal models. These include studies in flies, worms, rodents, and non-human primates. Animal models allow for an examination of the effect of the ageing process in an intact organism at the level of behaviour, functionality, organs, and cells under controlled experimental conditions which also include age at death and mode of death (hardly controllable in humans) - an important factor for the quality of investigated tissues. It further enables the investigation of the effects of environmental exposures such as stressors or treatment interventions. These studies have immensely contributed to our current understanding of affected molecules, genes, and pathways during the ageing process. However, successful translation to the clinic of potential drug candidates identified in animal models for brain-related pathologies is still challenging. [207] A possible explanation lies in evolutionary differences between humans and our model systems, partly due to the massive expansion of the primate and specifically human cortex [208, 209]. One of the most widely used animal models in the study of brain diseases (including psychiatric and neurodegenerative disease) is the mouse. However, the human brain volume is roughly a thousand times larger than the mouse brain [210]. Moreover, the human brain is gyrified,

having allowed the brain to expand in volume and surface area, while mice belong to the lissencephalic species presenting a smooth cortex surface [211]. And even though we can identify homologous brain areas between the two species, especially certain regions in the human cortex may lack specific counterparts in the mouse [212]. As mentioned in the introduction of this thesis, rodents (including rats and mice) do not naturally present hallmarks of neurodegenerative disease and some non-human primates show accumulation of Aβ but rarely NFTs [116, 117]. All in all, this underscores the importance of the use of human-specific model systems when studying both normal and pathological ageing.

Since the discovery by Takahashi and Yamanaka [213] that pluripotent stem cells could be induced via the expression of four transcription factors from adult somatic cells, this technology has been leveraged across scientific disciplines to reprogram cells from control donors and donors with a disease or phenotype of interest. These induced pluripotent stem cell (iPSC) lines can then be further differentiated into a cell type of interest, including the different cell types of the human brain. Additionally, subsequent research demonstrated the utility of iPSCs to differentiate 3D structures, so-called organoids, which represent tissue models. Cerebral organoids [214] show a similar cytoarchitecture to the cerebral cortex and contain both neuronal as well as glial cell types. Yet, they often contain only few glial cells, especially microglia, and they lack the vasculature present in brain. [215] iPSCs present other important limitations in particular for the research of ageing and ageing-related pathologies like the late-onset forms of neurodegenerative diseases: iPSC-derived neurons both as 2D cultures and in cerebral organoids resemble both in structure, function and transcriptome an embryonic stage of second-trimester pregnancy [216, 217]. Moreover, reprogramming of the somatic cells into iPSCs results in an embryonic-like cell state in which the epigenetic landscape has been reset and therefore information on cellular donor age is lost [218]. This is consistent with findings from various studies comparing iPSC-derived neurons from neurotypical controls and individuals with neurodegenerative disorders, such as AD and PD. These studies could only recapitulate some but not all pathological hallmarks and ageing-related features of the donor cells were lost. [218] While examination of neurons differentiated from iPSCs with genetic mutations associated with the familial forms of the disease provides insight into pathological mechanisms, it is not clear how these findings relate to the late-onset (sporadic) forms of neurodegenerative diseases, which are by far the most common form. This emphasizes that iPSC derived neural cell types may not be the model of choice for studying age-related processes and late-onset forms of neurodegenerative diseases.

Another promising technology is the direct induction of neurons (iNeurons) from somatic cells, which does not pass through an embryonic-like state. Direct induction of different subtypes of neurons including motor neurons [219], and dopaminergic neurons [220] has been successfully demonstrated. Importantly, Huh and colleagues [221] demonstrated that these neurons retain the age of the donor cells as estimated by DNA methylation via Horvath's multi-tissue clock. Moreover, other ageing features such as impaired mitochondrial function and nuclear pore defects [218, 222] are present in iNeurons derived from old donors. Mertens and colleagues [223] used fibroblasts from patients with AD and controls to differentiate iNeurons. They demonstrated that AD iNeurons show cellular defects and

transcriptomic alterations with a high concordance with data from human post-mortem brain. Most studies so far have focused on the direct conversion of fibroblasts to diverse neuronal subtypes but protocols for the direct conversion of glial cells have recently been developed [224-226] and are starting to be leveraged for the investigation of their roles in neurodegenerative disorders [227]. Yet, using direct conversion protocols only individual cell types can be derived and studied. Moreover, conversion efficiency is a critical factor and is often low. Besides, lower replication of fibroblasts from older donors (used for direct conversion) has been shown [218, 221]. In addition, the direction conversion does not result in an expandable intermediate cell state (like iPSCs) making scaling of experiments a challenge.

This highlights the need to directly investigate the adult human brain. Non-invasive imaging techniques such as structural and functional MRI can provide insights into regional volume changes and differences in functional network connectivity. However, little inference on the precise underlying molecular mechanism can be made. Human post-mortem brain represents the full complex organ and samples derived from this intact tissue have a donor-specific genetic background and contain all the diverse interconnected cell types in their mature state having undergone changes related to ageing or disease. While post-mortem brain provides a snapshot of the brain's state at the time of death, studies have shown that slices from human post-mortem brains, obtained within hours after death, have been successfully cultured thereby allowing a certain degree of experimental manipulation, including the assessment of new pharmaceuticals [207, 228]. Moreover, post-mortem brain samples of large cohorts have been used for the study of epigenetic, transcriptomic, and proteomic alterations during ageing and ageing-related disease [132, 133, 229, 230]. These studies investigating gene regulation, gene and protein expression have provided mechanistic insights into disease processes and helped pinpoint potential new drug targets as well as biomarkers. Overall, this underscores the importance of human post-mortem brain as a highly valuable complementary "model system" for the study of ageing and ageing-related pathologies.

5.2 Effect of ageing on the transcriptome at single cell resolution

sn-RNA-seq allowed us to examine the effects of ageing on the different cell types in the brain. The cell types we were able to identify using a label transfer algorithm and manual curation with cell type marker genes included different types of excitatory as well as inhibitory neurons and different glial cell types. These identified cell types are consistent with other sn-RNA-seq studies in the prefrontal cortex. Moreover, similar cell type proportions, with excitatory neurons constituting the vast majority of nuclei, have been previously reported [127, 128, 132, 133, 157]. We found that most of the cell types do not change in abundance with ageing except for VIP inhibitory neurons (In_VIP) and OPCs, which decrease with age. The decrease of OPCs goes hand in hand with an expected increase in the oligodendrocyte population and matches results from studies in mice [114] and rhesus macaque [115]. Overall,

these findings are in agreement with the idea that normal ageing does not lead to a substantial loss of neurons [99], whereas pathological ageing, such as in AD and PD, is linked to the death of (certain) neuronal cell populations.

Differential gene expression analysis enabled us to investigate the transcriptomic changes that occur during ageing within each of the 20 identified cell types. We could detect gene expression changes in all of the cell types, except for endothelial cells. Interestingly, the transcriptome of brain endothelial cells from mouse hippocampus has been shown to undergo age-related changes influenced by circulatory cues from the blood [231]. Moreover, brain endothelial cells in aged mice have reduced expression of tight junction proteins and increased expression of TNF-α indicative of BBB dysfunction [232]. The lack of age-related gene expression changes in endothelial cells in this thesis could result from insufficient statistical power since only ~ 13,600 endothelial nuclei were recovered. However, other cell types with fewer nuclei showed age-related gene expression changes. Another possibility could be region-specific differences in the effects of age on endothelial cells supported by MRI analysis in humans showing that the age-related breakdown of the BBB starts in the hippocampus [233].

Comparison of the genes affected by ageing between the cell types showed that the majority were age-regulated in a cell-type specific manner. This was only partly driven by genes uniquely expressed in these cell types. Microglia and upper-layer excitatory neurons (Exc_L2-3) were the cells with the most uniquely expressed genes identified as age-regulated. Within the microglia this is likely to reflect their unique roles in immune response and their different lineage origin. Upper-layer excitatory neurons were the cell type with more than 200,000 nuclei thus increasing the chance of detection of more lowly expressed genes compared to other neuronal cell types.

In an attempt to normalize differences in statistical power between cell types, we calculated the ratio of number of age DE genes per one million sequencing reads. This revealed that not all cell types are equally affected by the ageing process: LAMP5 inhibitory neurons seemed to be especially vulnerable. Despite the differences in age-regulated genes between the cell types, ORA identified disruption of synaptic signalling and G-protein-coupled receptor signalling as convergent affected pathways across neuronal and glial cell types. Importantly, several metabolic pathways were dysregulated within the inhibitory neurons. Age-regulated genes in LAMP5 inhibitory neurons were over-represented in pathways involved in oxidative phosphorylation and cellular respiration. This is indicative of mitochondrial dysfunction, a mechanism previously linked to both ageing and neurodegeneration [234]. In order for cells to function properly, ATP synthesis is crucial, particularly in neurons that have high metabolic needs. This is essential for the maintenance and regulation of ion gradients, facilitating transport along axons, and enabling firing. [235] Thus, dysfunctional mitochondria could provide a mechanistic explanation for why LAMP5 inhibitory neurons were identified as the most strongly affected cell type. Consistent with previous reports from several species of primed, aged microglia [115, 158, 236, 237], genes upregulated with age in microglia were over-represented in biological processes involved in immune response. While other studies in humans [159] and mice [238] have found evidence for reactive astrocytes in ageing, we did not. On the one hand, this could be due to differences in sampling, since Krawczyk and

colleagues [159] obtained their human brain samples from brain surgeries, not post-mortem. On the other hand, Clarke and colleagues [238] compared different brain regions in mice and found aged cortical astrocytes up-regulated fewer reactive astrocyte genes than aged astrocytes in hippocampus or striatum indicating brain-region-specific differences.

Disease enrichment for psychiatric and cognitive disorders amongst downregulated age DE genes of several cell types provided evidence for their involvement in the disease aetiology of these disorders. This is in line with age being one of the strongest risk factors for neurodegenerative disorders as well as studies suggesting similar biological pathways are affected by ageing and psychiatric disorders [239].

Importantly, we were able to validate age-regulated genes. Comparison of previous studies in human bulk tissue with our 'full pseudobulk' dataset derived by summing gene counts across all cell types showed good agreement. Moreover, the importance of examining cell-type-specific gene expression changes is highlighted by the fact that within our 'full pseudobulk' analysis 2,387 DE genes were identified in contrast to a total of 5,161 genes identified as DE in at least one of the cell types. This shows that certain cell-type-specific changes get diluted when looking at the bulk tissue. In addition, we used data from three additional studies to validate age-related gene expression changes in specific cell types; purified astrocytes [159] and microglia [158] combined with RNA sequencing and LAMP5 inhibitory neurons derived from another sn-RNA-seq dataset [157]. Within all three cell types, we were able to replicate a significant proportion of age-regulated genes and additionally show that the extent of the expression change (log2FC) was highly correlated. This strongly underlines the robustness of our results between datasets derived from different human samples and across methodologies.

5.3 LAMP5 inhibitory neurons - an inhibitory neuron class worth further exploration

In this thesis, LAMP5 inhibitory neurons were identified as a cell type particularly affected by the ageing process given the highest relative number of age DE genes, which could be linked to mitochondrial dysfunction. Interestingly, the number of LAMP5 inhibitory neurons was shown to be reduced in the cortex and hippocampus of a mouse model of AD [240]. These changes in cell type numbers were also seen in human brains of individuals with AD [240]. Several genes involved in mitochondrial function were downregulated with age in our LAMP5 inhibitory neurons and were also downregulated in inhibitory neurons of AD brains [132, 133]. Dysfunctional mitochondria could therefore represent a mechanistic link between ageing and AD: Age-related accumulation of malfunctioning mitochondria - in the presence of other AD risk factors - culminates in the loss of these LAMP5 inhibitory neurons.

Zooming in onto this cell type, we were able to identify two different subtypes. LAMP5 inhibitory neurons co-expressing *NRG1* and *FREM1* in contrast to LAMP5 inhibitory neurons co-expressing *LHX6* and *CHST9*. This subclustering analysis revealed that in fact, *LAMP5*+ *LHX6*+ inhibitory neurons had the most relative age DE genes. In 2018, Tasic and colleagues [74] described this cell type for the first time in the mouse cortex. They referred to it as ‘unusual’ given the co-expression of *Lamp5* (which is expressed in inhibitory neurons derived from the caudal ganglionic eminence) with *Lhx6* and *Nkx2.1* (transcription factors of the medial ganglionic eminence). A study by Krienen and colleagues [187] compared the different inhibitory neuron populations between primates and mice and showed that *LAMP5*+ *LHX6*+ cells were eight times more abundant in the primate compared to the mouse cortex. They also demonstrated differences in the distribution of *LAMP5*+ *LHX6*+ and *LAMP5*+ *LHX6*- inhibitory neurons. *LAMP5*+ *LHX6*+ cells were primarily located in L5 and L6, whereas *LAMP5*+ *LHX6*- cells were found across L1-5, with the largest proportions in L2/3. Interestingly, transcriptomically cortical primate *LAMP5*+ *LHX6*+ cells are most similar to *Lamp5*+ *Lhx6*+ ivy cells of the mouse hippocampus. Ivy cells form part of the neurogliaform family of cells, which present different characteristics than the other inhibitory neuron classes. Their synapses have a wider synaptic cleft and some synaptic boutons lack a clear postsynaptic target. [241]. They therefore can signal via volume transmission affecting several surrounding neurons [241, 242].

Overall, however, LAMP5 inhibitory neurons are a relatively recently assigned/denoted inhibitory neuron class, and we are therefore lacking detailed functional characterization. A recent study by Machold et al. [243] highlighted that cortical mouse *Id2* (*Lamp5*) expressing neurons are comprised of both neurogliaform cells and non-neurogliaform cells with different connectivity and spiking patterns. Since a subtype of LAMP5 inhibitory neurons has been shown to be primate-enriched in the neocortex and evidence from this thesis points to this subtype being strongly affected by the ageing process, further research warrants an in-depth characterization of the LAMP5 inhibitory class and subtypes in primate- or even human-specific model systems.

5.4 Ageing and Alzheimer - is it all about a threshold?

Since age is one of the most prominent risk factors for neurodegenerative diseases such as AD, we wanted to explore the relationship of age-regulated genes with genes dysregulated in AD. Comparison of age-regulated genes with AD DE genes in two studies comparing healthy controls and AD patients in individual cell types showed a significant overlap for upregulated DE genes in astrocytes and oligodendrocytes and for downregulated DE genes in astrocytes and excitatory neurons. This could suggest that astrocytes are especially susceptible to age-related changes relevant in the pathogenesis of AD. The overlap in astrocytes does not stem from changes related to reactive astrocytes, previously implicated in AD [244]. Rather, impairment in neuronal support seems to be a common feature. Interestingly, the expression level of several overlapping genes has been linked to measures of cognition or AD disease severity. For example, *GRM3* - a metabotropic glutamate receptor - is downregulated with age in astrocytes and shows lower expression in AD. An SNP in *GRM3*, resulting in trend-level lower expression in human PFC, was associated with poorer cognitive performance [196]. *RPH3A* is involved in synaptic vesicle exocytosis and downregulated during ageing and in AD. Reduced protein levels of RPH3A in the cortex of AD patients negatively correlated with Aβ burden [198]. Moreover, higher protein levels of RPH3A in human dorsolateral prefrontal cortex were shown to be associated with cognitive resilience [197]. Other examples of age-regulated genes that have been linked to AD include *NPTX2* and *NRGN*, two synaptic proteins. *NPTX2* is downregulated with age across several excitatory neuron types. Several proteomic studies have consistently shown NPTX2 to be downregulated in AD brains [245]. Moreover, reduction in its concentration was positively correlated with rates of cognitive decline and has therefore been proposed as a prognostic biomarker for AD [246]. *NRGN* is downregulated with age across several cell types including excitatory and inhibitory neurons, microglia and OPCs. In addition, *NRGN's* expression level has been shown to negatively correlate with Aβ and tau pathology burden and with dementia severity [247]. These only represent a few examples of genes whose expression level correlates with AD severity and age and may be unrelated. However, it is tempting to speculate - in analogy to PRS - that once a set of several interconnected genes (with individually small effects) involved in a variety of biological pathways surpasses an expression threshold, an individual may deviate from the path of healthy to pathological ageing in the presence of other risk factors (**Figure 5.1**). These risk factors include behaviour (diet, exercise, smoking), environmental exposures (stress, neurotoxins) and genetic make-up (SNPs). Surpassing of the threshold would result in a state where compensatory mechanisms have been exhausted which leads to the manifestation of the disease. These genes could therefore represent potential candidates for drug targeting; attempting to maintain/prolong 'a healthy' ageing trajectory.

In addition, we identified two genes (*KCTD17* and *LINGO1*) whose expression was regulated in opposite direction with age and in AD. *KCTD17* is a member of the potassium channel tetramerization domain containing protein family, which has been linked to neurodegeneration and psychiatric diseases [248]. *LINGO1* has been shown to regulate myelination [249] and to influence cleavage of Aβ precursor protein (APP) via direct interaction [250]. Even though these are only individual genes, and both ageing and

neurodegenerative processes are complex with multiple genes and pathways involved, these genes could also be interesting candidates for novel therapeutics. Interestingly so, a preclinical study in a transgenic mouse model of AD showed that the administration of an antibody directed against LINGO1 reduces Aβ burden and ameliorated cognitive defects [251]. However, a phase-II clinical trial for the use of LINGO1 antibody in multiple sclerosis failed to meet the primary endpoint of disability improvement [252]. Thus, further (pre-clinical) studies are needed to investigate the functional roles and evaluate the therapeutic potential of *KCTD17* and *LINGO1* for AD.

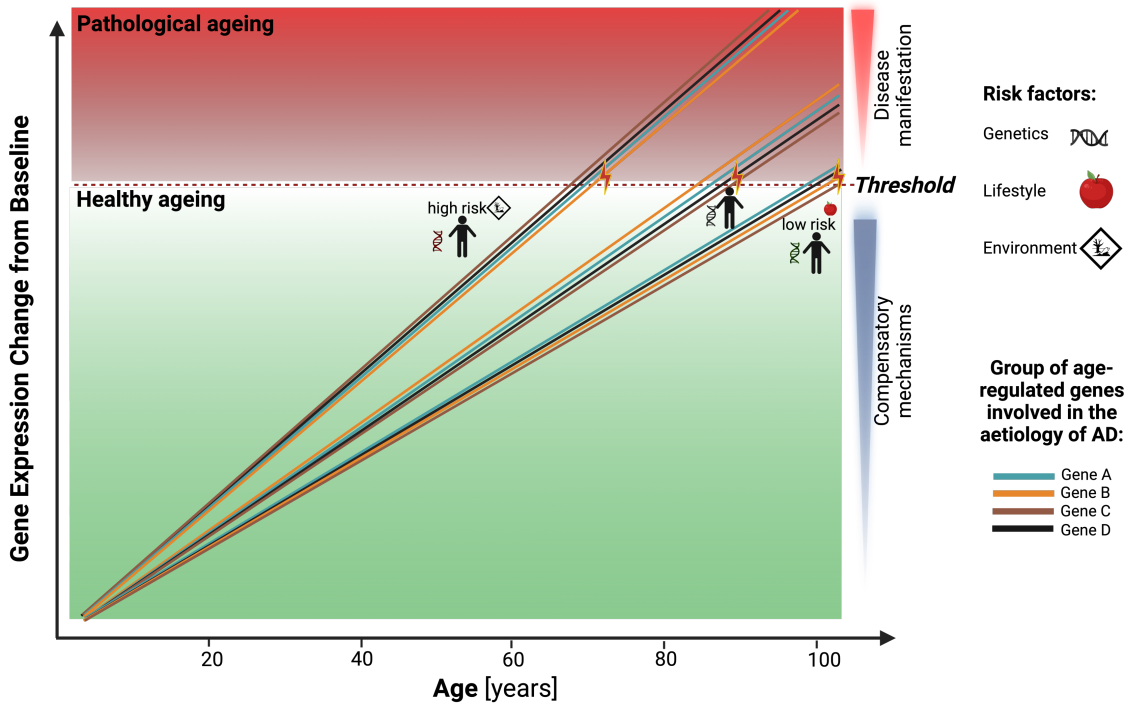

Figure 5.1: Hypothetical model of how cumulative effects of age-regulated genes lead to pathological ageing This figure displays a hypothetical model of how cumulative effects of age-regulated genes lead to pathological ageing in different individuals at different ages. Healthy brain function is brought about by the complex interplay of diverse cell types in the brain. Ageing leads to gradual gene expression changes in a cell-type-specific manner resulting in altered biological processes, part of which are compensatory. However, a set of several interconnected genes (with individually small effects) involved in a variety of biological pathways will surpass a critical cumulative expression threshold at a certain age. Since compensatory mechanisms have been exhausted the individual shifts from the path of healthy to pathological ageing resulting in the manifestation of neurodegenerative disease. The age at which this shift to pathological ageing occurs is different for each individual depending on other risk factors, including genetics (SNPs), lifestyle (diet) and the environment (exposure to neurotoxins). Figure was created using Biorender.com.

5.5 Accelerated ageing in psychiatric disease - Evidence from different biological measures

Studying the ageing process in humans is not a trivial task considering that chronological age is not necessarily representative of biological age. This is demonstrated by the great inter-individual variability in how fast individuals visibly age, differences in cognitive performance and age-related frailty [253]. Thus, several different biological measures derived from different tissues and using different modalities have been used as a means to estimate biological age. So-called epigenetic clocks are a commonly used method utilizing the methylation level of a set of cytosine guanine dinucleotides (CpGs) in the DNA for the prediction of biological (DNA methylation) age (DNAmAge). One of the first epigenetic clocks, the Hannum clock [254], was derived from whole blood samples, whereas Horvath's clock [163] was derived from multiple tissues. Other biological age predictors use gene expression to predict biological age. Peters et al. [255] estimated biological age from blood samples using the expression level of ~ 1500 genes. Lin et al. [49] used gene expression from ~ 70 genes from human post-mortem brain to construct a molecular brain age calculator. Moreover, structural MRI has been used as a neuroimaging biomarker to develop the brain age gap estimation (BrainAGE) to predict biological brain age. Common for all biological age predictors is that the deviation of the estimated biological age from the chronological age is used as a measure of age de- or acceleration.

Several lines of evidence indicate accelerated ageing in psychiatric disease. Severe mental disorders, across diagnosis, are linked to shorter life expectancy, which means on average dying 10 - 20 years earlier compared to the general population. [44] While a portion of this excess mortality is attributable to unnatural causes of death including suicide and accidents, more than two-thirds are due to physical disease [256]. These include cardiovascular and respiratory disease as well as infections [44]. The increased risk for cardiovascular disease is partly driven by lifestyle factors including lack of exercise, unhealthy diet and smoking [256]. Additionally, antipsychotic medication is linked to an increased risk for gaining weight and diabetes mellitus [256]. Furthermore, several studies have found associations with accelerated biological ageing and psychiatric disease. For example, Han and colleagues [46] found increased epigenetic age in individuals suffering from MDD based on biological age estimates from DNAm measurements in blood and post-mortem brain. Lin et al. [49] developed a transcriptomic brain age predictor and showed significantly accelerated brain ageing in individuals with SCZ and BPD. Moreover, structural brain ageing (BrainAge) was shown the be significantly accelerated in MDD, SCZ and BPD with psychosis [257, 258].

In this thesis, epigenetic age in brain was not accelerated in psychiatric cases. Given that the majority of psychiatric cases in our cohort suffered from SCZ, this finding is consistent with other studies in post-mortem brain examining epigenetic age [259, 260]. On the other hand, we were able to replicate the results of Lin et al. [49] demonstrating accelerated transcriptomic age in cases with psychiatric disorders. This 'discrepancy' between epigenetic and transcriptomic age acceleration demonstrates that different estimates of biological age are unlikely to capture the same component of the bio-physiological ageing process [261]. This is also underlined by the fact that e.g. different epigenetic clocks which are based on

the same biological measure - DNA methylation (though different CpGs) - do not necessarily show association to the same outcome variables [261]. Belsky and colleagues [262] compared three different CpG-based epigenetic clocks and their association with measures of physical and cognitive function. They showed that only one of the three clocks, the Hannum clock [254], was significantly associated with measures including balance and motor coordination as well as cognitive test scores [262]. In general, this highlights the necessity to deepen our understanding of the diverse biological measures used and which aspects of ageing they represent.

Additionally, using our sn-RNA-seq data, we showed that the expression of several genes is influenced both by age and psychiatric disease. A concordance in directionality of expression change with age and in psychiatric cases indicates a shared signature across multiple cell types. Our exploratory analysis using polygenic risk scores could indicate that genetic factors may contribute to some of the gene expression changes of age- and disease-associated genes. Overall, the identified transcriptional changes, likely influencing cellular connectivity, could therefore potentially represent the molecular underpinnings of structural and functional changes in the brain observed during ageing and in psychopathology. The use of psychiatric medication, which increases the risk for metabolic syndrome, could be a potential confounding factor contributing to the observed accelerated transcriptomic ageing. However, accelerated structural BrainAge was found in patients suffering from psychosis independent of being medicated or not and BrainAge was not linked to cumulative antipsychotic medication exposure [263]. In addition, our results indicate that gene expression is likely influenced by other factors besides genetics such as living with a chronic psychiatric disease, which entails behavioural and lifestyle adaptations and environmental exposures.

5.6 Limitations

Every study comes with certain limitations, and these should therefore be noted. Using human post-mortem brain does not allow the researchers to control for several variables as compared to studies in animal models. These include genotypic background, environmental exposures, lifestyle, medication use, and mode of death, which all contribute to inter-individual differences at the gene expression level. Additionally, all samples cannot be processed for experiments on the same day and effects of these experimental batches have been shown to influence results. It is therefore essential that during study design, experimental procedures in the laboratory and during the analysis both sample and experimental factors are taken into account. Thus, we assigned samples into experimental batches using a balanced design not confounded by our variables of interest including age and disease status. Moreover, European ancestry of all individuals within our cohort was confirmed by genotyping. In our statistical model, we included covariates shown to influence gene expression including PMI, RIN, pH, and biological sex. However, due to all these potentially confounding factors common to human post-mortem studies, replication using data obtained from independent cohorts is essential and ensures validity of findings. Thus, by comparing our results both at bulk and single-cell level to previously published datasets we demonstrate robustness of our results.

Even though we have shown evidence for accelerated transcriptomic ageing in psychiatric cases and identified genes with congruent regulation between age and disease, the contributions of genetic risk and additional factors that come with suffering from a psychiatric disease including lifestyle and medication use could not be disentangled. In order to do so, larger samples with a detailed longitudinal characterization of individuals such as from birth (e.g. via national health care registries) would be necessary. Despite the fact that this study presents one of the largest post-mortem cohorts profiled using sn-RNA-seq, future studies with even more samples and thus increased statistical power will likely identify additional genes associated with psychiatric disease in additional cell types. It will be interesting to examine if a part of these genes also shows congruent regulation with age-associated genes providing further insights into accelerated ageing at the cell-type-specific level. Additionally, some of the psychiatric cases within our cohort died by suicide. A recent study by Mullins and colleagues [264] showed that certain genetic loci contributing to risk for suicide are independent of those overlapping with risk for psychiatric disorders. However, since this subgroup within our cohort was relatively small, effects of suicide could not be further investigated.

sn-RNA-seq has become a widely applied technique over the last 5 - 10 years due to the suitability of nuclei isolated from frozen tissue for transcriptomic profiling. Compared to whole cells, nuclei even present certain advantages such as less bias in cell capture, which can lead to the (additional) identification of rare cell types [126, 265]. What is more, dissociation of intact cells from tissues can affect the transcriptome. Yet, nuclei do not allow for the examination of mitochondrial transcription, a process reported to be affected both in ageing and neurodegenerative disorders. Moreover, using the three-prime sequencing method applied examination of splicing, shown to be affected by ageing, in neurodegeneration [266, 267], and in psychiatric disorders [268, 269], is not possible. In addition, we were not able to

detect all cells of the cerebrovasculature, such as pericytes and vascular smooth muscle cells, impeding the investigation of the effects of the ageing process on their transcriptome. Due to their sparsity, enrichment methods are necessary to capture these cells in sufficient numbers and recent studies have started to characterize their diversity and their implications in neurodegenerative diseases [270, 271].

5.7 Future directions

Going forward several interesting questions are yet to be answered. Examination of the cell-type-specific regulatory landscape, including microRNAs, long non-coding RNAs, DNA methylation, histone marks and chromatin accessibility, and its changes during ageing will provide insights into the diverse gene regulatory mechanisms involved and their relation to observed gene expression changes. Moreover, the on-going development of methods to quantify the proteome of single cells will enable investigation of how the observed transcriptional changes are translated to changes in the proteome. Gene co-expression network analysis could be further applied to group genes with similar expression patterns and identify driver/hub genes. However, currently, methods that integrate co-expression networks across different cell types have yet to be developed. Exploring how a whole network of genes in interconnected cell types changes in expression would open the opportunity to understand changes seen at the circuit level. Furthermore, this thesis examined only linear age-related expression changes. Since it is probable that certain genes may present more complex patterns of expression during ageing, these should be explored in future studies.

The LAMP5 inhibitory neuron class is strongly affected by ageing (as shown in this thesis) and in AD awaits a deep characterisation of its subtypes including the distribution of these subtypes in different brain regions and cortical layers, electrophysiological properties and how these cells integrate on a circuit level. Understanding all these details will provide clues on what leads to their vulnerability to ageing and neurodegeneration.

This study correlated gene expression changes with age. However, the lack of information on cognitive measures of the individuals impeded the investigation of the relation to ageing-related outcomes including cognitive decline. Therefore, longitudinal prospective studies are needed which perform deep phenotyping (including cognitive measures, structural and function brain imaging) ante-mortem as well as pathological examination and molecular investigation of brain tissues post-mortem. The ROSEMAP project [272] is one such longitudinal study focusing on ageing and dementia. A recent publication [273] leveraging data from this project evaluated differences in cellular neocortical populations between individuals with different levels of cognitive function/impairment with and without AD pathology and diagnosis at time of death. The authors thereby identified altered cellular communities in AD.

5.8 Conclusions

We are part of an ageing society. While this demographic development is proof of immense improvements in prevention, diagnosis, and treatment of a variety of diseases, we are now facing a new pandemic with the rise in prevalence of age-related neurodegenerative disorders. Over the last decades, we have deepened our insights into both the normal and pathological ageing process of the brain using animal models, in-vitro model systems as well as human subjects. All of this scientific work revealed shared and species-specific changes at the structural, functional, cellular, and molecular level, however disease-modifying treatments for neurodegenerative disorders have yet to be identified.

To date, the work presented in this thesis is the first study to examine age-related gene expression changes in the human brain at cell-type resolution and to evaluate differences in the gene expression ageing trajectories between healthy controls and individuals with psychiatric disease. We identified a large number of age-regulated genes in individual cell types and showed that age-associated genes overlap on the cell-type level with changes observed in Alzheimer's disease, especially in astrocytes. Finally, we demonstrated that several genes are not only age-regulated but additionally associated with psychiatric diagnosis highlighting a convergence of the signature of ageing and psychopathology across multiple cell types. This could provide a biological explanation of the increased risk of cognitive decline and neurodegenerative disease in patients with psychiatric disorders. These findings have important clinical implications, as they highlight the need for better monitoring of patients with psychiatric diseases for age-related disorders such as cognitive decline. Moreover, early prevention and intervention strategies could improve outcomes for patients.

6 | Bibliography

1. United Nations, D.o.E.a.S.A., Population Division (2022),. *World Population Prospects 2022: Summary of Results. UN DESA/POP/2022/TR/NO. 3.* 2022; Available from: https://www.un.org/development/desa/pd/sites/www.un.org.development.desa.pd/files/wpp2022_summary_of_results.pdf.
2. Ritchie, H. and M. Roser. *Age Structure*. 2019 [cited 2023 April 9]; Available from: https://ourworldindata.org/age-structure.
3. Roser, M., et al. *World Population Growth*. 2013 [cited 2023 April 9]; Available from: https://ourworldindata.org/world-population-growth.
4. Checkoway, H., J.I. Lundin, and S.N. Kelada, *Neurodegenerative diseases.* IARC Sci Publ, 2011(163): p. 407-19.
5. World Health Organization. *Dementia*. [cited 2023 April 9]; Available from: https://www.who.int/news-room/fact-sheets/detail/dementia.
6. Gustavsson, A., et al., *Global estimates on the number of persons across the Alzheimer's disease continuum.* Alzheimers Dement, 2023. **19**(2): p. 658-670.
7. Igarashi, K.M., *Entorhinal cortex dysfunction in Alzheimer's disease.* Trends Neurosci, 2023. **46**(2): p. 124-136.
8. Penke, B., F. Bogar, and L. Fulop, *beta-Amyloid and the Pathomechanisms of Alzheimer's Disease: A Comprehensive View.* Molecules, 2017. **22**(10).
9. Cummings, J.L., G. Tong, and C. Ballard, *Treatment Combinations for Alzheimer's Disease: Current and Future Pharmacotherapy Options.* J Alzheimers Dis, 2019. **67**(3): p. 779-794.
10. Parkinson's Foundation. *Statistics Who has Parkinson's*. [cited 2023 April 9]; Available from: https://www.parkinson.org/understanding-parkinsons/statistics.
11. Poewe, W., et al., *Parkinson disease.* Nat Rev Dis Primers, 2017. **3**: p. 17013.
12. Jellinger, K.A., *The pathomechanisms underlying Parkinson's disease.* Expert Rev Neurother, 2014. **14**(2): p. 199-215.
13. Armstrong, M.J. and M.S. Okun, *Diagnosis and Treatment of Parkinson Disease: A Review.* JAMA, 2020. **323**(6): p. 548-560.
14. Europe, A., *Dementia in Europe Yearbook 2019 Estimating the prevalence of dementia in Europe*. 2020.
15. G. B. D. Collaborators, *Global mortality from dementia: Application of a new method and results from the Global Burden of Disease Study 2019.* Alzheimers Dement (N Y), 2021. **7**(1): p. e12200.
16. Collaborators, G.B.D.D., *Global, regional, and national burden of Alzheimer's disease and other dementias, 1990-2016: a systematic analysis for the Global Burden of Disease Study 2016.* Lancet Neurol, 2019. **18**(1): p. 88-106.
17. International., A.s.D., et al. *World Alzheimer Report 2015*. 2015 [cited 2023 April 10]; Available from: https://www.alzint.org/resource/world-alzheimer-report-2015/.
18. Collaborators, G.B.D.D.F., *Estimation of the global prevalence of dementia in 2019 and forecasted prevalence in 2050: an analysis for the Global Burden of Disease Study 2019.* Lancet Public Health, 2022. **7**(2): p. e105-e125.
19. Collaborators, G.B.D.M.D., *Global, regional, and national burden of 12 mental disorders in 204 countries and territories, 1990-2019: a systematic analysis for the Global Burden of Disease Study 2019.* Lancet Psychiatry, 2022. **9**(2): p. 137-150.

20. Sullivan, P.F. and D.H. Geschwind, *Defining the Genetic, Genomic, Cellular, and Diagnostic Architectures of Psychiatric Disorders.* Cell, 2019. **177**(1): p. 162-183.

21. Lee, P.H., Y.A. Feng, and J.W. Smoller, *Pleiotropy and Cross-Disorder Genetics Among Psychiatric Disorders.* Biol Psychiatry, 2021. **89**(1): p. 20-31.

22. Trubetskoy, V., et al., *Mapping genomic loci implicates genes and synaptic biology in schizophrenia.* Nature, 2022. **604**(7906): p. 502-508.

23. Howard, D.M., et al., *Genome-wide meta-analysis of depression identifies 102 independent variants and highlights the importance of the prefrontal brain regions.* Nat Neurosci, 2019. **22**(3): p. 343-352.

24. Stahl, E.A., et al., *Genome-wide association study identifies 30 loci associated with bipolar disorder.* Nat Genet, 2019. **51**(5): p. 793-803.

25. Hogg, B., et al., *Psychological trauma as a transdiagnostic risk factor for mental disorder: an umbrella meta-analysis.* Eur Arch Psychiatry Clin Neurosci, 2023. **273**(2): p. 397-410.

26. Paykel, E.S., *Life stress, depression and attempted suicide.* J Human Stress, 1976. **2**(3): p. 3-12.

27. Davis, M.T., et al., *Neurobiology of Chronic Stress-Related Psychiatric Disorders: Evidence from Molecular Imaging Studies.* Chronic Stress (Thousand Oaks), 2017. **1**.

28. Madhu, A., A. Deegan, and D. Cawthorpe, *Correlation Between Pregnancy and Childbirth Complications and the Mental Health of the Children Born.* European Psychiatry, 2015. **30**: p. 194.

29. Nielsen, S.M., et al., *Association between alcohol, cannabis, and other illicit substance abuse and risk of developing schizophrenia: a nationwide population based register study.* Psychol Med, 2017. **47**(9): p. 1668-1677.

30. Nemeroff, C.B., *The State of Our Understanding of the Pathophysiology and Optimal Treatment of Depression: Glass Half Full or Half Empty?* Am J Psychiatry, 2020. **177**(8): p. 671-685.

31. Hasler, G., *Pathophysiology of depression: do we have any solid evidence of interest to clinicians?* World Psychiatry, 2010. **9**(3): p. 155-61.

32. McCutcheon, R.A., R.S.E. Keefe, and P.K. McGuire, *Cognitive impairment in schizophrenia: aetiology, pathophysiology, and treatment.* Mol Psychiatry, 2023.

33. Patel, K.R., et al., *Schizophrenia: overview and treatment options.* P T, 2014. **39**(9): p. 638-45.

34. Zimmermann, G., et al., *The effect of cognitive behavioral treatment on the positive symptoms of schizophrenia spectrum disorders: a meta-analysis.* Schizophr Res, 2005. **77**(1): p. 1-9.

35. Bighelli, I., et al., *Psychological interventions to reduce positive symptoms in schizophrenia: systematic review and network meta-analysis.* World Psychiatry, 2018. **17**(3): p. 316-329.

36. Riehle, M., et al., *Efficacy of Psychological Treatments for Patients With Schizophrenia and Relevant Negative Symptoms: A Meta-Analysis.* Clin Psychol Eur, 2020. **2**(3): p. e2899.

37. Magioncalda, P. and M. Martino, *A unified model of the pathophysiology of bipolar disorder.* Mol Psychiatry, 2022. **27**(1): p. 202-211.

38. Geddes, J.R. and D.J. Miklowitz, *Treatment of bipolar disorder.* Lancet, 2013. **381**(9878): p. 1672-82.

39. Perugi, G., et al., *The Role of Electroconvulsive Therapy (ECT) in Bipolar Disorder: Effectiveness in 522 Patients with Bipolar Depression, Mixed-state, Mania and Catatonic Features.* Curr Neuropharmacol, 2017. **15**(3): p. 359-371.

40. Popiolek, K., et al., *Electroconvulsive therapy in bipolar depression - effectiveness and prognostic factors.* Acta Psychiatr Scand, 2019. **140**(3): p. 196-204.

41. Correll, C.U., et al., *Prevalence, incidence and mortality from cardiovascular disease in patients with pooled and specific severe mental illness: a large-scale meta-analysis of 3,211,768 patients and 113,383,368 controls.* World Psychiatry, 2017. **16**(2): p. 163-180.

42. Richmond-Rakerd, L.S., et al., *Longitudinal Associations of Mental Disorders With Dementia: 30-Year Analysis of 1.7 Million New Zealand Citizens.* JAMA Psychiatry, 2022. **79**(4): p. 333-340.

43. Viron, M.J. and T.A. Stern, *The impact of serious mental illness on health and healthcare.* Psychosomatics, 2010. **51**(6): p. 458-65.

44. Liu, N.H., et al., *Excess mortality in persons with severe mental disorders: a multilevel intervention framework and priorities for clinical practice, policy and research agendas.* World Psychiatry, 2017. **16**(1): p. 30-40.

45. Wertz, J., et al., *Association of History of Psychopathology With Accelerated Aging at Midlife.* JAMA Psychiatry, 2021. **78**(5): p. 530-539.

46. Han, L.K.M., et al., *Epigenetic Aging in Major Depressive Disorder.* Am J Psychiatry, 2018. **175**(8): p. 774-782.

47. Teeuw, J., et al., *Accelerated aging in the brain, epigenetic aging in blood, and polygenic risk for schizophrenia.* Schizophr Res, 2021. **231**: p. 189-197.

48. Yusupov, N., et al., *Transdiagnostic evaluation of epigenetic age acceleration and burden of psychiatric disorders.* Neuropsychopharmacology, 2023.

49. Lin, C.W., et al., *Older molecular brain age in severe mental illness.* Mol Psychiatry, 2021. **26**(7): p. 3646-3656.

50. Wrigglesworth, J., et al., *Factors associated with brain ageing - a systematic review.* BMC Neurol, 2021. **21**(1): p. 312.

51. Richter, D., et al., *Is the global prevalence rate of adult mental illness increasing? Systematic review and meta-analysis.* Acta Psychiatr Scand, 2019. **140**(5): p. 393-407.

52. Collaborators, C.-M.D., *Global prevalence and burden of depressive and anxiety disorders in 204 countries and territories in 2020 due to the COVID-19 pandemic.* Lancet, 2021. **398**(10312): p. 1700-1712.

53. Sinclair, L.I., et al., *Characterization of Depressive Symptoms in Dementia and Examination of Possible Risk Factors.* J Alzheimers Dis Rep, 2023. **7**(1): p. 213-225.

54. Ismail, Z., et al., *Psychosis in Alzheimer disease - mechanisms, genetics and therapeutic opportunities.* Nat Rev Neurol, 2022. **18**(3): p. 131-144.

55. Gallagher, D.A. and A. Schrag, *Psychosis, apathy, depression and anxiety in Parkinson's disease.* Neurobiol Dis, 2012. **46**(3): p. 581-9.

56. Asmer, M.S., et al., *Meta-Analysis of the Prevalence of Major Depressive Disorder Among Older Adults With Dementia.* J Clin Psychiatry, 2018. **79**(5).

57. Pearlson, G.D., et al., *Association between family history of affective disorder and the depressive syndrome of Alzheimer's disease.* Am J Psychiatry, 1990. **147**(4): p. 452-6.

58. Strauss, M.E. and P.K. Ogrocki, *Confirmation of an association between family history of affective disorder and the depressive syndrome in Alzheimer's disease.* Am J Psychiatry, 1996. **153**(10): p. 1340-2.

59. Zahodne, L.B., et al., *Longitudinal relationships between Alzheimer disease progression and psychosis, depressed mood, and agitation/aggression.* Am J Geriatr Psychiatry, 2015. **23**(2): p. 130-40.

60. Aarsland, D., et al., *Depression in Parkinson disease--epidemiology, mechanisms and management.* Nat Rev Neurol, 2011. **8**(1): p. 35-47.

61. Stang, C.D., et al., *Incidence, Prevalence, and Mortality of Psychosis Associated with Parkinson's Disease (1991-2010).* J Parkinsons Dis, 2022. **12**(4): p. 1319-1327.

62. Samudra, N., et al., *Psychosis in Parkinson Disease: A Review of Etiology, Phenomenology, and Management.* Drugs Aging, 2016. **33**(12): p. 855-863.

63. Patel, R.S., et al., *Impact of Depression on Hospitalization and Related Outcomes for Parkinson's Disease Patients: A Nationwide Inpatient Sample-Based Retrospective Study.* Cureus, 2017. **9**(9): p. e1648.

64. Smeland, O.B., et al., *Genome-wide Association Analysis of Parkinson's Disease and Schizophrenia Reveals Shared Genetic Architecture and Identifies Novel Risk Loci.* Biol Psychiatry, 2021. **89**(3): p. 227-235.

65. Wingo, T.S., et al., *Shared mechanisms across the major psychiatric and neurodegenerative diseases.* Nat Commun, 2022. **13**(1): p. 4314.

66. Sadeghi, I., et al., *Brain transcriptomic profiling reveals common alterations across neurodegenerative and psychiatric disorders.* Comput Struct Biotechnol J, 2022. **20**: p. 4549-4561.

67. Brodal, P. and P. Brodal, *Functions of the Neocortex*, in *The Central Nervous System*. 2016, Oxford University Press.

68. Nieuwenhuys, R., *The neocortex. An overview of its evolutionary development, structural organization and synaptology.* Anat Embryol (Berl), 1994. **190**(4): p. 307-37.

69. Molyneaux, B.J., et al., *Neuronal subtype specification in the cerebral cortex.* Nat Rev Neurosci, 2007. **8**(6): p. 427-37.

70. Belgard, T.G., et al., *A transcriptomic atlas of mouse neocortical layers.* Neuron, 2011. **71**(4): p. 605-16.

71. Bernard, A., et al., *Transcriptional architecture of the primate neocortex.* Neuron, 2012. **73**(6): p. 1083-99.

72. Sorensen, S.A., et al., *Correlated gene expression and target specificity demonstrate excitatory projection neuron diversity.* Cereb Cortex, 2015. **25**(2): p. 433-49.

73. Tasic, B., et al., *Adult mouse cortical cell taxonomy revealed by single cell transcriptomics.* Nat Neurosci, 2016. **19**(2): p. 335-46.

74. Tasic, B., et al., *Shared and distinct transcriptomic cell types across neocortical areas.* Nature, 2018. **563**(7729): p. 72-78.

75. Kepecs, A. and G. Fishell, *Interneuron cell types are fit to function.* Nature, 2014. **505**(7483): p. 318-26.

76. Huang, Z.J. and A. Paul, *The diversity of GABAergic neurons and neural communication elements.* Nat Rev Neurosci, 2019. **20**(9): p. 563-572.

77. Fishell, G. and A. Kepecs, *Interneuron Types as Attractors and Controllers.* Annu Rev Neurosci, 2020. **43**: p. 1-30.

78. Jiang, X., et al., *Principles of connectivity among morphologically defined cell types in adult neocortex.* Science, 2015. **350**(6264): p. aac9462.

79. Markram, H., et al., *Reconstruction and Simulation of Neocortical Microcircuitry.* Cell, 2015. **163**(2): p. 456-92.

80. Mayer, C., et al., *Developmental diversification of cortical inhibitory interneurons.* Nature, 2018. **555**(7697): p. 457-462.

81. Ben Haim, L. and D.H. Rowitch, *Functional diversity of astrocytes in neural circuit regulation.* Nat Rev Neurosci, 2017. **18**(1): p. 31-41.

82. Oberheim, N.A., et al., *Astrocytic complexity distinguishes the human brain.* Trends Neurosci, 2006. **29**(10): p. 547-53.

83. Kimelberg, H.K. and M. Nedergaard, *Functions of astrocytes and their potential as therapeutic targets.* Neurotherapeutics, 2010. **7**(4): p. 338-53.

84. Oberheim, N.A., S.A. Goldman, and M. Nedergaard, *Heterogeneity of astrocytic form and function.* Methods Mol Biol, 2012. **814**: p. 23-45.

85. Hughes, E.G., et al., *Oligodendrocyte progenitors balance growth with self-repulsion to achieve homeostasis in the adult brain.* Nat Neurosci, 2013. **16**(6): p. 668-76.

86. Akay, L.A., A.H. Effenberger, and L.H. Tsai, *Cell of all trades: oligodendrocyte precursor cells in synaptic, vascular, and immune function.* Genes Dev, 2021. **35**(3-4): p. 180-198.

87. Kirby, L., et al., *Oligodendrocyte precursor cells present antigen and are cytotoxic targets in inflammatory demyelination.* Nat Commun, 2019. **10**(1): p. 3887.

88. Caldwell, J.H., et al., *Sodium channel Na(v)1.6 is localized at nodes of ranvier, dendrites, and synapses.* Proc Natl Acad Sci U S A, 2000. **97**(10): p. 5616-20.

89. Stadelmann, C., et al., *Myelin in the Central Nervous System: Structure, Function, and Pathology.* Physiol Rev, 2019. **99**(3): p. 1381-1431.

90. Ginhoux, F., et al., *Fate mapping analysis reveals that adult microglia derive from primitive macrophages.* Science, 2010. **330**(6005): p. 841-5.

91. Kriegstein, A. and A. Alvarez-Buylla, *The glial nature of embryonic and adult neural stem cells.* Annu Rev Neurosci, 2009. **32**: p. 149-84.

92. Colonna, M. and O. Butovsky, *Microglia Function in the Central Nervous System During Health and Neurodegeneration.* Annu Rev Immunol, 2017. **35**: p. 441-468.

93. Kadry, H., B. Noorani, and L. Cucullo, *A blood-brain barrier overview on structure, function, impairment, and biomarkers of integrity.* Fluids Barriers CNS, 2020. **17**(1): p. 69.

94. Pong, S., et al., *The Role of Brain Microvascular Endothelial Cell and Blood-Brain Barrier Dysfunction in Schizophrenia.* Complex Psychiatry, 2020. **6**(1-2): p. 30-46.

95. Cabezas, R., et al., *Astrocytic modulation of blood brain barrier: perspectives on Parkinson's disease.* Front Cell Neurosci, 2014. **8**: p. 211.

96. Maki, T., *Novel roles of oligodendrocyte precursor cells in the developing and damaged brain.* Clinical and Experimental Neuroimmunology, 2017. **8**(1): p. 33-42.

97. Hedden, T. and J.D. Gabrieli, *Insights into the ageing mind: a view from cognitive neuroscience.* Nat Rev Neurosci, 2004. **5**(2): p. 87-96.

98. Andrews-Hanna, J.R., et al., *Disruption of large-scale brain systems in advanced aging.* Neuron, 2007. **56**(5): p. 924-35.

99. Teissier, T., E. Boulanger, and V. Deramecourt, *Normal ageing of the brain: Histological and biological aspects.* Rev Neurol (Paris), 2020. **176**(9): p. 649-660.

100. Lee, J. and H.J. Kim, *Normal Aging Induces Changes in the Brain and Neurodegeneration Progress: Review of the Structural, Biochemical, Metabolic, Cellular, and Molecular Changes.* Front Aging Neurosci, 2022. **14**: p. 931536.

101. Masliah, E., et al., *Quantitative synaptic alterations in the human neocortex during normal aging.* Neurology, 1993. **43**(1 Part 1): p. 192-192.

102. Itoh, Y., et al., *An immunohistochemical study of centenarian brains: a comparison.* J Neurol Sci, 1998. **157**(1): p. 73-81.

103. Scheff, S.W., D.A. Price, and D.L. Sparks, *Quantitative assessment of possible age-related change in synaptic numbers in the human frontal cortex.* Neurobiol Aging, 2001. **22**(3): p. 355-65.

104. Michiels, L., et al., *Synaptic density in healthy human aging is not influenced by age or sex: a (11)C-UCB-J PET study.* Neuroimage, 2021. **232**: p. 117877.

105. Pyo, J.O., et al., *Overexpression of Atg5 in mice activates autophagy and extends lifespan.* Nat Commun, 2013. **4**: p. 2300.

106. Lapierre, L.R., et al., *The TFEB orthologue HLH-30 regulates autophagy and modulates longevity in Caenorhabditis elegans.* Nat Commun, 2013. **4**: p. 2267.

107. Toth, M.L., et al., *Longevity pathways converge on autophagy genes to regulate life span in Caenorhabditis elegans.* Autophagy, 2008. **4**(3): p. 330-8.

108. Hara, T., et al., *Suppression of basal autophagy in neural cells causes neurodegenerative disease in mice.* Nature, 2006. **441**(7095): p. 885-9.

109. Komatsu, M., et al., *Loss of autophagy in the central nervous system causes neurodegeneration in mice.* Nature, 2006. **441**(7095): p. 880-4.

110. Bishop, N.A., T. Lu, and B.A. Yankner, *Neural mechanisms of ageing and cognitive decline.* Nature, 2010. **464**(7288): p. 529-35.

111. Gleichmann, M. and M.P. Mattson, *Neuronal calcium homeostasis and dysregulation.* Antioxid Redox Signal, 2011. **14**(7): p. 1261-73.

112. Chandran, R., et al., *Cellular calcium signaling in the aging brain.* J Chem Neuroanat, 2019. **95**: p. 95-114.

113. Loerch, P.M., et al., *Evolution of the aging brain transcriptome and synaptic regulation.* PLoS One, 2008. **3**(10): p. e3329.

114. Ximerakis, M., et al., *Single-cell transcriptomic profiling of the aging mouse brain.* Nat Neurosci, 2019. **22**(10): p. 1696-1708.

115. Chiou, K.L., et al., *Multiregion transcriptomic profiling of the primate brain reveals signatures of aging and the social environment.* Nat Neurosci, 2022. **25**(12): p. 1714-1723.

116. Heuer, E., et al., *Nonhuman primate models of Alzheimer-like cerebral proteopathy.* Curr Pharm Des, 2012. **18**(8): p. 1159-69.

117. Toledano, A., et al., *Does Alzheimer's disease exist in all primates? Alzheimer pathology in non-human primates and its pathophysiological implications (I).* Neurología (English Edition), 2012. **27**(6): p. 354-369.

118. Hanseeuw, B.J., et al., *Association of Amyloid and Tau With Cognition in Preclinical Alzheimer Disease: A Longitudinal Study.* JAMA Neurol, 2019. **76**(8): p. 915-924.

119. Sperling, R.A., et al., *The impact of amyloid-beta and tau on prospective cognitive decline in older individuals.* Ann Neurol, 2019. **85**(2): p. 181-193.

120. Hwang, B., J.H. Lee, and D. Bang, *Single-cell RNA sequencing technologies and bioinformatics pipelines.* Exp Mol Med, 2018. **50**(8): p. 1-14.

121. Clark, S. *Single cell RNA-seq: An introductory overview and tools for getting started*. 2022 [cited 2023 July 11]; Available from: https://www.10xgenomics.com/blog/single-cell-rna-seq-an-introductory-overview-and-tools-for-getting-started.

122. Tang, F., et al., *mRNA-Seq whole-transcriptome analysis of a single cell.* Nat Methods, 2009. **6**(5): p. 377-82.

123. Ziegenhain, C., et al., *Comparative Analysis of Single-Cell RNA Sequencing Methods.* Mol Cell, 2017. **65**(4): p. 631-643 e4.

124. Lake, B.B., et al., *A comparative strategy for single-nucleus and single-cell transcriptomes confirms accuracy in predicted cell-type expression from nuclear RNA.* Sci Rep, 2017. **7**(1): p. 6031.

125. Bakken, T.E., et al., *Comparative cellular analysis of motor cortex in human, marmoset and mouse.* Nature, 2021. **598**(7879): p. 111-119.

126. Wu, H., et al., *Advantages of Single-Nucleus over Single-Cell RNA Sequencing of Adult Kidney: Rare Cell Types and Novel Cell States Revealed in Fibrosis.* J Am Soc Nephrol, 2019. **30**(1): p. 23-32.

127. Velmeshev, D., et al., *Single-cell genomics identifies cell type-specific molecular changes in autism.* Science, 2019. **364**(6441): p. 685-689.

128. Nagy, C., et al., *Single-nucleus transcriptomics of the prefrontal cortex in major depressive disorder implicates oligodendrocyte precursor cells and excitatory neurons.* Nat Neurosci, 2020. **23**(6): p. 771-781.

129. Reiner, B.C., et al., *Single-nuclei transcriptomics of schizophrenia prefrontal cortex primarily implicates neuronal subtypes.* bioRxiv, 2020: p. 2020.07.29.227355.

130. Ruzicka, W.B., et al., *Single-cell dissection of schizophrenia reveals neurodevelopmental-synaptic axis and transcriptional resilience.* medRxiv, 2020: p. 2020.11.06.20225342.

131. Smajić, S., et al., *Single-cell sequencing of human midbrain reveals glial activation and a Parkinson-specific neuronal state.* Brain, 2021. **145**(3): p. 964-978.

132. Mathys, H., et al., *Single-cell transcriptomic analysis of Alzheimer's disease.* Nature, 2019. **570**(7761): p. 332-337.

133. Lau, S.F., et al., *Single-nucleus transcriptome analysis reveals dysregulation of angiogenic endothelial cells and neuroprotective glia in Alzheimer's disease.* Proc Natl Acad Sci U S A, 2020. **117**(41): p. 25800-25809.

134. Jobson, D.D., et al., *The role of the medial prefrontal cortex in cognition, ageing and dementia.* Brain Commun, 2021. **3**(3): p. fcab125.

135. Resnick, S.M., M. Lamar, and I. Driscoll, *Vulnerability of the orbitofrontal cortex to age-associated structural and functional brain changes.* Ann N Y Acad Sci, 2007. **1121**: p. 562-75.

136. Xie, C., et al., *Reward Versus Nonreward Sensitivity of the Medial Versus Lateral Orbitofrontal Cortex Relates to the Severity of Depressive Symptoms.* Biol Psychiatry Cogn Neurosci Neuroimaging, 2021. **6**(3): p. 259-269.

137. Mladinov, M., et al., *Gene expression profiling of the dorsolateral and medial orbitofrontal cortex in schizophrenia.* Transl Neurosci, 2016. **7**(1): p. 139-150.

138. 10x Genomics. *Chromium Single Cell 3' Reagent Kits User Guide (v3.1 Chemistry)*. 2022 [cited 2023 July 11]; Available from: https://www.10xgenomics.com/support/single-cell-gene-expression/documentation/steps/library-prep/chromium-single-cell-3-reagent-kits-user-guide-v-3-1-chemistry.

139. Slovin, S., et al., *Single-Cell RNA Sequencing Analysis: A Step-by-Step Overview*, in *RNA Bioinformatics*, E. Picardi, Editor. 2021, Springer US: New York, NY. p. 343-365.

140. Yan, L., et al., *OSAT: a tool for sample-to-batch allocations in genomics experiments.* BMC Genomics, 2012. **13**: p. 689.

141. Matevossian, A. and S. Akbarian, *Neuronal nuclei isolation from human postmortem brain tissue.* J Vis Exp, 2008(20).

142. Wolf, F.A., P. Angerer, and F.J. Theis, *SCANPY: large-scale single-cell gene expression data analysis.* Genome Biol, 2018. **19**(1): p. 15.

143. Gayoso, A. and J. Shor. *JonathanShor/DoubletDetection: doubletdetection v4.2*. 2022; Available from: https://zenodo.org/record/6349517#.ZHdK4-xBxAc.

144. Hafemeister, C. and R. Satija, *Normalization and variance stabilization of single-cell RNA-seq data using regularized negative binomial regression.* Genome Biol, 2019. **20**(1): p. 296.

145. Lotfollahi, M., et al., *Mapping single-cell data to reference atlases by transfer learning.* Nat Biotechnol, 2022. **40**(1): p. 121-130.

146. Love, M.I., W. Huber, and S. Anders, *Moderated estimation of fold change and dispersion for RNA-seq data with DESeq2.* Genome Biol, 2014. **15**(12): p. 550.

147. Ritchie, M.E., et al., *limma powers differential expression analyses for RNA-sequencing and microarray studies.* Nucleic Acids Res, 2015. **43**(7): p. e47.

148. Hoffman, G.E. and E.E. Schadt, *variancePartition: interpreting drivers of variation in complex gene expression studies.* BMC Bioinformatics, 2016. **17**(1): p. 483.

149. Harrell, F.E.J. *Hmisc: Harrell Miscellaneous. R package version 5.0-1*. 2023 [cited 2023 30 May]; Available from: https://CRAN.R-project.org/package=Hmisc.

150. Robinson, M.D., D.J. McCarthy, and G.K. Smyth, *edgeR: a Bioconductor package for differential expression analysis of digital gene expression data.* Bioinformatics, 2010. **26**(1): p. 139-40.

151. Chen, Y., A.T. Lun, and G.K. Smyth, *From reads to genes to pathways: differential expression analysis of RNA-Seq experiments using Rsubread and the edgeR quasi-likelihood pipeline.* F1000Res, 2016. **5**: p. 1438.

152. Zimmerman, K.D., M.A. Espeland, and C.D. Langefeld, *A practical solution to pseudoreplication bias in single-cell studies.* Nat Commun, 2021. **12**(1): p. 738.

153. Squair, J.W., et al., *Confronting false discoveries in single-cell differential expression.* Nat Commun, 2021. **12**(1): p. 5692.

154. Lu, T., et al., *Gene regulation and DNA damage in the ageing human brain.* Nature, 2004. **429**(6994): p. 883-91.

155. Kumar, A., et al., *Age-associated changes in gene expression in human brain and isolated neurons.* Neurobiol Aging, 2013. **34**(4): p. 1199-209.

156. Shen, L. and Icahn School of Medicine at Mount Sinai. *GeneOverlap: Test and visualize gene overlaps. R package version 1.28.0*. 2021; Available from: https://github.com/shenlab-sinai/GeneOverlap.

157. Chatzinakos, C., et al., *Single-nucleus transcriptome profiling of dorsolateral prefrontal cortex reveals mechanistic roles for neuronal gene expression, including the 17q21.31 locus, in PTSD stress response.* The American Journal of Psychiatry, in press 2023.

158. Galatro, T.F., et al., *Transcriptomic analysis of purified human cortical microglia reveals age-associated changes.* Nat Neurosci, 2017. **20**(8): p. 1162-1171.

159. Krawczyk, M.C., et al., *Human Astrocytes Exhibit Tumor Microenvironment-, Age-, and Sex-Related Transcriptomic Signatures.* J Neurosci, 2022. **42**(8): p. 1587-1603.

160. Wu, T., et al., *clusterProfiler 4.0: A universal enrichment tool for interpreting omics data.* Innovation (Camb), 2021. **2**(3): p. 100141.

161. Yu, G., et al., *DOSE: an R/Bioconductor package for disease ontology semantic and enrichment analysis.* Bioinformatics, 2015. **31**(4): p. 608-9.

162. Reijnders, M. and R.M. Waterhouse, *Summary Visualizations of Gene Ontology Terms With GO-Figure!* Front Bioinform, 2021. **1**: p. 638255.

163. Horvath, S., *DNA methylation age of human tissues and cell types.* Genome Biol, 2013. **14**(10): p. R115.

164. Shireby, G.L., et al., *Recalibrating the epigenetic clock: implications for assessing biological age in the human cortex.* Brain, 2020. **143**(12): p. 3763-3775.

165. Aryee, M.J., et al., *Minfi: a flexible and comprehensive Bioconductor package for the analysis of Infinium DNA methylation microarrays.* Bioinformatics, 2014. **30**(10): p. 1363-9.

166. Touleimat, N. and J. Tost, *Complete pipeline for Infinium((R)) Human Methylation 450K BeadChip data processing using subset quantile normalization for accurate DNA methylation estimation.* Epigenomics, 2012. **4**(3): p. 325-41.

167. Maksimovic, J., B. Phipson, and A. Oshlack, *A cross-package Bioconductor workflow for analysing methylation array data.* F1000Res, 2016. **5**: p. 1281.

168. Teschendorff, A.E., et al., *A beta-mixture quantile normalization method for correcting probe design bias in Illumina Infinium 450 k DNA methylation data.* Bioinformatics, 2013. **29**(2): p. 189-96.

169. Pidsley, R., et al., *A data-driven approach to preprocessing Illumina 450K methylation array data.* BMC Genomics, 2013. **14**: p. 293.

170. Gorrie-Stone, T.J., et al., *Bigmelon: tools for analysing large DNA methylation datasets.* Bioinformatics, 2019. **35**(6): p. 981-986.

171. Leek, J.T., et al., *The sva package for removing batch effects and other unwanted variation in high-throughput experiments.* Bioinformatics, 2012. **28**(6): p. 882-3.

172. Westra, H.J., et al., *MixupMapper: correcting sample mix-ups in genome-wide datasets increases power to detect small genetic effects.* Bioinformatics, 2011. **27**(15): p. 2104-11.

173. Pelegi-Siso, D., et al., *methylclock: a Bioconductor package to estimate DNA methylation age.* Bioinformatics, 2021. **37**(12): p. 1759-1760.

174. Shireby, G.L. *CorticalClock*. 2021; Available from: https://github.com/gemmashireby/CorticalClock.

175. Guintivano, J., M.J. Aryee, and Z.A. Kaminsky, *A cell epigenotype specific model for the correction of brain cellular heterogeneity bias and its application to age, brain region and major depression.* Epigenetics, 2013. **8**(3): p. 290-302.

176. Purcell, S., et al., *PLINK: a tool set for whole-genome association and population-based linkage analyses.* Am J Hum Genet, 2007. **81**(3): p. 559-75.

177. Delaneau, O., J. Marchini, and J.F. Zagury, *A linear complexity phasing method for thousands of genomes.* Nat Methods, 2011. **9**(2): p. 179-81.

178. Marchini, J., et al., *A new multipoint method for genome-wide association studies by imputation of genotypes.* Nat Genet, 2007. **39**(7): p. 906-13.

179. Cross-Disorder Group of the Psychiatric Genomics Consortium. Electronic address, p.m.h.e. and C. Cross-Disorder Group of the Psychiatric Genomics, *Genomic Relationships, Novel Loci, and Pleiotropic Mechanisms across Eight Psychiatric Disorders.* Cell, 2019. **179**(7): p. 1469-1482 e11.

180. Ge, T., et al., *Polygenic prediction via Bayesian regression and continuous shrinkage priors.* Nat Commun, 2019. **10**(1): p. 1776.

181. Ge, T. *PRS-CS*. 2019; Available from: https://github.com/getian107/PRScs.

182. Chang, C.C. *PLINK 1.90 beta*. 2023; Available from: https://www.cog-genomics.org/plink/1.9/.

183. Chang, C.C., et al., *Second-generation PLINK: rising to the challenge of larger and richer datasets.* Gigascience, 2015. **4**: p. 7.

184. Highet, B., et al., *RNA Quality in Post-mortem Human Brain Tissue Is Affected by Alzheimer's Disease.* Front Mol Neurosci, 2021. **14**: p. 780352.

185. Benjamini, Y. and Y. Hochberg, *Controlling The False Discovery Rate - A Practical And Powerful Approach To Multiple Testing.* J. Royal Statist. Soc., Series B, 1995. **57**: p. 289-300.

186. Wu, H., C. Wang, and Z. Wu, *PROPER: comprehensive power evaluation for differential expression using RNA-seq.* Bioinformatics, 2015. **31**(2): p. 233-41.

187. Krienen, F.M., et al., *Innovations present in the primate interneuron repertoire.* Nature, 2020. **586**(7828): p. 262-269.

188. Lonze, B.E. and D.D. Ginty, *Function and regulation of CREB family transcription factors in the nervous system.* Neuron, 2002. **35**(4): p. 605-23.

189. Matosin, N., et al., *Associations of psychiatric disease and ageing with FKBP5 expression converge on superficial layer neurons of the neocortex.* Acta Neuropathol, 2023.

190. Antunez, C., et al., *The membrane-spanning 4-domains, subfamily A (MS4A) gene cluster contains a common variant associated with Alzheimer's disease.* Genome Med, 2011. **3**(5): p. 33.

191. Hollingworth, P., et al., *Common variants at ABCA7, MS4A6A/MS4A4E, EPHA1, CD33 and CD2AP are associated with Alzheimer's disease.* Nat Genet, 2011. **43**(5): p. 429-35.

192. Timmers, P.R.H.J., et al., *Mendelian randomization of genetically independent aging phenotypes identifies LPA and VCAM1 as biological targets for human aging.* Nature Aging, 2022. **2**(1): p. 19-30.

193. Lambert, J.C., et al., *Meta-analysis of 74,046 individuals identifies 11 new susceptibility loci for Alzheimer's disease.* Nat Genet, 2013. **45**(12): p. 1452-8.

194. Kohli, M.A., et al., *The neuronal transporter gene SLC6A15 confers risk to major depression.* Neuron, 2011. **70**(2): p. 252-65.

195. Ni, H., et al., *The GWAS Risk Genes for Depression May Be Actively Involved in Alzheimer's Disease.* J Alzheimers Dis, 2018. **64**(4): p. 1149-1161.

196. Egan, M.F., et al., *Variation in GRM3 affects cognition, prefrontal glutamate, and risk for schizophrenia.* Proc Natl Acad Sci U S A, 2004. **101**(34): p. 12604-9.

197. Yu, L., et al., *Cortical Proteins Associated With Cognitive Resilience in Community-Dwelling Older Persons.* JAMA Psychiatry, 2020. **77**(11): p. 1172-1180.

198. Tan, M.G., et al., *Decreased rabphilin 3A immunoreactivity in Alzheimer's disease is associated with Abeta burden.* Neurochem Int, 2014. **64**: p. 29-36.

199. Chang, C.K., et al., *Life expectancy at birth for people with serious mental illness and other major disorders from a secondary mental health care case register in London.* PLoS One, 2011. **6**(5): p. e19590.

200. Huo, Y.X., et al., *Identification of SLC25A37 as a major depressive disorder risk gene.* J Psychiatr Res, 2016. **83**: p. 168-175.

201. Lavdovskaia, E., et al., *Dual function of GTPBP6 in biogenesis and recycling of human mitochondrial ribosomes.* Nucleic Acids Res, 2020. **48**(22): p. 12929-12942.

202. Cao, M., et al., *Identification of age- and gender-associated long noncoding RNAs in the human brain with Alzheimer's disease.* Neurobiol Aging, 2019. **81**: p. 116-126.

203. Mills, J.D., et al., *LINC00507 Is Specifically Expressed in the Primate Cortex and Has Age-Dependent Expression Patterns.* J Mol Neurosci, 2016. **59**(4): p. 431-9.

204. Lombard, D.B., et al., *DNA repair, genome stability, and aging.* Cell, 2005. **120**(4): p. 497-512.

205. Su, J., et al., *Collagen XIX is expressed by interneurons and contributes to the formation of hippocampal synapses.* J Comp Neurol, 2010. **518**(2): p. 229-53.

206. Dittman, J.S., *Unc13: a multifunctional synaptic marvel.* Curr Opin Neurobiol, 2019. **57**: p. 17-25.

207. Qi, X.R., et al., *Human Brain Slice Culture: A Useful Tool to Study Brain Disorders and Potential Therapeutic Compounds.* Neurosci Bull, 2019. **35**(2): p. 244-252.

208. Kaas, J.H., *The evolution of neocortex in primates.* Prog Brain Res, 2012. **195**: p. 91-102.

209. Buckner, R.L. and F.M. Krienen, *The evolution of distributed association networks in the human brain.* Trends Cogn Sci, 2013. **17**(12): p. 648-65.

210. Murray, S.J. and N.L. Mitchell, *The Translational Benefits of Sheep as Large Animal Models of Human Neurological Disorders.* Front Vet Sci, 2022. **9**: p. 831838.

211. Sun, T. and R.F. Hevner, *Growth and folding of the mammalian cerebral cortex: from molecules to malformations.* Nat Rev Neurosci, 2014. **15**(4): p. 217-32.

212. Beauchamp, A., et al., *Whole-brain comparison of rodent and human brains using spatial transcriptomics.* Elife, 2022. **11**.

213. Takahashi, K. and S. Yamanaka, *Induction of pluripotent stem cells from mouse embryonic and adult fibroblast cultures by defined factors.* Cell, 2006. **126**(4): p. 663-76.

214. Lancaster, M.A., et al., *Cerebral organoids model human brain development and microcephaly.* Nature, 2013. **501**(7467): p. 373-9.

215. Wu, Y.Y., et al., *Opportunities and challenges for the use of induced pluripotent stem cells in modelling neurodegenerative disease.* Open Biol, 2019. **9**(1): p. 180177.

216. Camp, J.G., et al., *Human cerebral organoids recapitulate gene expression programs of fetal neocortex development.* Proc Natl Acad Sci U S A, 2015. **112**(51): p. 15672-7.

217. Vadodaria, K.C., et al., *Modeling Brain Disorders Using Induced Pluripotent Stem Cells.* Cold Spring Harb Perspect Biol, 2020. **12**(6).

218. Aversano, S., C. Caiazza, and M. Caiazzo, *Induced pluripotent stem cell-derived and directly reprogrammed neurons to study neurodegenerative diseases: The impact of aging signatures.* Front Aging Neurosci, 2022. **14**: p. 1069482.

219. Tang, Y., et al., *Direct Reprogramming Rather than iPSC-Based Reprogramming Maintains Aging Hallmarks in Human Motor Neurons.* Front Mol Neurosci, 2017. **10**: p. 359.

220. Drouin-Ouellet, J., et al., *Age-related pathological impairments in directly reprogrammed dopaminergic neurons derived from patients with idiopathic Parkinson's disease.* Stem Cell Reports, 2022. **17**(10): p. 2203-2219.

221. Huh, C.J., et al., *Maintenance of age in human neurons generated by microRNA-based neuronal conversion of fibroblasts.* Elife, 2016. **5**.

222. Mertens, J., et al., *Aging in a Dish: iPSC-Derived and Directly Induced Neurons for Studying Brain Aging and Age-Related Neurodegenerative Diseases.* Annu Rev Genet, 2018. **52**: p. 271-293.

223. Mertens, J., et al., *Age-dependent instability of mature neuronal fate in induced neurons from Alzheimer's patients.* Cell Stem Cell, 2021. **28**(9): p. 1533-1548 e6.

224. Caiazzo, M., et al., *Direct conversion of fibroblasts into functional astrocytes by defined transcription factors.* Stem Cell Reports, 2015. **4**(1): p. 25-36.

225. Najm, F.J., et al., *Transcription factor-mediated reprogramming of fibroblasts to expandable, myelinogenic oligodendrocyte progenitor cells.* Nat Biotechnol, 2013. **31**(5): p. 426-33.

226. Quist, E., et al., *Transcription factor-based direct conversion of human fibroblasts to functional astrocytes.* Stem Cell Reports, 2022. **17**(7): p. 1620-1635.

227. Meyer, K., et al., *Direct conversion of patient fibroblasts demonstrates non-cell autonomous toxicity of astrocytes to motor neurons in familial and sporadic ALS.* Proc Natl Acad Sci U S A, 2014. **111**(2): p. 829-32.

228. Verwer, R.W., et al., *Cells in human postmortem brain tissue slices remain alive for several weeks in culture.* FASEB J, 2002. **16**(1): p. 54-60.

229. Nativio, R., et al., *Dysregulation of the epigenetic landscape of normal aging in Alzheimer's disease.* Nat Neurosci, 2018. **21**(4): p. 497-505.

230. Kandigian, S.E., et al., *Proteomic characterization of post-mortem human brain tissue following ultracentrifugation-based subcellular fractionation.* Brain Commun, 2022. **4**(3): p. fcac103.

231. Chen, M.B., et al., *Brain Endothelial Cells Are Exquisite Sensors of Age-Related Circulatory Cues.* Cell Rep, 2020. **30**(13): p. 4418-4432 e4.

232. Elahy, M., et al., *Blood-brain barrier dysfunction developed during normal aging is associated with inflammation and loss of tight junctions but not with leukocyte recruitment.* Immun Ageing, 2015. **12**: p. 2.

233. Montagne, A., et al., *Blood-brain barrier breakdown in the aging human hippocampus.* Neuron, 2015. **85**(2): p. 296-302.

234. Grimm, A. and A. Eckert, *Brain aging and neurodegeneration: from a mitochondrial point of view.* J Neurochem, 2017. **143**(4): p. 418-431.

235. Sheng, Z.H. and Q. Cai, *Mitochondrial transport in neurons: impact on synaptic homeostasis and neurodegeneration.* Nat Rev Neurosci, 2012. **13**(2): p. 77-93.

236. Norden, D.M. and J.P. Godbout, *Review: microglia of the aged brain: primed to be activated and resistant to regulation.* Neuropathol Appl Neurobiol, 2013. **39**(1): p. 19-34.

237. Pan, J., et al., *Transcriptomic profiling of microglia and astrocytes throughout aging.* J Neuroinflammation, 2020. **17**(1): p. 97.

238. Clarke, L.E., et al., *Normal aging induces A1-like astrocyte reactivity.* Proc Natl Acad Sci U S A, 2018. **115**(8): p. E1896-E1905.

239. Ding, Y., et al., *Molecular and Genetic Characterization of Depression: Overlap with other Psychiatric Disorders and Aging.* Mol Neuropsychiatry, 2015. **1**(1): p. 1-12.

240. Deng, Y., et al., *Loss of LAMP5 interneurons drives neuronal network dysfunction in Alzheimer's disease.* Acta Neuropathol, 2022. **144**(4): p. 637-650.

241. Armstrong, C., E. Krook-Magnuson, and I. Soltesz, *Neurogliaform and Ivy Cells: A Major Family of nNOS Expressing GABAergic Neurons.* Front Neural Circuits, 2012. **6**: p. 23.

242. Olah, S., et al., *Regulation of cortical microcircuits by unitary GABA-mediated volume transmission.* Nature, 2009. **461**(7268): p. 1278-81.

243. Machold, R., et al., *Id2 GABAergic interneurons: a neglected fourth major group of cortical inhibitory cells.* bioRxiv, 2022.

244. Chun, H., et al., *Severe reactive astrocytes precipitate pathological hallmarks of Alzheimer's disease via H(2)O(2)(-) production.* Nat Neurosci, 2020. **23**(12): p. 1555-1566.

245. Haytural, H., et al., *Insights into the changes in the proteome of Alzheimer disease elucidated by a meta-analysis.* Sci Data, 2021. **8**(1): p. 312.

246. Libiger, O., et al., *Longitudinal CSF proteomics identifies NPTX2 as a prognostic biomarker of Alzheimer's disease.* Alzheimers Dement, 2021. **17**(12): p. 1976-1987.

247. Sun, X., et al., *Association of neurogranin gene expression with Alzheimer's disease pathology in the perirhinal cortex.* Alzheimers Dement (N Y), 2021. **7**(1): p. e12162.

248. Teng, X., et al., *KCTD: A new gene family involved in neurodevelopmental and neuropsychiatric disorders.* CNS Neurosci Ther, 2019. **25**(7): p. 887-902.

249. Mi, S., et al., *LINGO-1 negatively regulates myelination by oligodendrocytes.* Nat Neurosci, 2005. **8**(6): p. 745-51.

250. Fernandez-Enright, F. and J.L. Andrews, *Lingo-1: a novel target in therapy for Alzheimer's disease?* Neural Regen Res, 2016. **11**(1): p. 88-9.

251. He, Q., et al., *Anti-LINGO-1 antibody ameliorates cognitive impairment, promotes adult hippocampal neurogenesis, and increases the abundance of CB1R-rich CCK-GABAergic interneurons in AD mice.* Neurobiol Dis, 2021. **156**: p. 105406.

252. Cadavid, D., et al., *Safety and efficacy of opicinumab in patients with relapsing multiple sclerosis (SYNERGY): a randomised, placebo-controlled, phase 2 trial.* Lancet Neurol, 2019. **18**(9): p. 845-856.

253. Bell, C.G., et al., *DNA methylation aging clocks: challenges and recommendations.* Genome Biol, 2019. **20**(1): p. 249.

254. Hannum, G., et al., *Genome-wide methylation profiles reveal quantitative views of human aging rates.* Mol Cell, 2013. **49**(2): p. 359-367.

255. Peters, M.J., et al., *The transcriptional landscape of age in human peripheral blood.* Nat Commun, 2015. **6**: p. 8570.

256. Nielsen, R.E., J. Banner, and S.E. Jensen, *Cardiovascular disease in patients with severe mental illness.* Nat Rev Cardiol, 2021. **18**(2): p. 136-145.

257. Koutsouleris, N., et al., *Accelerated brain aging in schizophrenia and beyond: a neuroanatomical marker of psychiatric disorders.* Schizophr Bull, 2014. **40**(5): p. 1140-53.

258. Demro, C., et al., *Advanced Brain-Age in Psychotic Psychopathology: Evidence for Transdiagnostic Neurodevelopmental Origins.* Front Aging Neurosci, 2022. **14**: p. 872867.

259. McKinney, B.C., et al., *DNA methylation evidence against the accelerated aging hypothesis of schizophrenia.* NPJ Schizophr, 2017. **3**: p. 13.

260. Voisey, J., et al., *Epigenetic analysis confirms no accelerated brain aging in schizophrenia.* NPJ Schizophr, 2017. **3**(1): p. 26.

261. Jylhava, J., N.L. Pedersen, and S. Hagg, *Biological Age Predictors.* EBioMedicine, 2017. **21**: p. 29-36.

262. Belsky, D.W., et al., *Eleven Telomere, Epigenetic Clock, and Biomarker-Composite Quantifications of Biological Aging: Do They Measure the Same Thing?* Am J Epidemiol, 2018. **187**(6): p. 1220-1230.

263. Franke, K. and C. Gaser, *Ten Years of BrainAGE as a Neuroimaging Biomarker of Brain Aging: What Insights Have We Gained?* Front Neurol, 2019. **10**: p. 789.

264. Mullins, N., et al., *Dissecting the Shared Genetic Architecture of Suicide Attempt, Psychiatric Disorders, and Known Risk Factors.* Biol Psychiatry, 2022. **91**(3): p. 313-327.

265. Andrews, T.S., et al., *Single-Cell, Single-Nucleus, and Spatial RNA Sequencing of the Human Liver Identifies Cholangiocyte and Mesenchymal Heterogeneity.* Hepatol Commun, 2022. **6**(4): p. 821-840.

266. Mazin, P., et al., *Widespread splicing changes in human brain development and aging.* Mol Syst Biol, 2013. **9**: p. 633.

267. Tollervey, J.R., et al., *Analysis of alternative splicing associated with aging and neurodegeneration in the human brain.* Genome Res, 2011. **21**(10): p. 1572-82.

268. Reble, E., A. Dineen, and C.L. Barr, *The contribution of alternative splicing to genetic risk for psychiatric disorders.* Genes Brain Behav, 2018. **17**(3): p. e12430.

269. Zhang, C.Y., et al., *An alternative splicing hypothesis for neuropathology of schizophrenia: evidence from studies on historical candidate genes and multi-omics data.* Mol Psychiatry, 2022. **27**(1): p. 95-112.

270. Garcia, F.J., et al., *Single-cell dissection of the human brain vasculature.* Nature, 2022. **603**(7903): p. 893-899.

271. Yang, A.C., et al., *A human brain vascular atlas reveals diverse mediators of Alzheimer's risk.* Nature, 2022. **603**(7903): p. 885-892.

272. Bennett, D.A., et al., *Religious Orders Study and Rush Memory and Aging Project.* J Alzheimers Dis, 2018. **64**(s1): p. S161-S189.

273. Cain, A., et al., *Multicellular communities are perturbed in the aging human brain and Alzheimer's disease.* Nat Neurosci, 2023.

7 | Appendix

7.1 Supplementary Tables

Supplementary Table 1: Comparison of number of nuclei per cell type between controls and psychiatric cases.

Cell Type	Controls (N)	Cases (N)	Statistic	Df	p-value	Normally distributed	Variance	Test
Astro_FB	33	54	1.12	N/A	0.264	No	unequal	brunner-munzel test
Astro_PP	33	54	-1.42	85.00	0.159	Yes	equal	t-test
Endothelial	33	54	954.00	N/A	0.585	No	equal	wilcox
Exc_L2-3	33	54	872.00	N/A	0.871	No	equal	wilcox
Exc_L3-5	33	54	871.00	N/A	0.865	No	equal	wilcox
Exc_L4-6_1	33	54	-0.87	85.00	0.386	Yes	equal	t-test
Exc_L4-6_2	33	54	-0.67	85.00	0.506	Yes	equal	t-test
Exc_L4-6_3	33	52	682.50	N/A	0.115	No	equal	wilcox
Exc_L5-6_1	33	53	751.00	N/A	0.275	No	equal	wilcox
Exc_L5-6_2	32	50	661.50	N/A	0.189	No	equal	wilcox
Exc_L5-6_HTR2C	32	53	750.00	N/A	0.376	No	equal	wilcox
In_LAMP5	33	54	-1.17	85.00	0.243	Yes	equal	t-test
In_PVALB_Ba	33	54	-0.72	85.00	0.472	Yes	equal	t-test
In_PVALB_Ch	33	54	-0.30	85.00	0.766	Yes	equal	t-test
In_RELN	33	54	748.00	N/A	0.213	No	equal	wilcox
In_SST	33	54	1.43	53.11	0.160	Yes	unequal	t-test
In_VIP	33	54	-0.77	85.00	0.445	Yes	equal	t-test
Microglia	33	54	1039.50	N/A	0.195	No	equal	wilcox
Oligodendrocyte	33	54	884.50	N/A	0.958	No	equal	wilcox
OPC	33	54	-0.977	85	0.33	Yes	equal	t-test

Supplementary Table 2: Top ten upregulated DE genes (based on log2FC) per cell type

Upregulated DE genes				
Cell type	**Ensembl ID**	**Gene name**	**logFC**	**FDR-adj. p-value**
Astro_FB	ENSG00000287704	AC012405.1	0.031	0.007
	ENSG00000111907	TPD52L1	0.027	0.016
	ENSG00000083067	TRPM3	0.026	0.016
	ENSG00000188596	CFAP54	0.020	0.022
	ENSG00000157445	CACNA2D3	0.020	0.082
	ENSG00000052126	PLEKHA5	0.018	0.007
	ENSG00000106351	AGFG2	0.017	0.052
	ENSG00000132470	ITGB4	0.017	0.016
	ENSG00000100364	KIAA0930	0.017	0.016
	ENSG00000034677	RNF19A	0.016	0.056
Astro_PP	ENSG00000174776	WDR49	0.039	0.038
	ENSG00000132470	ITGB4	0.036	0.001
	ENSG00000038427	VCAN	0.036	0.003
	ENSG00000106624	AEBP1	0.034	0.066
	ENSG00000069535	MAOB	0.025	0.067
	ENSG00000188596	CFAP54	0.023	0.004
	ENSG00000233420	AC002069.2	0.023	0.067
	ENSG00000259616	AC104574.2	0.023	0.033
	ENSG00000253642	AF279873.3	0.021	0.083
	ENSG00000283913	AL512662.2	0.021	0.033
Exc_L2-3	ENSG00000096060	FKBP5	0.047	0.000
	ENSG00000286619	AC119673.2	0.046	0.084
	ENSG00000261543	AC010931.3	0.037	0.003
	ENSG00000176387	HSD11B2	0.034	0.001
	ENSG00000125378	BMP4	0.034	0.001
	ENSG00000124749	COL21A1	0.033	0.000
	ENSG00000047936	ROS1	0.033	0.000
	ENSG00000196104	SPOCK3	0.030	0.000
	ENSG00000189295	ANKRD62P1-PARP4P3	0.030	0.002
	ENSG00000123560	PLP1	0.029	0.063
Exc_L3-5	ENSG00000112038	OPRM1	0.026	0.000
	ENSG00000138378	STAT4	0.025	0.019
	ENSG00000196975	ANXA4	0.021	0.001
	ENSG00000168830	HTR1E	0.021	0.015
	ENSG00000146555	SDK1	0.020	0.059
	ENSG00000029534	ANK1	0.020	0.026
	ENSG00000182836	PLCXD3	0.019	0.030
	ENSG00000172554	SNTG2	0.019	0.060
	ENSG00000155974	GRIP1	0.018	0.074
	ENSG00000180287	PLD5	0.018	0.015

Supplementary Table 2 *CONTINUED*

Upregulated DE genes				
Cell type	**Ensembl ID**	**Gene name**	**logFC**	**FDR-adj. p-value**
Exc_L4-6_1	ENSG00000136546	SCN7A	0.035	0.000
	ENSG00000047936	ROS1	0.031	0.001
	ENSG00000253642	AF279873.3	0.030	0.000
	ENSG00000181031	RPH3AL	0.029	0.000
	ENSG00000167693	NXN	0.028	0.003
	ENSG00000151136	BTBD11	0.028	0.001
	ENSG00000172986	GXYLT2	0.025	0.000
	ENSG00000267098	AC113137.1	0.024	0.055
	ENSG00000174498	IGDCC3	0.024	0.000
	ENSG00000158683	PKD1L1	0.023	0.000
Exc_L4-6_2	ENSG00000141314	RHBDL3	0.045	0.000
	ENSG00000181031	RPH3AL	0.041	0.000
	ENSG00000286619	AC119673.2	0.040	0.092
	ENSG00000166002	SMCO4	0.029	0.001
	ENSG00000253642	AF279873.3	0.029	0.000
	ENSG00000092421	SEMA6A	0.027	0.000
	ENSG00000029534	ANK1	0.026	0.000
	ENSG00000183785	TUBA8	0.024	0.000
	ENSG00000146555	SDK1	0.023	0.016
	ENSG00000255595	AC007368.1	0.023	0.004
Exc_L4-6_3	ENSG00000096060	FKBP5	0.037	0.000
	ENSG00000104043	ATP8B4	0.030	0.007
	ENSG00000141314	RHBDL3	0.028	0.000
	ENSG00000261543	AC010931.3	0.023	0.087
	ENSG00000099250	NRP1	0.020	0.028
	ENSG00000058866	DGKG	0.019	0.000
	ENSG00000197635	DPP4	0.019	0.039
	ENSG00000197892	KIF13B	0.018	0.000
	ENSG00000244040	IL12A-AS1	0.018	0.050
	ENSG00000233559	LINC00513	0.017	0.009
Exc_L5-6_1	ENSG00000122574	WIPF3	0.028	0.002
	ENSG00000141314	RHBDL3	0.022	0.010
	ENSG00000077943	ITGA8	0.019	0.046
	ENSG00000109452	INPP4B	0.018	0.020
	ENSG00000141668	CBLN2	0.016	0.041
	ENSG00000183722	LHFPL6	0.016	0.018
	ENSG00000177119	ANO6	0.015	0.018
	ENSG00000137672	TRPC6	0.015	0.046
	ENSG00000081803	CADPS2	0.015	0.032
	ENSG00000233559	LINC00513	0.015	0.014

Supplementary Table 2 *CONTINUED*

Upregulated DE genes				
Cell type	**Ensembl ID**	**Gene name**	**logFC**	**FDR-adj. p-value**
Exc_L5-6_2	ENSG00000058866	DGKG	0.015	0.041
	ENSG00000038532	CLEC16A	0.015	0.020
	ENSG00000120594	PLXDC2	0.014	0.053
	ENSG00000108684	ASIC2	0.013	0.010
	ENSG00000079691	CARMIL1	0.012	0.039
	ENSG00000140262	TCF12	0.012	0.075
	ENSG00000183722	LHFPL6	0.012	0.075
	ENSG00000251562	MALAT1	0.011	0.067
	ENSG00000156299	TIAM1	0.010	0.067
	ENSG00000084676	NCOA1	0.009	0.053
Exc_L5-6_HTR2C	ENSG00000185666	SYN3	0.023	0.040
	ENSG00000175471	MCTP1	0.016	0.040
	ENSG00000152583	SPARCL1	0.015	0.083
	ENSG00000249335	AC093523.1	0.015	0.078
	ENSG00000157445	CACNA2D3	0.013	0.001
	ENSG00000095066	HOOK2	0.012	0.040
	ENSG00000133226	SRRM1	0.012	0.059
	ENSG00000076356	PLXNA2	0.011	0.078
	ENSG00000168830	HTR1E	0.010	0.100
	ENSG00000004866	ST7	0.010	0.081
In_LAMP5	ENSG00000286619	AC119673.2	0.039	0.066
	ENSG00000282885	AL627171.2	0.026	0.032
	ENSG00000196218	RYR1	0.023	0.004
	ENSG00000227240	AL136456.1	0.018	0.002
	ENSG00000227486	AL050309.1	0.017	0.005
	ENSG00000119227	PIGZ	0.016	0.009
	ENSG00000184500	PROS1	0.016	0.006
	ENSG00000077943	ITGA8	0.016	0.006
	ENSG00000224905	AP001347.1	0.016	0.012
	ENSG00000130653	PNPLA7	0.015	0.008
In_PVALB_Ba	ENSG00000146376	ARHGAP18	0.025	0.048
	ENSG00000226149	AL356124.1	0.023	0.061
	ENSG00000250101	AC106795.3	0.020	0.037
	ENSG00000254746	AC103855.2	0.019	0.081
	ENSG00000285955	BX842242.1	0.017	0.056
	ENSG00000159231	CBR3	0.015	0.082
	ENSG00000205476	CCDC85C	0.013	0.082
	ENSG00000257458	AC069437.1	0.013	0.082
	ENSG00000233559	LINC00513	0.011	0.085
	ENSG00000159433	STARD9	0.011	0.029

Supplementary Table 2 *CONTINUED*

Upregulated DE genes				
Cell type	**Ensembl ID**	**Gene name**	**logFC**	**FDR-adj. p-value**
In_PVALB_Ch	ENSG00000158683	PKD1L1	0.018	0.019
	ENSG00000146966	DENND2A	0.017	0.000
	ENSG00000145416	MARCH1	0.016	0.052
	ENSG00000187609	EXD3	0.015	0.038
	ENSG00000204677	FAM153CP	0.014	0.038
	ENSG00000136699	SMPD4	0.014	0.038
	ENSG00000134882	UBAC2	0.013	0.015
	ENSG00000125351	UPF3B	0.013	0.089
	ENSG00000114648	KLHL18	0.012	0.085
	ENSG00000145996	CDKAL1	0.012	0.003
In_RELN	ENSG00000096060	FKBP5	0.029	0.073
	ENSG00000282885	AL627171.2	0.028	0.067
	ENSG00000087253	LPCAT2	0.016	0.052
	ENSG00000197971	MBP	0.016	0.052
	ENSG00000109458	GAB1	0.015	0.093
	ENSG00000186417	GLDN	0.014	0.077
	ENSG00000125122	LRRC29	0.013	0.073
	ENSG00000130653	PNPLA7	0.012	0.039
	ENSG00000168026	TTC21A	0.012	0.073
	ENSG00000256824	AP000721.2	0.012	0.073
In_SST	ENSG00000136546	SCN7A	0.029	0.001
	ENSG00000231533	AL391840.1	0.022	0.025
	ENSG00000248898	AC022126.1	0.021	0.097
	ENSG00000248359	AC010280.1	0.019	0.002
	ENSG00000213949	ITGA1	0.017	0.043
	ENSG00000249335	AC093523.1	0.016	0.016
	ENSG00000117266	CDK18	0.016	0.054
	ENSG00000088756	ARHGAP28	0.016	0.040
	ENSG00000162669	HFM1	0.015	0.034
	ENSG00000011426	ANLN	0.015	0.095
In_VIP	ENSG00000267761	MIR4527HG	0.045	0.001
	ENSG00000286619	AC119673.2	0.042	0.078
	ENSG00000096060	FKBP5	0.029	0.003
	ENSG00000282885	AL627171.2	0.026	0.027
	ENSG00000147459	DOCK5	0.022	0.060
	ENSG00000166960	CCDC178	0.020	0.065
	ENSG00000178075	GRAMD1C	0.020	0.033
	ENSG00000254101	LINC02055	0.019	0.016
	ENSG00000021826	CPS1	0.018	0.100
	ENSG00000130653	PNPLA7	0.017	0.003

Supplementary Table 2 *CONTINUED*

Upregulated DE genes				
Cell type	**Ensembl ID**	**Gene name**	**logFC**	**FDR-adj. p-value**
Microglia	ENSG00000110077	MS4A6A	0.059	0.000
	ENSG00000147459	DOCK5	0.048	0.000
	ENSG00000117115	PADI2	0.042	0.001
	ENSG00000188641	DPYD	0.039	0.002
	ENSG00000114861	FOXP1	0.034	0.000
	ENSG00000006747	SCIN	0.028	0.091
	ENSG00000132122	SPATA6	0.027	0.062
	ENSG00000237484	LINC01684	0.026	0.028
	ENSG00000197081	IGF2R	0.024	0.026
	ENSG00000135678	CPM	0.024	0.019
Oligodenrocyte	ENSG00000196169	KIF19	0.037	0.003
	ENSG00000004799	PDK4	0.030	0.007
	ENSG00000100906	NFKBIA	0.023	0.031
	ENSG00000161791	FMNL3	0.022	0.045
	ENSG00000287299	AC012459.1	0.022	0.025
	ENSG00000072041	SLC6A15	0.022	0.000
	ENSG00000044524	EPHA3	0.021	0.063
	ENSG00000165175	MID1IP1	0.021	0.029
	ENSG00000273118	AC093865.1	0.020	0.090
	ENSG00000154864	PIEZO2	0.019	0.025
OPC	ENSG00000096060	FKBP5	0.035	0.019
	ENSG00000147459	DOCK5	0.034	0.030
	ENSG00000175445	LPL	0.032	0.009
	ENSG00000127325	BEST3	0.027	0.001
	ENSG00000124440	HIF3A	0.026	0.087
	ENSG00000103319	EEF2K	0.025	0.014
	ENSG00000228526	MIR34AHG	0.025	0.013
	ENSG00000173805	HAP1	0.024	0.073
	ENSG00000253642	AF279873.3	0.021	0.021
	ENSG00000103264	FBXO31	0.021	0.012

Supplementary Table 3: Top ten downregulated DE genes (based on log2FC) per cell type.

Downregulated DE genes				
Cell type	**Ensembl ID**	**Gene name**	**logFC**	**FDR-adj. p-value**
Astro_FB	ENSG00000151572	ANO4	-0.032	0.016
	ENSG00000183662	TAFA1	-0.029	0.000
	ENSG00000211448	DIO2	-0.026	0.032
	ENSG00000100095	SEZ6L	-0.024	0.064
	ENSG00000104112	SCG3	-0.023	0.000
	ENSG00000173406	DAB1	-0.023	0.007
	ENSG00000144218	AFF3	-0.023	0.007
	ENSG00000112715	VEGFA	-0.022	0.078
	ENSG00000198822	GRM3	-0.022	0.016
	ENSG00000112902	SEMA5A	-0.022	0.078
Astro_PP	ENSG00000258416	AF123462.1	-0.034	0.007
	ENSG00000258637	AC008056.1	-0.034	0.007
	ENSG00000141837	CACNA1A	-0.032	0.004
	ENSG00000172247	C1QTNF4	-0.027	0.033
	ENSG00000157851	DPYSL5	-0.025	0.068
	ENSG00000117600	PLPPR4	-0.024	0.049
	ENSG00000152495	CAMK4	-0.023	0.009
	ENSG00000156687	UNC5D	-0.022	0.009
	ENSG00000130558	OLFM1	-0.022	0.004
	ENSG00000144366	GULP1	-0.022	0.037
Exc_L2-3	ENSG00000050628	PTGER3	-0.052	0.000
	ENSG00000197261	C6orf141	-0.050	0.000
	ENSG00000234464	AL356010.2	-0.044	0.000
	ENSG00000231877	AL359551.1	-0.043	0.001
	ENSG00000250190	LINC02364	-0.042	0.000
	ENSG00000188133	TMEM215	-0.040	0.000
	ENSG00000286321	AC093791.2	-0.040	0.007
	ENSG00000287373	AL122014.1	-0.039	0.000
	ENSG00000144681	STAC	-0.039	0.000
	ENSG00000237250	AL359924.1	-0.039	0.000
Exc_L3-5	ENSG00000256193	LINC00507	-0.027	0.006
	ENSG00000185053	SGCZ	-0.026	0.057
	ENSG00000258312	AC016152.1	-0.026	0.014
	ENSG00000106236	NPTX2	-0.025	0.022
	ENSG00000071205	ARHGAP10	-0.022	0.028
	ENSG00000111962	UST	-0.021	0.060
	ENSG00000185008	ROBO2	-0.019	0.021
	ENSG00000237250	AL359924.1	-0.018	0.030
	ENSG00000229618	AC011287.1	-0.018	0.034
	ENSG00000126432	PRDX5	-0.018	0.032

Supplementary Table 3 *CONTINUED*

Downregulated DE genes				
Cell type	**Ensembl ID**	**Gene name**	**logFC**	**FDR-adj. p-value**
Exc_L4-6_1	ENSG00000106236	NPTX2	-0.043	0.002
	ENSG00000146648	EGFR	-0.034	0.002
	ENSG00000198576	ARC	-0.033	0.059
	ENSG00000120738	EGR1	-0.030	0.036
	ENSG00000135919	SERPINE2	-0.030	0.000
	ENSG00000164125	GASK1B	-0.029	0.000
	ENSG00000250387	LINC02197	-0.028	0.007
	ENSG00000234156	AL359636.2	-0.028	0.027
	ENSG00000256193	LINC00507	-0.027	0.006
	ENSG00000162551	ALPL	-0.027	0.002
Exc_L4-6_2	ENSG00000071205	ARHGAP10	-0.055	0.000
	ENSG00000179796	LRRC3B	-0.043	0.000
	ENSG00000119547	ONECUT2	-0.043	0.000
	ENSG00000203685	STUM	-0.042	0.000
	ENSG00000106236	NPTX2	-0.037	0.000
	ENSG00000198576	ARC	-0.037	0.019
	ENSG00000240086	AC092969.1	-0.034	0.000
	ENSG00000229618	AC011287.1	-0.034	0.000
	ENSG00000185008	ROBO2	-0.032	0.000
	ENSG00000120738	EGR1	-0.032	0.005
Exc_L4-6_3	ENSG00000050628	PTGER3	-0.051	0.001
	ENSG00000110723	EXPH5	-0.038	0.000
	ENSG00000120738	EGR1	-0.036	0.022
	ENSG00000288087	AC112770.1	-0.034	0.009
	ENSG00000106236	NPTX2	-0.033	0.013
	ENSG00000248431	AC021134.1	-0.030	0.009
	ENSG00000135919	SERPINE2	-0.028	0.000
	ENSG00000239440	LINC02008	-0.027	0.007
	ENSG00000038295	TLL1	-0.026	0.025
	ENSG00000071205	ARHGAP10	-0.026	0.001
Exc_L5-6_1	ENSG00000134986	NREP	-0.051	0.000
	ENSG00000178568	ERBB4	-0.023	0.009
	ENSG00000154975	CA10	-0.023	0.002
	ENSG00000135272	MDFIC	-0.022	0.003
	ENSG00000285638	AL138927.1	-0.022	0.058
	ENSG00000285939	AC034268.2	-0.020	0.021
	ENSG00000174473	GALNTL6	-0.020	0.008
	ENSG00000229989	MIR181A1HG	-0.019	0.009
	ENSG00000229618	AC011287.1	-0.019	0.027
	ENSG00000128989	ARPP19	-0.018	0.009

Supplementary Table 3 *CONTINUED*

Downregulated DE genes				
Cell type	**Ensembl ID**	**Gene name**	**logFC**	**FDR-adj. p-value**
Exc_L5-6_2	ENSG00000128989	ARPP19	-0.027	0.017
	ENSG00000117152	RGS4	-0.021	0.059
	ENSG00000154146	NRGN	-0.021	0.037
	ENSG00000143933	CALM2	-0.017	0.070
	ENSG00000269821	KCNQ1OT1	-0.015	0.067
	ENSG00000198216	CACNA1E	-0.014	0.067
	ENSG00000184838	PRR16	-0.014	0.067
	ENSG00000101489	CELF4	-0.013	0.060
	ENSG00000150627	WDR17	-0.011	0.063
	ENSG00000134318	ROCK2	-0.010	0.067
Exc_L5-6_HTR2C	ENSG00000253693	AC008415.1	-0.028	0.031
	ENSG00000241956	AC109466.1	-0.026	0.013
	ENSG00000164112	TMEM155	-0.022	0.001
	ENSG00000176771	NCKAP5	-0.018	0.015
	ENSG00000167508	MVD	-0.015	0.024
	ENSG00000167964	RAB26	-0.015	0.024
	ENSG00000113161	HMGCR	-0.015	0.064
	ENSG00000178031	ADAMTSL1	-0.015	0.055
	ENSG00000006468	ETV1	-0.013	0.055
	ENSG00000171617	ENC1	-0.013	0.100
In_LAMP5	ENSG00000147571	CRH	-0.023	0.034
	ENSG00000054803	CBLN4	-0.023	0.008
	ENSG00000272398	CD24	-0.022	0.020
	ENSG00000241563	CORT	-0.021	0.049
	ENSG00000196418	ZNF124	-0.021	0.005
	ENSG00000102468	HTR2A	-0.020	0.010
	ENSG00000138741	TRPC3	-0.019	0.006
	ENSG00000114646	CSPG5	-0.019	0.004
	ENSG00000224982	TMEM233	-0.019	0.043
	ENSG00000135919	SERPINE2	-0.019	0.012
In_PVALB_Ba	ENSG00000153993	SEMA3D	-0.025	0.072
	ENSG00000227220	AL133346.1	-0.021	0.056
	ENSG00000188290	HES4	-0.020	0.059
	ENSG00000135919	SERPINE2	-0.020	0.095
	ENSG00000188157	AGRN	-0.019	0.071
	ENSG00000119125	GDA	-0.018	0.071
	ENSG00000162981	LRATD1	-0.017	0.061
	ENSG00000152467	ZSCAN1	-0.015	0.072
	ENSG00000134917	ADAMTS8	-0.015	0.095
	ENSG00000196972	SMIM10L2B	-0.015	0.029

Supplementary Table 3 *CONTINUED*

Downregulated DE genes				
Cell type	**Ensembl ID**	**Gene name**	**logFC**	**FDR-adj. p-value**
In_PVALB_Ch	ENSG00000185532	PRKG1	-0.024	0.015
	ENSG00000147571	CRH	-0.021	0.023
	ENSG00000162631	NTNG1	-0.021	0.013
	ENSG00000139289	PHLDA1	-0.020	0.013
	ENSG00000159216	RUNX1	-0.018	0.077
	ENSG00000256287	LINC02398	-0.017	0.056
	ENSG00000087494	PTHLH	-0.017	0.042
	ENSG00000100362	PVALB	-0.016	0.013
	ENSG00000187094	CCK	-0.015	0.092
	ENSG00000229117	RPL41	-0.014	0.030
In_RELN	ENSG00000157005	SST	-0.028	0.025
	ENSG00000054803	CBLN4	-0.021	0.052
	ENSG00000171159	C9orf16	-0.016	0.025
	ENSG00000110975	SYT10	-0.016	0.073
	ENSG00000135919	SERPINE2	-0.014	0.073
	ENSG00000179455	MKRN3	-0.014	0.039
	ENSG00000198755	RPL10A	-0.013	0.077
	ENSG00000171617	ENC1	-0.013	0.027
	ENSG00000172247	C1QTNF4	-0.013	0.098
	ENSG00000166557	TMED3	-0.013	0.098
In_SST	ENSG00000249853	HS3ST5	-0.036	0.004
	ENSG00000182348	ZNF804B	-0.030	0.000
	ENSG00000054803	CBLN4	-0.029	0.001
	ENSG00000148848	ADAM12	-0.029	0.001
	ENSG00000104327	CALB1	-0.027	0.001
	ENSG00000083857	FAT1	-0.025	0.016
	ENSG00000184384	MAML2	-0.023	0.000
	ENSG00000171502	COL24A1	-0.023	0.006
	ENSG00000152953	STK32B	-0.022	0.008
	ENSG00000249484	LINC01470	-0.021	0.042
In_VIP	ENSG00000272398	CD24	-0.021	0.000
	ENSG00000175274	TP53I11	-0.020	0.000
	ENSG00000158270	COLEC12	-0.020	0.011
	ENSG00000162975	KCNF1	-0.018	0.007
	ENSG00000102924	CBLN1	-0.018	0.010
	ENSG00000052802	MSMO1	-0.017	0.036
	ENSG00000274956	NKAIN3-IT1	-0.017	0.020
	ENSG00000115461	IGFBP5	-0.017	0.022
	ENSG00000260192	LINC02240	-0.016	0.059
	ENSG00000167614	TTYH1	-0.016	0.011

Supplementary Table 3 *CONTINUED*

Downregulated DE genes				
Cell type	**Ensembl ID**	**Gene name**	**logFC**	**FDR-adj. p-value**
Microglia	ENSG00000287950	AC009432.2	-0.048	0.049
	ENSG00000232591	LINC02642	-0.034	0.089
	ENSG00000152092	ASTN1	-0.032	0.000
	ENSG00000166833	NAV2	-0.030	0.005
	ENSG00000140945	CDH13	-0.025	0.076
	ENSG00000110436	SLC1A2	-0.024	0.026
	ENSG00000144218	AFF3	-0.024	0.094
	ENSG00000198797	BRINP2	-0.024	0.035
	ENSG00000173436	MICOS10	-0.024	0.091
	ENSG00000099954	CECR2	-0.024	0.028
Oligodenrocyte	ENSG00000110436	SLC1A2	-0.025	0.028
	ENSG00000135919	SERPINE2	-0.025	0.002
	ENSG00000185942	NKAIN3	-0.024	0.074
	ENSG00000018625	ATP1A2	-0.024	0.054
	ENSG00000198838	RYR3	-0.023	0.063
	ENSG00000134986	NREP	-0.021	0.025
	ENSG00000152495	CAMK4	-0.020	0.017
	ENSG00000171408	PDE7B	-0.018	0.079
	ENSG00000046889	PREX2	-0.018	0.003
	ENSG00000130558	OLFM1	-0.018	0.025
OPC	ENSG00000197921	HES5	-0.032	0.054
	ENSG00000137766	UNC13C	-0.028	0.044
	ENSG00000112715	VEGFA	-0.026	0.093
	ENSG00000137872	SEMA6D	-0.026	0.001
	ENSG00000144810	COL8A1	-0.024	0.073
	ENSG00000178531	CTXN1	-0.024	0.006
	ENSG00000172247	C1QTNF4	-0.023	0.003
	ENSG00000185742	C11orf87	-0.023	0.019
	ENSG00000152818	UTRN	-0.023	0.000
	ENSG00000149972	CNTN5	-0.023	0.044

Supplementary Table 4: Over-representation analysis of biological processes in upregulated age DE genes - summarized using semantic similarity analysis (only cluster representative shown).

Cell Type	Cluster representative	Description	FDR adj. p-value
Exc_L4-6_1	GO:0071417	cellular response to organonitrogen compound	0.001
	GO:0030036	actin filament-based process	0.009
	GO:0007169	transmembrane receptor protein tyrosine kinase signaling pathway	0.014
	GO:0055086	nucleobase-containing small molecule metabolic process	0.024
	GO:0120031	plasma membrane bounded cell projection assembly	0.024
	GO:0097435	supramolecular fiber organization	0.025
	GO:0030334	regulation of cell motility	0.040
	GO:0035295	tube development	0.047
Exc_L4-6_2	GO:0010942	positive regulation of cell death	0.016
	GO:0097435	supramolecular fiber organization	0.050
	GO:0035295	tube development	0.050
	GO:0055086	nucleobase-containing small molecule metabolic process	0.050
	GO:0030036	actin cytoskeleton organization	0.050
In_LAMP5	GO:0034330	cell junction organization	0.019
	GO:0044089	positive regulation of cellular component biogenesis	0.022
	GO:0072359	circulatory system development	0.022
	GO:0016311	dephosphorylation	0.022
	GO:0098609	cell-cell adhesion	0.023
	GO:1901987	regulation of cell cycle phase transition	0.023
	GO:0120031	cell projection assembly	0.022
	GO:0035295	tube development	0.033
	GO:0051270	regulation of cellular component movement	0.034
	GO:0051493	regulation of cytoskeleton organization	0.034
	GO:1903047	mitotic cell cycle process	0.036
	GO:0030155	regulation of cell adhesion	0.038
In_VIP	GO:0030031	cell projection assembly	0.000
	GO:0000226	microtubule-based movement	0.000
	GO:0044089	positive regulation of cellular component biogenesis	0.019
	GO:0008380	RNA splicing	0.022
	GO:0007346	regulation of mitotic cell cycle	0.022
	GO:0030334	regulation of cell migration	0.025
Microglia	GO:0098542	defense response to other organism	0.014
	GO:0030216	keratinocyte differentiation	0.015
	GO:2000106	regulation of leukocyte apoptotic process	0.017
	GO:0042127	regulation of cell population proliferation	0.018
	GO:0002456	T cell mediated immunity	0.018
	GO:0071887	leukocyte apoptotic process	0.018
	GO:0008544	epidermis development	0.018
	GO:0032956	regulation of actin cytoskeleton organization	0.020
	GO:0051865	protein autoubiquitination	0.023
	GO:0030041	actin filament polymerization	0.026
	GO:0043547	regulation of GTPase activity	0.023
	GO:0046634	regulation of alpha-beta T cell activation	0.026
	GO:0008283	cell population proliferation	0.029
	GO:0071346	response to interferon-gamma	0.015
	GO:0002520	immune system development	0.033
	GO:0001816	cytokine production	0.034
	GO:1903900	regulation of viral life cycle	0.034
	GO:0030029	actin filament-based process	0.046
	GO:0019886	antigen processing and presentation of exogenous peptide antigen via MHC class II	0.047
	GO:0090066	regulation of anatomical structure size	0.049
Oligodendrocyte	GO:0071396	cellular response to lipid	0.032
OPC	GO:0031589	cell-substrate adhesion	0.014
	GO:0010769	regulation of cell morphogenesis involved in differentiation	0.014
	GO:0050773	regulation of dendrite development	0.015

Supplementary Table 5: Over-representation analysis of biological processes in downregulated age DE genes - summarized using semantic similarity analysis (only cluster representative shown).

Cell Type	Cluster representative	Description	FDR adj. p-value
Astro_FB	GO:0120035	regulation of plasma membrane bounded cell projection organization	0.001
	GO:0048666	neuron development	0.001
	GO:0031175	neuron projection development	0.001
	GO:0000904	cell morphogenesis involved in differentiation	0.001
	GO:0030182	neuron differentiation	0.002
	GO:0048858	cell projection morphogenesis	0.005
	GO:0007155	cell adhesion	0.011
	GO:0048846	axon extension involved in axon guidance	0.020
	GO:1902692	regulation of neuroblast proliferation	0.020
	GO:0022603	regulation of anatomical structure morphogenesis	0.021
	GO:0035249	synaptic transmission. glutamatergic	0.022
	GO:0045685	regulation of glial cell differentiation	0.023
	GO:0010811	positive regulation of cell-substrate adhesion	0.023
	GO:0021549	cerebellum development	0.023
	GO:0002690	positive regulation of leukocyte chemotaxis	0.024
	GO:0045765	regulation of angiogenesis	0.024
	GO:0022037	metencephalon development	0.024
	GO:0010720	positive regulation of cell development	0.029
	GO:0007405	neuroblast proliferation	0.030
	GO:0014013	regulation of gliogenesis	0.032
	GO:0016525	negative regulation of angiogenesis	0.034
	GO:0007215	glutamate receptor signaling pathway	0.035
	GO:0098916	anterograde trans-synaptic signaling	0.035
	GO:0050900	leukocyte migration	0.036
	GO:0030308	negative regulation of cell growth	0.036
	GO:0043687	post-translational protein modification	0.041
	GO:0050808	synapse organization	0.047
Astro_PP	GO:1902692	regulation of neuroblast proliferation	0.009
	GO:0007268	chemical synaptic transmission	0.009
	GO:0007405	neuroblast proliferation	0.011
	GO:0010469	regulation of signaling receptor activity	0.014
	GO:0042987	amyloid precursor protein catabolic process	0.014
	GO:0007215	glutamate receptor signaling pathway	0.014
	GO:0048678	response to axon injury	0.014
	GO:0010976	positive regulation of neuron projection development	0.016
	GO:0002576	platelet degranulation	0.023
	GO:0051208	sequestering of calcium ion	0.023
	GO:0010811	positive regulation of cell-substrate adhesion	0.026
	GO:0007186	G protein-coupled receptor signaling pathway	0.027
	GO:0006954	inflammatory response	0.027
	GO:0016311	dephosphorylation	0.027
	GO:0097553	calcium ion transmembrane import into cytosol	0.027
	GO:0002685	regulation of leukocyte migration	0.027
	GO:0030595	leukocyte chemotaxis	0.029
	GO:0061564	axon development	0.029
	GO:0001817	regulation of cytokine production	0.037
	GO:0001816	cytokine production	0.049
Exc_L2-3	GO:0048667	cell morphogenesis involved in neuron differentiation	1.48E-10
Exc_L3-5	GO:0061337	cardiac conduction	8.36E-06
	GO:0003015	heart process	8.36E-06
	GO:0008016	regulation of heart contraction	1.50E-04
	GO:0072507	divalent inorganic cation homeostasis	2.19E-04
	GO:0098662	inorganic cation transmembrane transport	2.40E-04
	GO:0051480	regulation of cytosolic calcium ion concentration	0.001
	GO:0006875	cellular metal ion homeostasis	0.001
	GO:0055065	metal ion homeostasis	0.001
	GO:0050801	ion homeostasis	0.002
	GO:0051651	maintenance of location in cell	0.002
	GO:0007269	neurotransmitter secretion	0.003
	GO:0031346	positive regulation of cell projection organization	0.003
	GO:0006873	cellular ion homeostasis	0.003
	GO:0043270	positive regulation of ion transport	0.004
	GO:0051223	regulation of protein transport	0.009
	GO:0050803	regulation of synapse structure or activity	0.011
	GO:1903530	regulation of secretion by cell	0.014
	GO:0060322	head development	0.016
	GO:0010035	response to inorganic substance	0.018
	GO:0051222	positive regulation of protein transport	0.020
	GO:0051345	positive regulation of hydrolase activity	0.021
	GO:0019216	regulation of lipid metabolic process	0.023
	GO:0007268	chemical synaptic transmission	0.026
	GO:0032970	regulation of actin filament-based process	0.043
	GO:0062012	regulation of small molecule metabolic process	0.047
	GO:0061564	axon development	0.047
	GO:0007186	G protein-coupled receptor signaling pathway	0.047

Supplementary Table 5 *CONTINUED*

Cell Type	Cluster representative	Description	FDR adj. p-value
Exc_L4-6_1	GO:0007268	chemical synaptic transmission	2.51E-17
	GO:0099177	regulation of trans-synaptic signaling	1.17E-14
	GO:0048812	neuron projection morphogenesis	1.97E-10
	GO:1903530	regulation of secretion by cell	7.05E-09
	GO:0044057	regulation of system process	7.05E-09
	GO:0048667	cell morphogenesis involved in neuron differentiation	1.69E-08
	GO:0007186	G protein-coupled receptor signaling pathway	2.39E-08
	GO:0023061	signal release	1.06E-07
	GO:0050808	synapse organization	3.36E-06
	GO:0098662	inorganic cation transmembrane transport	3.74E-06
	GO:0060627	regulation of vesicle-mediated transport	4.02E-06
	GO:0098609	cell-cell adhesion	5.10E-06
	GO:0120035	regulation of plasma membrane bounded cell projection organization	8.92E-06
	GO:0003013	circulatory system process	2.10E-05
	GO:0055082	cellular chemical homeostasis	1.45E-04
	GO:0006935	chemotaxis	3.68E-04
	GO:0007610	behavior	3.73E-04
	GO:0051223	regulation of protein transport	3.75E-04
	GO:0030029	actin filament-based process	0.002
	GO:0051093	negative regulation of developmental process	0.003
	GO:0051347	positive regulation of transferase activity	0.005
	GO:0040008	regulation of growth	0.006
	GO:1901137	carbohydrate derivative biosynthetic process	0.009
	GO:0042327	positive regulation of phosphorylation	0.016
	GO:0007169	transmembrane receptor protein tyrosine kinase signaling pathway	0.021
	GO:0007420	brain development	0.033
	GO:0008610	lipid biosynthetic process	0.038
Exc_L4-6_2	GO:0007268	chemical synaptic transmission	6.92E-13
	GO:0050808	synapse organization	2.40E-11
	GO:0048812	neuron projection morphogenesis	4.32E-11
	GO:0048667	cell morphogenesis involved in neuron differentiation	3.63E-10
	GO:0050804	modulation of chemical synaptic transmission	8.22E-10
	GO:0007186	G protein-coupled receptor signaling pathway	8.22E-10
	GO:0044057	regulation of system process	3.18E-07
	GO:0050877	nervous system process	6.59E-07
	GO:0120035	regulation of plasma membrane bounded cell projection organization	8.25E-07
	GO:0006935	chemotaxis	3.04E-06
	GO:0098660	inorganic ion transmembrane transport	5.47E-05
	GO:0098609	cell-cell adhesion	1.78E-04
	GO:0007420	brain development	1.96E-04
	GO:0007610	behavior	2.82E-04
	GO:0044089	positive regulation of cellular component biogenesis	3.13E-04
	GO:0034765	regulation of ion transmembrane transport	4.65E-04
	GO:0030029	actin filament-based process	0.001
	GO:0000165	MAPK cascade	0.001
	GO:0016311	dephosphorylation	0.001
	GO:0050801	ion homeostasis	0.001
	GO:0045597	positive regulation of cell differentiation	0.001
	GO:0051345	positive regulation of hydrolase activity	0.003
	GO:1901137	carbohydrate derivative biosynthetic process	0.042
	GO:0045055	regulated exocytosis	0.049
Exc_L4-6_3	GO:0007409	axonogenesis	3.80E-07
	GO:0006935	chemotaxis	2.28E-06
	GO:0007411	axon guidance	5.42E-06
	GO:0007268	chemical synaptic transmission	1.30E-05
	GO:0050804	modulation of chemical synaptic transmission	2.61E-05
	GO:0007186	G protein-coupled receptor signaling pathway	4.23E-05
	GO:0050877	nervous system process	8.48E-05
	GO:0007610	behavior	1.08E-04
	GO:0010720	positive regulation of cell development	1.69E-04
	GO:0120035	regulation of plasma membrane bounded cell projection organization	2.06E-04
	GO:0044057	regulation of system process	4.52E-04
	GO:0030334	regulation of cell migration	0.001
	GO:0007417	central nervous system development	0.001
	GO:0050808	synapse organization	0.001
	GO:0098609	cell-cell adhesion	0.003
	GO:0043547	positive regulation of GTPase activity	0.008
	GO:0040008	regulation of growth	0.011
	GO:0045936	negative regulation of phosphate metabolic process	0.017
	GO:0098655	cation transmembrane transport	0.020
	GO:0016311	dephosphorylation	0.031
	GO:1901699	cellular response to nitrogen compound	0.031
	GO:0000165	MAPK cascade	0.047
Exc_L5-6_2	GO:0060079	excitatory postsynaptic potential	0.036
	GO:0099565	chemical synaptic transmission. postsynaptic	0.036
	GO:0006412	translation	0.036
	GO:0031400	negative regulation of protein modification process	0.036
	GO:0043086	negative regulation of catalytic activity	0.045
	GO:1904062	regulation of cation transmembrane transport	0.045
	GO:0010611	regulation of cardiac muscle hypertrophy	0.045
	GO:0034250	positive regulation of cellular amide metabolic process	0.046
	GO:0098655	cation transmembrane transport	0.048

Supplementary Table 5 *CONTINUED*

Cell Type	Cluster representative	Description	FDR adj. p-value
Exc_L5-6_HTR2C	GO:1905606	regulation of presynapse assembly	0.018
	GO:1902930	regulation of alcohol biosynthetic process	0.018
	GO:1903530	regulation of secretion by cell	0.018
	GO:0007157	heterophilic cell-cell adhesion via plasma membrane cell adhesion molecules	0.021
	GO:0099054	presynapse assembly	0.027
	GO:0046165	alcohol biosynthetic process	0.040
	GO:0140352	export from cell	0.045
In_LAMP5	GO:0006119	oxidative phosphorylation	1.50E-20
	GO:0042775	mitochondrial ATP synthesis coupled electron transport	2.51E-19
	GO:0022904	respiratory electron transport chain	8.87E-19
	GO:0045333	cellular respiration	1.05E-17
	GO:0007268	chemical synaptic transmission	4.24E-10
	GO:0099537	trans-synaptic signaling	9.08E-10
	GO:0055082	cellular chemical homeostasis	9.57E-09
	GO:0098660	inorganic ion transmembrane transport	1.27E-08
	GO:0023061	signal release	9.88E-08
	GO:0050801	ion homeostasis	9.88E-08
	GO:0007005	mitochondrion organization	9.88E-08
	GO:0030003	cellular cation homeostasis	2.71E-07
	GO:0045055	regulated exocytosis	1.03E-06
	GO:0043270	positive regulation of ion transport	1.11E-06
	GO:0050804	modulation of chemical synaptic transmission	3.51E-06
	GO:0090150	establishment of protein localization to membrane	9.84E-06
	GO:0044070	regulation of anion transport	1.75E-05
	GO:1903530	regulation of secretion by cell	4.83E-05
	GO:0010035	response to inorganic substance	7.42E-05
	GO:0009150	purine ribonucleotide metabolic process	9.93E-05
	GO:0006163	purine nucleotide metabolic process	1.23E-04
	GO:0043254	regulation of protein-containing complex assembly	1.41E-04
	GO:0060341	regulation of cellular localization	1.45E-04
	GO:0044057	regulation of system process	3.14E-04
	GO:0002444	myeloid leukocyte mediated immunity	3.43E-04
	GO:0070201	regulation of establishment of protein localization	3.90E-04
	GO:0002275	myeloid cell activation involved in immune response	3.90E-04
	GO:0016311	dephosphorylation	8.55E-04
	GO:0097190	apoptotic signaling pathway	0.001
	GO:0043086	negative regulation of catalytic activity	0.001
	GO:0009117	nucleotide metabolic process	0.002
	GO:0050877	nervous system process	0.003
	GO:0043066	negative regulation of apoptotic process	0.004
	GO:0007186	G protein-coupled receptor signaling pathway	0.005
	GO:0030162	regulation of proteolysis	0.005
	GO:0006914	autophagy	0.005
	GO:0007610	behavior	0.006
	GO:0071417	cellular response to organonitrogen compound	0.007
	GO:0045936	negative regulation of phosphate metabolic process	0.008
	GO:0000165	MAPK cascade	0.011
	GO:0022411	cellular component disassembly	0.011
	GO:0007169	transmembrane receptor protein tyrosine kinase signaling pathway	0.014
	GO:0120035	regulation of plasma membrane bounded cell projection organization	0.032
	GO:0040008	regulation of growth	0.039
In_PVALB_Ba	GO:0006026	aminoglycan catabolic process	5.20E-04
	GO:0072507	divalent inorganic cation homeostasis	0.001
	GO:0055065	metal ion homeostasis	0.003
	GO:0048708	astrocyte differentiation	0.004
	GO:0051960	regulation of nervous system development	0.006
	GO:0051924	regulation of calcium ion transport	0.008
	GO:0030308	negative regulation of cell growth	0.008
	GO:0030198	extracellular matrix organization	0.011
	GO:0098660	inorganic ion transmembrane transport	0.011
	GO:0099536	synaptic signaling	0.011
	GO:0050714	positive regulation of protein secretion	0.012
	GO:0050803	regulation of synapse structure or activity	0.013
	GO:0010951	negative regulation of endopeptidase activity	0.015
	GO:0061337	cardiac conduction	0.016
	GO:0060401	cytosolic calcium ion transport	0.022
	GO:1904062	regulation of cation transmembrane transport	0.022
	GO:0071248	cellular response to metal ion	0.025
	GO:0007416	synapse assembly	0.027
	GO:0008015	blood circulation	0.027
	GO:0009101	glycoprotein biosynthetic process	0.027
	GO:0070372	regulation of ERK1 and ERK2 cascade	0.028
	GO:0044272	sulfur compound biosynthetic process	0.030
	GO:0070371	ERK1 and ERK2 cascade	0.031
	GO:0021700	developmental maturation	0.038
	GO:0048667	cell morphogenesis involved in neuron differentiation	0.042
	GO:0023061	signal release	0.042
	GO:0060560	developmental growth involved in morphogenesis	0.043

Supplementary Table 5 *CONTINUED*

Cell Type	Cluster representative	Description	FDR adj. p-value
	GO:0019646	aerobic electron transport chain	0.027
	GO:0003254	regulation of membrane depolarization	0.027
	GO:0010976	positive regulation of neuron projection development	0.027
	GO:0031175	neuron projection development	0.027
	GO:0086065	cell communication involved in cardiac conduction	0.032
	GO:0098662	inorganic cation transmembrane transport	0.032
	GO:0046034	ATP metabolic process	0.032
ln_PVALB_Ch	GO:0051241	negative regulation of multicellular organismal process	0.033
	GO:0070509	calcium ion import	0.035
	GO:0071417	cellular response to organonitrogen compound	0.038
	GO:0090150	establishment of protein localization to membrane	0.039
	GO:2000649	regulation of sodium ion transmembrane transporter activity	0.042
	GO:0048839	inner ear development	0.045
	GO:0009205	purine ribonucleoside triphosphate metabolic process	0.049
	GO:0140353	lipid export from cell	0.049
	GO:0006091	generation of precursor metabolites and energy	3.78E-05
	GO:0098660	inorganic ion transmembrane transport	3.78E-05
	GO:0055082	cellular chemical homeostasis	3.78E-05
	GO:0019932	second-messenger-mediated signaling	3.78E-05
	GO:0009150	purine ribonucleotide metabolic process	2.81E-04
	GO:0043270	positive regulation of ion transport	3.32E-04
	GO:0005996	monosaccharide metabolic process	0.001
	GO:0000904	cell morphogenesis involved in differentiation	0.001
	GO:0044057	regulation of system process	0.003
	GO:0061061	muscle structure development	0.003
	GO:0023061	signal release	0.003
	GO:0008015	blood circulation	0.003
ln_SST	GO:0007186	G protein-coupled receptor signaling pathway	0.005
	GO:0098609	cell-cell adhesion	0.006
	GO:0007268	chemical synaptic transmission	0.006
	GO:0034329	cell junction assembly	0.009
	GO:0006935	chemotaxis	0.009
	GO:0050804	modulation of chemical synaptic transmission	0.009
	GO:0007005	mitochondrion organization	0.010
	GO:0071417	cellular response to organonitrogen compound	0.012
	GO:0030155	regulation of cell adhesion	0.016
	GO:0072359	circulatory system development	0.017
	GO:0045596	negative regulation of cell differentiation	0.028
	GO:0061564	axon development	0.036
	GO:0007015	actin filament organization	0.038
	GO:0007169	transmembrane receptor protein tyrosine kinase signaling pathway	0.041
	GO:0045047	protein targeting to ER	8.28E-15
	GO:0090150	establishment of protein localization to membrane	9.07E-14
	GO:0006413	translational initiation	2.51E-10
	GO:0000184	nuclear-transcribed mRNA catabolic process. nonsense-mediated decay	2.51E-10
	GO:0050801	ion homeostasis	4.50E-08
	GO:0019080	viral gene expression	6.06E-08
	GO:0055082	cellular chemical homeostasis	8.43E-08
	GO:0019083	viral transcription	8.43E-08
	GO:0030003	cellular cation homeostasis	1.42E-07
	GO:0043270	positive regulation of ion transport	1.42E-07
	GO:0098662	inorganic cation transmembrane transport	1.77E-07
	GO:0007268	chemical synaptic transmission	2.91E-07
	GO:1903530	regulation of secretion by cell	1.10E-06
	GO:0006402	mRNA catabolic process	1.27E-06
	GO:0023061	signal release	4.52E-06
	GO:0051222	positive regulation of protein transport	1.13E-05
	GO:0051223	regulation of protein transport	5.14E-05
	GO:0044057	regulation of system process	7.68E-05
	GO:0008015	blood circulation	1.53E-04
	GO:0034655	nucleobase-containing compound catabolic process	1.74E-04
	GO:0002446	neutrophil mediated immunity	2.03E-04
ln_VIP	GO:0050804	modulation of chemical synaptic transmission	3.39E-04
	GO:0002275	myeloid cell activation involved in immune response	4.97E-04
	GO:0043312	neutrophil degranulation	7.50E-04
	GO:0032386	regulation of intracellular transport	8.14E-04
	GO:0007186	G protein-coupled receptor signaling pathway	8.77E-04
	GO:0098609	cell-cell adhesion	0.001
	GO:0043086	negative regulation of catalytic activity	0.001
	GO:0050808	synapse organization	0.004
	GO:0060284	regulation of cell development	0.004
	GO:0043065	positive regulation of apoptotic process	0.004
	GO:0006163	purine nucleotide metabolic process	0.005
	GO:0097190	apoptotic signaling pathway	0.005
	GO:0007420	brain development	0.007
	GO:0030029	actin filament-based process	0.012
	GO:0061564	axon development	0.014
	GO:0030162	regulation of proteolysis	0.014
	GO:0040008	regulation of growth	0.014
	GO:0071417	cellular response to organonitrogen compound	0.017
	GO:0002684	positive regulation of immune system process	0.020
	GO:0048812	neuron projection morphogenesis	0.021
	GO:0120035	regulation of plasma membrane bounded cell projection organization	0.021
	GO:0009117	nucleotide metabolic process	0.027
	GO:0007169	transmembrane receptor protein tyrosine kinase signaling pathway	0.049

Supplementary Table 5 *CONTINUED*

Cell Type	Cluster representative	Description	FDR adj. p-value
Microglia	GO:0006816	calcium ion transport	0.037
	GO:0014910	regulation of smooth muscle cell migration	0.037
	GO:0014909	smooth muscle cell migration	0.037
	GO:0021537	telencephalon development	0.037
	GO:0014902	myotube differentiation	0.037
	GO:2001257	regulation of cation channel activity	0.044
	GO:0003007	heart morphogenesis	0.045
	GO:0030032	lamellipodium assembly	0.045
	GO:0050679	positive regulation of epithelial cell proliferation	0.045
Oligodendrocyte	GO:0098916	anterograde trans-synaptic signaling	0.004
	GO:0099173	postsynapse organization	0.004
	GO:0014065	phosphatidylinositol 3-kinase signaling	0.004
	GO:0030534	adult behavior	0.004
	GO:1903779	regulation of cardiac conduction	0.007
	GO:0050877	nervous system process	0.011
	GO:0098712	L-glutamate import across plasma membrane	0.018
	GO:0010766	negative regulation of sodium ion transport	0.019
	GO:0070633	transepithelial transport	0.019
	GO:0071625	vocalization behavior	0.019
	GO:0010996	response to auditory stimulus	0.019
	GO:0015813	L-glutamate transmembrane transport	0.019
	GO:0098739	import across plasma membrane	0.020
	GO:0007158	neuron cell-cell adhesion	0.020
	GO:0089718	amino acid import across plasma membrane	0.022
	GO:0061337	cardiac conduction	0.024
	GO:1902414	protein localization to cell junction	0.024
	GO:0070527	platelet aggregation	0.026
	GO:0050865	regulation of cell activation	0.029
	GO:0035176	social behavior	0.031
	GO:0001941	postsynaptic membrane organization	0.032
	GO:0007416	synapse assembly	0.032
	GO:0032956	regulation of actin cytoskeleton organization	0.032
	GO:0044091	membrane biogenesis	0.033
	GO:0150104	transport across blood-brain barrier	0.033
	GO:1903522	regulation of blood circulation	0.037
	GO:0051480	regulation of cytosolic calcium ion concentration	0.037
	GO:0061041	regulation of wound healing	0.037
	GO:0048813	dendrite morphogenesis	0.038
	GO:0006814	sodium ion transport	0.038
	GO:0060047	heart contraction	0.040
	GO:0051966	regulation of synaptic transmission. glutamatergic	0.042
	GO:0009582	detection of abiotic stimulus	0.046
	GO:0001775	cell activation	0.046
OPC	GO:0008015	blood circulation	1.22E-04
	GO:0048667	cell morphogenesis involved in neuron differentiation	4.70E-04
	GO:0019932	second-messenger-mediated signaling	4.70E-04
	GO:0032412	regulation of ion transmembrane transporter activity	5.62E-04
	GO:0048469	cell maturation	6.16E-04
	GO:0044057	regulation of system process	7.50E-04
	GO:0072657	protein localization to membrane	8.73E-04
	GO:0042391	regulation of membrane potential	8.80E-04
	GO:0007411	axon guidance	0.002
	GO:0007268	chemical synaptic transmission	0.003
	GO:0007269	neurotransmitter secretion	0.003
	GO:0006935	chemotaxis	0.004
	GO:0000184	nuclear-transcribed mRNA catabolic process. nonsense-mediated decay	0.004
	GO:0007186	G protein-coupled receptor signaling pathway	0.004
	GO:0010810	regulation of cell-substrate adhesion	0.005
	GO:0045596	negative regulation of cell differentiation	0.006
	GO:0001822	kidney development	0.007
	GO:0050808	synapse organization	0.007
	GO:0072001	renal system development	0.007
	GO:0090287	regulation of cellular response to growth factor stimulus	0.007
	GO:0019083	viral transcription	0.012
	GO:0031589	cell-substrate adhesion	0.012
	GO:0071363	cellular response to growth factor stimulus	0.018
	GO:0019080	viral gene expression	0.019
	GO:0006413	translational initiation	0.022
	GO:0098662	inorganic cation transmembrane transport	0.022
	GO:0007178	transmembrane receptor protein serine/threonine kinase signaling pathway	0.022
	GO:0001558	regulation of cell growth	0.026

Supplementary Table 6: Disease enrichment of upregulated age DE genes.

Cell Type	ID	Description	GeneRatio	BgRatio	FDR adj. p-value	Count
Exc_L3-5	DOID:0050615	respiratory system cancer	7/25	183/3001	0.021	7
	DOID:5520	head and neck squamous cell carcinoma	4/25	55/3001	0.021	4
	DOID:3905	lung carcinoma	6/25	154/3001	0.021	6
	DOID:1324	lung cancer	6/25	181/3001	0.024	6
	DOID:1542	head and neck carcinoma	4/25	77/3001	0.024	4
	DOID:3908	non-small cell lung carcinoma	5/25	128/3001	0.024	5
	DOID:11934	head and neck cancer	4/25	78/3001	0.024	4
	DOID:2151	malignant ovarian surface epithelial-stromal neoplasm	4/25	86/3001	0.024	4
	DOID:2152	ovary epithelial cancer	4/25	86/3001	0.024	4
	DOID:4001	ovarian carcinoma	4/25	86/3001	0.024	4
	DOID:305	carcinoma	7/25	273/3001	0.024	7
	DOID:120	female reproductive organ cancer	5/25	145/3001	0.024	5
	DOID:2394	ovarian cancer	4/25	93/3001	0.025	4
	DOID:4450	renal cell carcinoma	4/25	97/3001	0.027	4
	DOID:1749	squamous cell carcinoma	6/25	228/3001	0.031	6
	DOID:4451	renal carcinoma	4/25	108/3001	0.034	4
	DOID:7148	rheumatoid arthritis	4/25	112/3001	0.037	4
	DOID:193	reproductive organ cancer	6/25	248/3001	0.038	6
	DOID:3459	breast carcinoma	4/25	124/3001	0.043	4
	DOID:201	connective tissue cancer	4/25	125/3001	0.043	4
	DOID:263	kidney cancer	4/25	125/3001	0.043	4
Exc_L4-6_1	DOID:178	vascular disease	29/157	448/4206	0.008	29
	DOID:0050828	artery disease	24/157	359/4206	0.008	24
	DOID:0060158	acquired metabolic disease	23/157	396/4206	0.034	23
	DOID:630	genetic disease	25/157	452/4206	0.034	25
Exc_L4-6_3	DOID:7148	rheumatoid arthritis	9/59	127/3211	0.007	9
	DOID:1287	cardiovascular system disease	15/59	374/3211	0.014	15
	DOID:848	arthritis	9/59	163/3211	0.014	9
	DOID:3342	bone inflammation disease	9/59	172/3211	0.015	9
	DOID:0080001	bone disease	10/59	218/3211	0.019	10
	DOID:178	vascular disease	12/59	299/3211	0.020	12
	DOID:17	musculoskeletal system disease	14/59	395/3211	0.023	14
	DOID:0050828	artery disease	10/59	240/3211	0.023	10
	DOID:65	connective tissue disease	10/59	269/3211	0.043	10
Exc_L5-6_1	DOID:114	heart disease	7/30	70/1845	0.004	7
	DOID:1287	cardiovascular system disease	10/30	202/1845	0.017	10
	DOID:10763	hypertension	6/30	75/1845	0.017	6
	DOID:0050828	artery disease	7/30	128/1845	0.034	7
	DOID:178	vascular disease	8/30	164/1845	0.034	8
	DOID:557	kidney disease	5/30	69/1845	0.034	5
	DOID:18	urinary system disease	5/30	70/1845	0.034	5
Exc_L5-6_2	DOID:15	reproductive system disease	2/6	15/629	0.045	2
In_PVALB_Ba	DOID:4766	embryoma	2/7	161/4052	0.037	2
	DOID:688	embryonal cancer	2/7	173/4052	0.037	2
	DOID:2994	germ cell cancer	2/7	185/4052	0.037	2
In_VIP	DOID:65	connective tissue disease	17/95	406/4180	0.018	17
	DOID:2914	immune system disease	17/95	444/4180	0.021	17
Microglia	DOID:7148	rheumatoid arthritis	11/43	131/1876	0.009	11
	DOID:10608	celiac disease	4/43	19/1876	0.022	4
	DOID:848	arthritis	11/43	166/1876	0.022	11
	DOID:0060031	autoimmune disease of gastrointestinal tract	4/43	21/1876	0.022	4
	DOID:3342	bone inflammation disease	11/43	176/1876	0.024	11
	DOID:5082	liver cirrhosis	5/43	40/1876	0.025	5
	DOID:417	hypersensitivity reaction type II disease	9/43	134/1876	0.030	9
	DOID:0080001	bone disease	11/43	201/1876	0.043	11
Oligodendrocyte	DOID:11335	sarcoidosis	45201	401647	0.011	2
	DOID:2916	hypersensitivity reaction type IV disease	45201	401647	0.011	2
	DOID:4989	pancreatitis	45201	21/2999	0.033	2
	DOID:0050736	autosomal dominant disease	45203	183/2999	0.033	4
OPC	DOID:0050013	carbohydrate metabolism disease	9/41	254/3492	0.042	9
	DOID:4194	glucose metabolism disease	9/41	254/3492	0.042	9

Supplementary Table 7: Number of differentially expressed genes associated with cross-disorder (CrossD) PRS and schizophrenia (SCZ) PRS shown per cell type at FDR-adjusted p-value < 0.1.

Cell type	PRS_CrossD FDR < 0.1	PRS_SCZ FDR < 0.1
Astro_FB	0	0
Astro_PP	0	0
Endothelial	0	0
Exc_L2-3	0	0
Exc_L3-5	0	0
Exc_L4-6_1	0	0
Exc_L4-6_2	1	0
Exc_L4-6_3	2	0
Exc_L5-6_1	0	0
Exc_L5-6_2	0	2
Exc_L5-6_HTR2C	0	0
In_LAMP5	0	0
In_PVALB_Ba	0	0
In_PVALB_Ch	0	0
In_RELN	0	0
In_SST	0	0
In_VIP	0	0
Microglia	0	0
Oligodendrocyte	0	0
OPC	0	0

List of Figures

List of Tables

Declaration of Contributions

Brain tissue acquisition	Elisabeth Binder, Natalie Matosin
Conceptualisation of research	Anna Fröhlich, Elisabeth Binder
Randomisation of samples for sn-RNA-seq	Anna Fröhlich, Nathalie Gerstner
Nuclei extraction of post-mortem brains	Anna Fröhlich, Miriam Gagliardi
Loading of 10x Genomics Chromium Controller	Anna Fröhlich, Miriam Gagliardi
10x library preparation	Anna Fröhlich, Maik Ködel
Sequencing alignment (CellRanger)	Nathalie Gerstner, Vanessa Murek
Quality control of sn-RNA-seq data	Anna Fröhlich, Nathalie Gerstner
Label transfer for cell type assignment	Nathalie Gerstner
Manual curation of cell type labels	Anna Fröhlich
Differential gene expression analysis	Anna Fröhlich
Over-representation analysis of biological processes	Anna Fröhlich
Disease enrichment analysis	Anna Fröhlich
Comparison with previously published datasets	Anna Fröhlich
LAMP5 inhibitory neurons (replication dataset) provided by	Nikoloas Daskalakis
Differential expression analysis in LAMP5 replication dataset	Chris Chatzinakos
Randomisation for genotyping and DNA methylation measurements	Anna Fröhlich
DNA extraction for genotyping and DNA methylation analysis	Anna Fröhlich
Prepping of DNA for genotyping and DNA methylation measurements	Maik Ködel, Susann Sauer
Pre-processing of DNA methylation data and calculation of epigenetic clocks	Natan Yusupov
Processing and imputation of genotyping data	Darina Czamara, Jade Martins
Calculation of polygenic risk scores	Nathalie Gerstner
Graphs and figures	Anna Fröhlich

Acknowledgements

I would like to start by thanking Prof. Dr. Elisabeth Binder for offering me the opportunity to conduct my doctoral studies in her lab. I am grateful to her for allowing me to grow professionally by advising me, giving me space and time to develop my (computational) skill set as well as scientific ideas and enabling me to attend several scientific conferences, retreats and courses promoting scientific knowledge exchange and networking.

I would also like to thank PD Dr. Mathias Schmidt, Prof. Dr. Wolfgang Enard and Prof. Dr. Michael Ziller for being part of my thesis advisory committee and providing helpful feedback, input, and suggestions.

I would also like to thank the donors and their families for the donations of brain tissue. Without them this research would not have been possible.

All my work throughout the years has been supported by a lot of people both in the wet and dry lab as well as outside of work:

I would like to thank Marta Labeur, an inspiring scientist, whose love and fascination for scientific discovery never wanes, not even in the most difficult and frustrating moments in the lab. Thank you for your supervision, ideas, guidance, and especially for your positive attitude - it is contagious.

I would like to thank Monika Rex-Haffner for support with project organization and making sure that the lab runs smoothly.

Barbara Wölfel, Maik Ködel, Susann Sauer, Vincenza Sportelli and Laura Diener - thank you for your excellent technical help with all the experiments conducted and for teaching me your wet-lab tricks.

I am grateful to Leander Dony for supporting me, especially in the beginning, by sharing code and taking the time to explain all the details to a complete newbie. It helped me realise fast that coding was fun.

To Natalie Matosin and Nathalie Gerstner - thank you for the great collaboration throughout the years.

To Anthi Krontira and Lea Kaspar - This journey would have been very different and much more difficult without you. I am glad that besides being office mates, I can now call you my friends. Anthi, you have accompanied me through all the up’s and down’s of a PhD journey - thank you for all the conversations, scientific discussion, laughter and tears (of joy) and sharing your passion for science. Lea, your great humour made long days in the lab and office much more bearable. Your eye for the detail and creativity have been inspiring.

To my students, Kira Höffler, Catarina Raimundo, and Laura Pohlenz - It was great fun teaching you, seeing you grow and sharing the moments when experiments finally worked. But you also taught me a lot: how to be more patient, how to share knowledge and explain techniques, how to guide and supervise.

To Lotte van Doeselaar and Muriel Frisch - From the moment we met at our interviews for our PhD positions, we clicked. I am thankful for spending our PhD journey together, for the

endless conversations and dinners we had, for you building me up and telling me to keep pushing through.

To Nina Blaimschein and Katharina Pointner - My scientific journey started together with you in Salzburg. I cannot imagine how my bachelor studies would have turned out without you. After all, you helped me accomplish what I have accomplished up until now. I am grateful for our friendship, for our long skype conversations and for having you close whenever needed even though we live in three different countries.

Gerhard Engleder - Thank you for your advice on life and PhD studies. You made it clear to me that the most important aspect of PhD studies was to find a topic you are passionate about - thanks for insisting.

Sabine and Robert Fröhlich - Thank you supporting me throughout my (long) studies and for enabling me to study and live abroad. I am also thankful for you having genuine interest in my work even though sometimes I am not capable of explaining it in a more generally intelligible way. Thanks for always listening and having my back.

Michael Fröhlich - I am happy we finally got to live in the same city and spend more time together. Your perseverance and ambition are impressive. Thank you for your support throughout the years, the delicious dinners at your place and pushing me to always aim higher.

Javier García González - There are not enough words to express my gratitude. Thank you. Thank you for always being by my side (even in the distance), for supporting me (scientifically), for trying to understand me, for calming me down when I was stressing out or overthinking.

Tissues received from the New South Wales Brain Tissue Resource Centre at the University of Sydney were supported by the University of Sydney. Research reported in this publication was supported by the National Institute of Alcohol Abuse and Alcoholism of the National Institutes of Health under Award Number NIAAA012725-15. The content is solely the responsibility of the authors and does not represent the official views of the National Institutes of Health.